Cement and Concrete Research 172 (2023) 107250

Contents lists available at ScienceDirect

Cement and Concrete Research

journal homepage: www.elsevier.com/locate/cemconres

Kinetics of Al uptake in synthetic calcium silicate hydrate (C-S-H)

Yiru Yan [a,b,*], Ellina Bernard [a], G. Dan Miron [c], Daniel Rentsch [d], Bin Ma [a,c], Karen Scrivener [b], Barbara Lothenbach [a,e,f]

[a] Empa, Swiss Federal Laboratories for Materials Science and Technology, Laboratory for Asphalt and Concrete, Überlandstrasse 129, 8600 Dübendorf, Switzerland
[b] EPFL STI IMX LMC, MXG 230, Station 12, CH-1015 Lausanne, Switzerland
[c] Paul Scherrer Institute, Laboratory for Waste Management, Forschungsstrasse 111, 5232 Villigen PSI, Switzerland
[d] Empa, Swiss Federal Laboratories for Materials Science and Technology, Laboratory for Functional Polymers, Überlandstrasse 129, 8600 Dübendorf, Switzerland
[e] University of Bern, Institute of Geological Sciences, Hochschulstrasse 6, 3102 Bern, Switzerland
[f] NTNU, Department of Structural Engineering, 7491 Trondheim, Norway

ARTICLE INFO

Keywords:
Calcium silicate hydrate (C-S-H)
Aluminium uptake
Kinetics
Equilibration time
Thermodynamic modelling

ABSTRACT

The effect of equilibration time on the composition, structure and solubility of calcium aluminate silicate hydrate (C-A-S-H) was investigated in 0.5 M NaOH solutions at Al/Si = 0.1. Longer equilibration time led to longer silica chains, to less Na and, to more Ca in C-A-S-H, as well as to an increased fraction of tetrahedral Al(IV) charge-balanced by Ca^{2+}. Aluminium, calcium and silicon concentrations in solution changed rapidly during the first day, while after 14 days only minor changes were observed. The long-term concentrations could be reproduced well by the thermodynamic CASH+ model. Over a longer time span of up to 10 years, a slow redistribution of Si and Al in C-A-S-H as well as the partial replacement of Na^{+} by Ca^{2+} in the interlayer space was observed. This study highlights the importance of considering the effect of time on C-A-S-H structure.

1. Introduction

The equilibration time in cement-based materials is an important factor. Cement hydration occurs at the moment of contact between cement and water and the rock-like cementitious processes in Roman concrete are continuing to take place even after 2000 years [1]. Equilibration time can influence the variety of hydrates formed in cementitious systems. In Portland cements and many blended cements portlandite initially precipitates and might be then (partially) consumed by reacting with Si- or Al-rich supplementary cementitious materials (SCMs). Ettringite forms during early hydration and can then convert to monosulphate phases later in the absence of carbonate. Although C-A-S-H is still the main hydration product, zeolites (phillipsite) and Al-tobermorite have been observed in Roman concrete equilibrated for 2000 years [1], indicating that also the composition and structure of C-(A-)S-H could be affected by the equilibration time.

The structure of calcium silicate hydrate containing aluminium (C-A-S-H) has been studied for decades. These products have a layered structure, similar to the tobermorite group minerals shown in Fig. 1, which contain calcium oxide sheets sandwiched between aluminosilicate chains in a “dreierketten” arrangement. The two “pairing” silicate tetrahedra in the aluminosilicate chains are coordinated with CaO in the main layer. A third tetrahedron with bridging Si links two pairs of silicate units. The silicon in the bridging tetrahedral site can be substituted by aluminium [2–5]. Also cross-linking between aluminosilicate chains has been observed in low-Ca (Ca/Si < 1) cements [6,7] and at elevated temperatures [8–11] resulting in disordered analogues of ‘double chain’ calcium silicate minerals, such as 11 Å tobermorite (Fig. 1(a)). The long-range order of C-(A-)S-H is reported to increase with higher curing temperature [11].

Despite numerous studies on the chemistry and structure of C-(A-)S-H [4,10,11,13–25], the effect of equilibration time on its solubility, composition and structure is poorly understood. A recent in-situ FTIR study from John et al. [26] showed a development of the silicate structure of synthetic C-S-H from 0 to 24 h and Pardal et al. [27] reported clear changes in calcium, aluminium and silicon concentrations in the aqueous phase of C-A-S-H with Ca/Si 0.66 from 0.05 to 20 days; unfortunately the solids present have not been characterized. Sun et al. [4] studied the effects of Al on C-S-H with synthesis time ranging from 1 week to 4 months and observed no clear difference. L’Hôpital et al.

* Corresponding author at: Empa, Swiss Federal Laboratories for Materials Science and Technology, Laboratory for Asphalt and Concrete, Überlandstrasse 129, 8600 Dübendorf, Switzerland.
E-mail addresses: yiru.yan@empa.ch, yiru.yan@alumni.epfl.ch (Y. Yan).

https://doi.org/10.1016/j.cemconres.2023.107250
Received 17 February 2023; Received in revised form 17 June 2023; Accepted 25 June 2023
Available online 11 July 2023

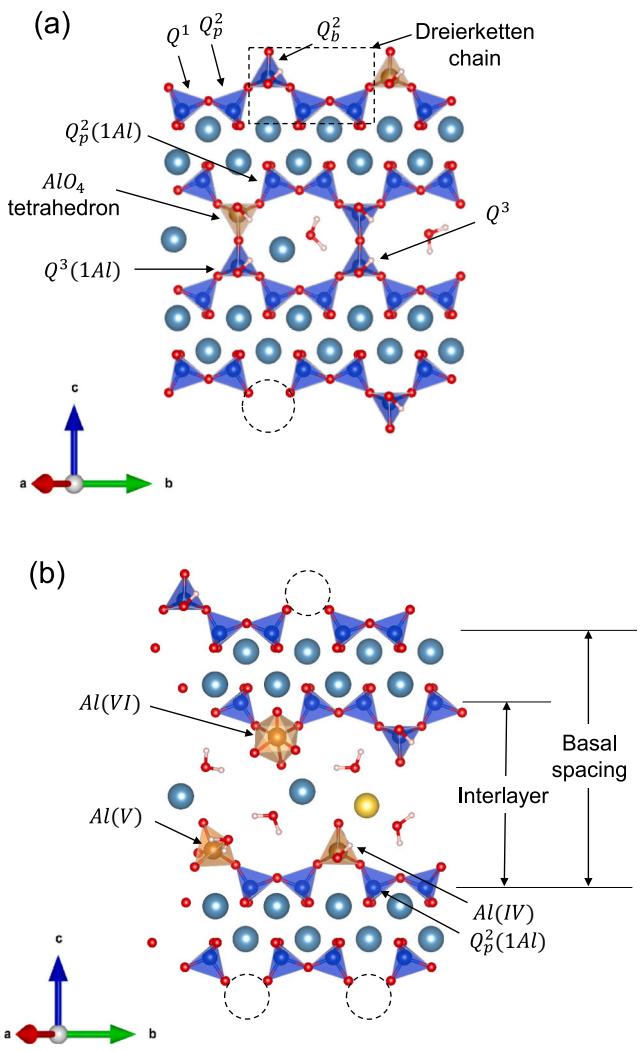

Fig. 1. Schematic structure of (a) cross-linked 11 Å Al-tobermorite and (b) non-cross-linked C-A-S-H, adapted from [12]. Spheres of blue, golden, turquoise, yellow, red and white colors represent Si, Al, Ca, Na, O and H, respectively. The dashed circles are Si tetrahedra vacancies in bridging sites. Q^n: n indicates the numbers of Si tetrahedral neighbors. Subscripts: b: bridging position, p: pairing position, Al(IV): Al in tetrahedral coordination, Al(V): Al in pentahedral coordination and Al(VI): Al in octahedral coordination. (For interpretation of the references to colour in this figure legend, the reader is referred to the web version of this article.)

[18,19], also reported little change in the aqueous phase when studying C-A-S-H with a Ca/Si ratio of 1.0–1.6 over a period of 30 days to 2 years. However, they did observe a decrease in the amount of secondary phases, such as katoite and porlandite, which indicate the presence of additional Al and Ca in C-S-H. A better ordering C-S-H is also observed with longer equilibration time. Barzgar et al. [28] similarly reported a decrease in secondary phases and also a decrease in the aqueous Al concentration over time, indicating a slow restructuring of C-A-S-H. However, the use of different preparation methods for the short-term and long-term experiments in these studies led to considerable scatters in the results.

In this study, 61 C-A-S-H samples with different equilibration time from 6 h up to 10 years were synthesized and characterized to assess the time influence on the C-A-S-H composition and structure. This study is also focused on the interplay between the aqueous concentrations of relevant ions, composition, Al and Na uptake and the C-A-S-H structure. The availability of a comprehensive set of solubility data for C-A-S-H with different equilibration time is necessary for the development of more accurate models to describe kinetics, hydration, durability and performance of cement-based materials. The experimental results are compared with the predictions generated by the CASH+ thermodynamic solid solution model [29–32] that accounts for the uptake of aluminium and alkali in C-S-H.

2. Materials and method

2.1. Synthesis procedure

SiO_2 (Aerosil 200, Evonik), CaO, $CaO{\cdot}Al_2O_3$ (CA) and 0.5 M NaOH solutions at a liquid/solid ratio of 40 or 45 (mL/g) were used to synthesize C-N-A-S-H. The synthesis of CaO and CA followed the procedure in [18]. The target molar ratios of Ca/Si in C-A-S-H samples were $Ca/Si_{target} = 0.6, 0.8, 1.0, 1.2, 1.4$ and 1.6; the target molar ratio of Al/Si was $Al/Si_{target} = 0.1$. The mixing proportions used to prepare C-A-S-H are shown in Table A1.

Different mixtures were equilibrated for varying durations to study the behavior of C-A-S-H. Short-term C-A-S-H slurries, with a liquid/solid ratio of 40 (mL/g), were equilibrated for durations ranging from 6 h to 90 days. Long-term C-A-S-H slurries, with a liquid/solid ratio of 45 (mL/g), were equilibrated for durations ranging from 90 days to 10 years (3650 days). The C-A-S-H sample preparation, filtration (nylon filter, 0.45 μm), washing, drying and storage at 35 % relative humidity prior to characterization, followed the same procedure described in detail by L'Hôpital et al. [19].

2.2. Analytical techniques

2.2.1. Solution analysis

The composition of the liquid phase was analyzed by ion chromatography (IC) as soon as possible after filtration (and diluted if necessary with MilliQ water) to avoid any carbonation and/or precipitation. The concentrations of Ca, Na, Al and Si were quantified using a Dionex DP series ICS-3000 ionic chromatography system. Independent measurements of solutions with known compositions indicated a measurement error of ≤10 %.

The pH measurements were carried out in a non-diluted fraction of the solution with the Knick pH meter (pHMeter 766) equipped with the Knick SE100 electrode. The pH electrode was calibrated against NaOH solutions of known concentrations to minimize alkali error using the method detailed in [33]. The pH values were measured at laboratory temperature (23 to 24 °C) and corrected to 20 °C by adding +0.1 pH unit to take into account the effect of temperature on the pH measurement [18].

2.2.2. Solid phase analysis

Thermogravimetric analysis (TGA) was conducted on ground powder (≈20–30 mg) under nitrogen atmosphere at a heating rate of 20 °C/min from 30 to 980 °C with a Mettler Toledo TGA/SDTA 8513 instrument. Mass losses between 30 and ≈ 600 °C were assigned to dehydration and dehydroxylation of C-A-S-H and portlandite during heating. Portlandite was quantified based on the weight loss between ≈ 350 and ≈ 500 °C using the tangential method [34] and double-checked with X-ray diffraction and Rietveld refinement analysis. Assignment of the weight loss peaks to the different hydrates was done based on the reference measurements given in [34].

Powder X-ray diffraction (XRD) data were collected using a PANalytical X'Pert Pro MPD diffractometer equipped with rotating sample stage in a θ–2θ configuration applying Cu radiation (λ = 1.54 Å) at 40 mV voltage and 40 mA, with steps of 0.019° 2θ with a fixed divergence slit size and an anti-scattering slit on the incident beam of 0.25° and 0.5° 2θ. The samples were scanned between 5° and 70° 2θ with an X'Celerator detector. Profile fittings were performed to determine the d-spacing and the full width at half maximum (FWHM) of the (001) reflection of C-S-H. The diffraction profiles were generated using the Pseudo-*V*oigt

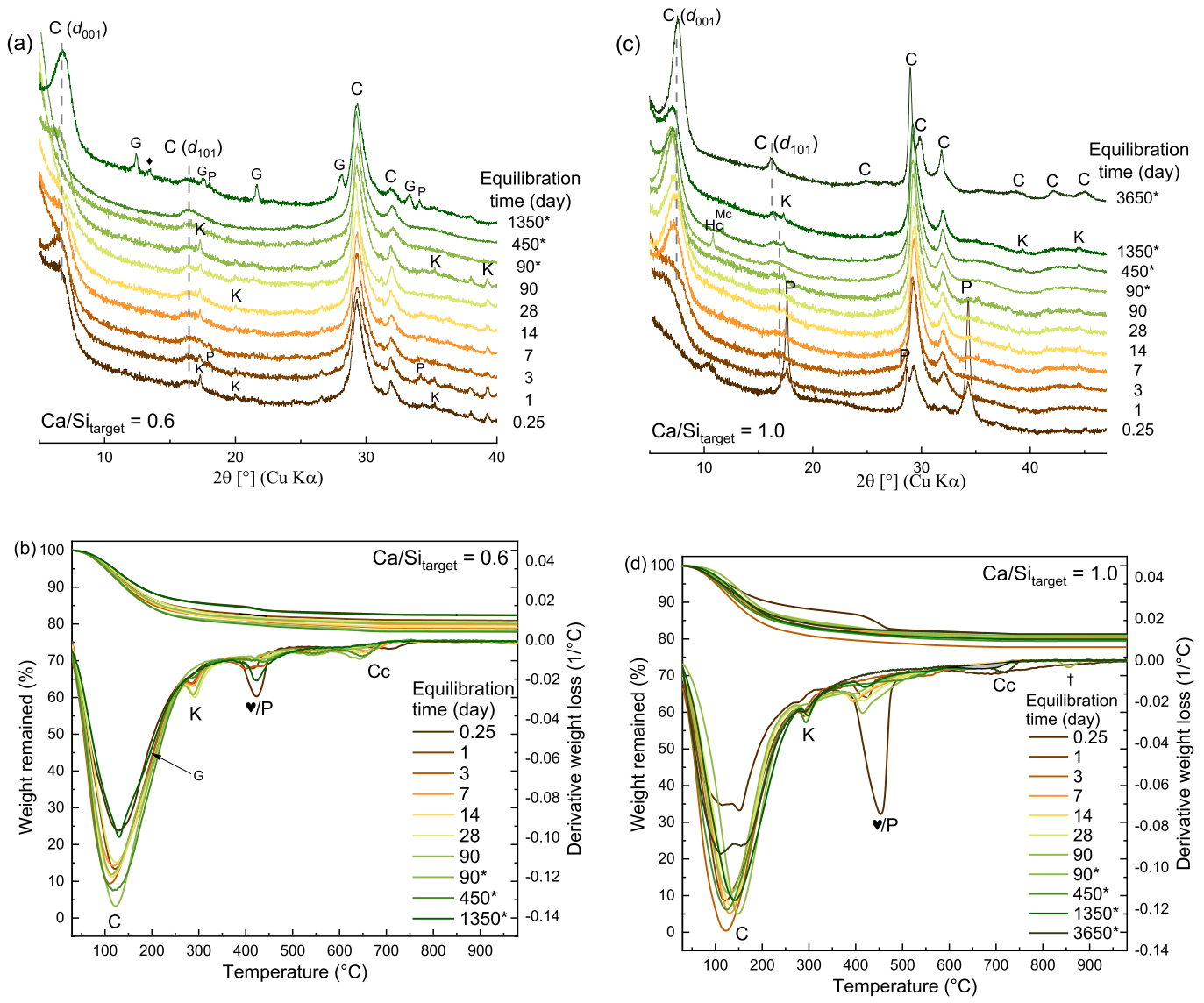

Fig. 2. XRD and TGA of C-A-S-H with (a) and (b) target Ca/Si = 0.6, (c) and (d) target Ca/Si = 1.0, (e) and (f) target Ca/Si = 1.4 synthesized in NaOH 0.5 M with initial Al/Si 0.1, equilibrated for different time from 0.25 day to 3650 days. C: C-A-S-H, P: portlandite ($Ca(OH)_2$, PDF# 00-004-733), K: katoite ($Ca_3Al_2(OH)_6$, PDF# 00-024-0217), Hc: hemicarbonate ($Ca_4Al_2(OH)_{12}(OH)(CO_3)_{0.5}(H_2O)_5$, PDF# 00-029-0285), Mc: monocarbonate ($Ca_4Al_2(OH)_{12}(OH)(CO_3)(H_2O)_5$, PDF# 00-029-0285). G: gismondine-P1-Na ($Na_6Al_6Si_{10}O_{32}$•$12H_2O$, PDF# 01-071-0962). ◆: unidentified phase. ♥: The weight loss from C-A-S-H Ca/Si$_{target}$ = 0.6 and 1.0 at later ages is tentatively assigned to C-N-A-S-H, as portlandite is absent in XRD and FTIR, and the solutions are strongly undersaturated with respect to portlandite. †: The weight loss from C-A-S-H synthesized for 90 days between 850 and 900 °C in (d) is assigned to phase transformation of C-N-A-S-H to wollastonite. *: samples synthesized with water/solid = 45.

function in the Highscore Plus V 3.0e software package. The identified reflections were assigned based on the Powder Diffraction File for tobermorite MDO2 (11 Å tobermorite structure) as reported by Merlino et al. [35] for C-S-H.

Attenuated total reflectance (ATR) Fourier Transformation Infrared (FTIR) spectra were collected by averaging 32 scans measured on a Bruker Tensor 27 FTIR spectrometer by transmittance between 340 and 4000 cm^{-1} at a resolution of 4 cm^{-1} on ≈ 3 mg of powder. The IR spectral data obtained were preprocessed using the software package OPUS (Bruker Optics GmbH, Ettlingen, Germany). Baseline correction and normalization to the intensity of the peak at around 950 cm^{-1} were applied to every recorded spectrum. The second derivative of FTIR spectra was used in order to identify the different bands and differentiate the wavenumbers.

Raman spectra were recorded using a WITec Alpha 300 R confocal Raman microscope in backscattering geometry. A diode-pumped green laser with a wavelength of 532 nm was used in combination with a 50× objective lens. The Rayleigh scattered light was blocked by an edge filter. The backscattered light was coupled to a 300 mm lens-based spectrometer with a grating of 600 g/mm equipped with a cooled deep-depletion CCD. Back- illuminated CCD chip with 1024 × 127 pixel format, pixel size 26 × 26 μm. The laser output power was set to 20 mW. To diminish possible carbonation, the C-A-S-H powders were loaded and sealed in quartz glass capillary tubes with a 2.0 mm out diameter and 0.01 mm wall thickness. Raman spectra of the loaded and empty tubes were recorded, with the spectrum of the empty tube being subsequently subtracted. Each C-A-S-H phase was measured and averaged at 10 spots with an exposure time of 10 s and 10 accumulations for each spectrum. Spectral analysis, including glass tube signal subtraction, individual baseline correction, spectra average and smoothing, was conducted

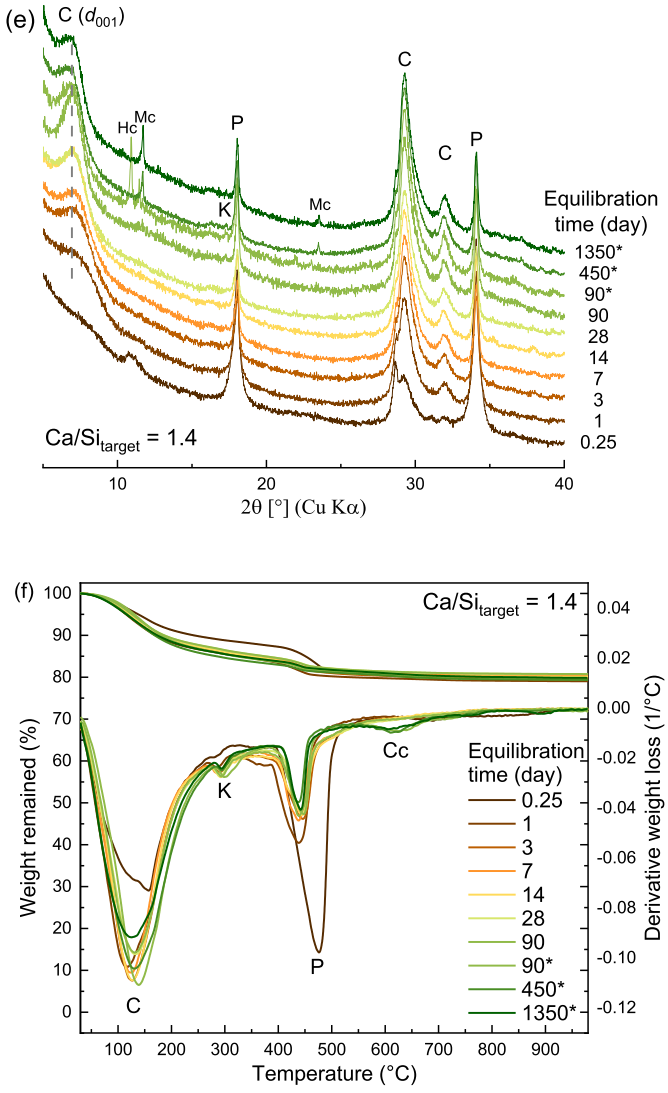

Fig. 2. (*continued*).

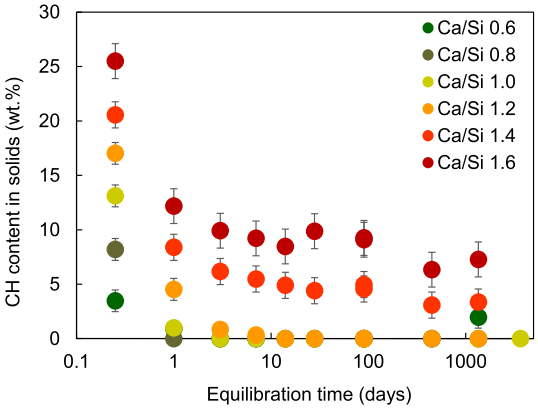

Fig. 3. Portlandite content in solid phases as a function of time, quantification obtained by TGA analysis.

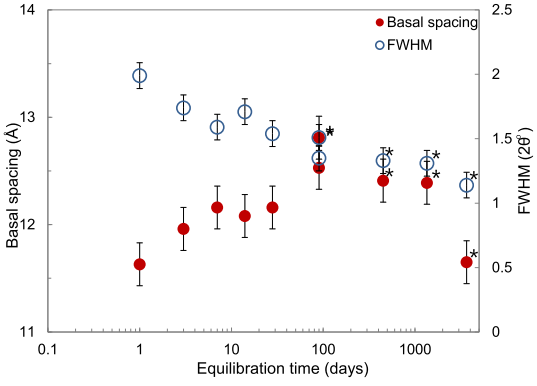

Fig. 4. Variation of mean basal spacing and the FWHM of the d_{001} reflection as a function of equilibration time for C-A-S-H with Ca/Si = 1.0, solid red symbols: mean basal spacing, empty blue symbols: FWHM. *: samples synthesized with water/solid = 45. (For interpretation of the references to colour in this figure legend, the reader is referred to the web version of this article.)

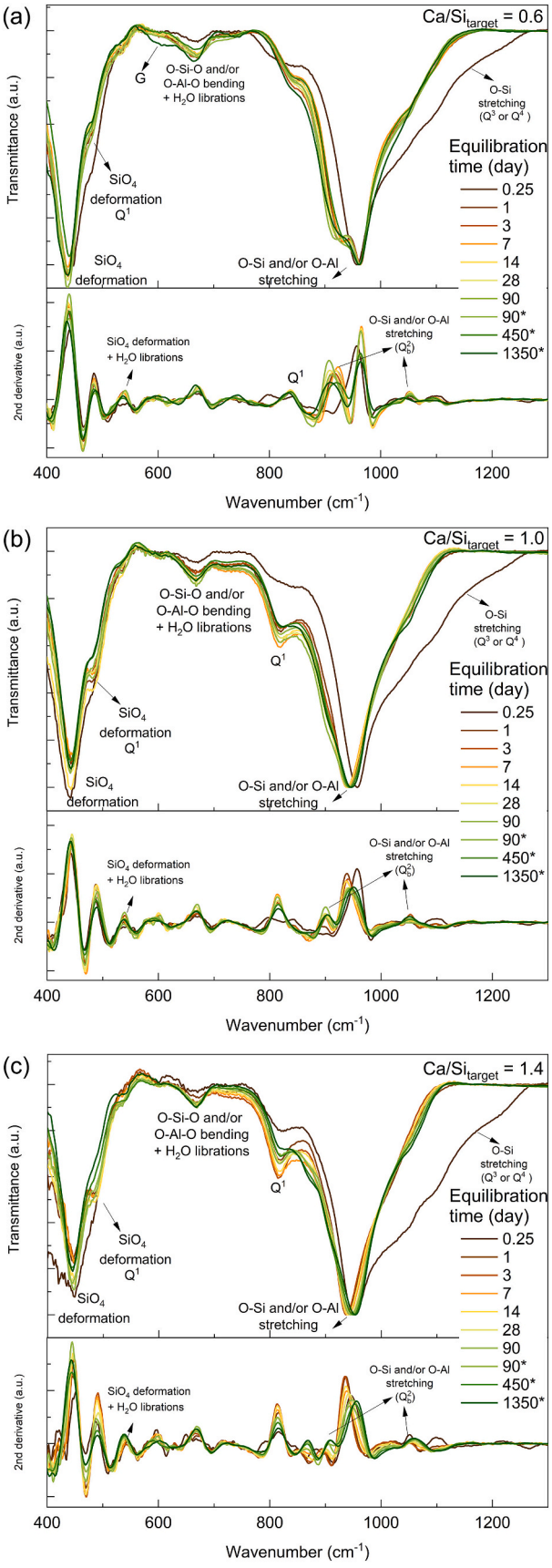

Fig. 5. FTIR spectra with second derivatives of C-A-S-H with Ca/Si_{target} = (a) 0.6, (b) 1.0 and (c) 1.4 after different equilibration time synthesized in 0.5 M NaOH. The spectra are normalized to the most intensive band at ≈ 970 cm^{-1} of FTIR. C-A-S-H equilibrated for 0.25–90 days: synthesized with water/solid = 40, C-A-S-H equilibrated for 90*, 450*, 1350* and 3650* days: synthesized with water/solid = 45. Δ: Si—O and/or Al—O stretching of Q^3.

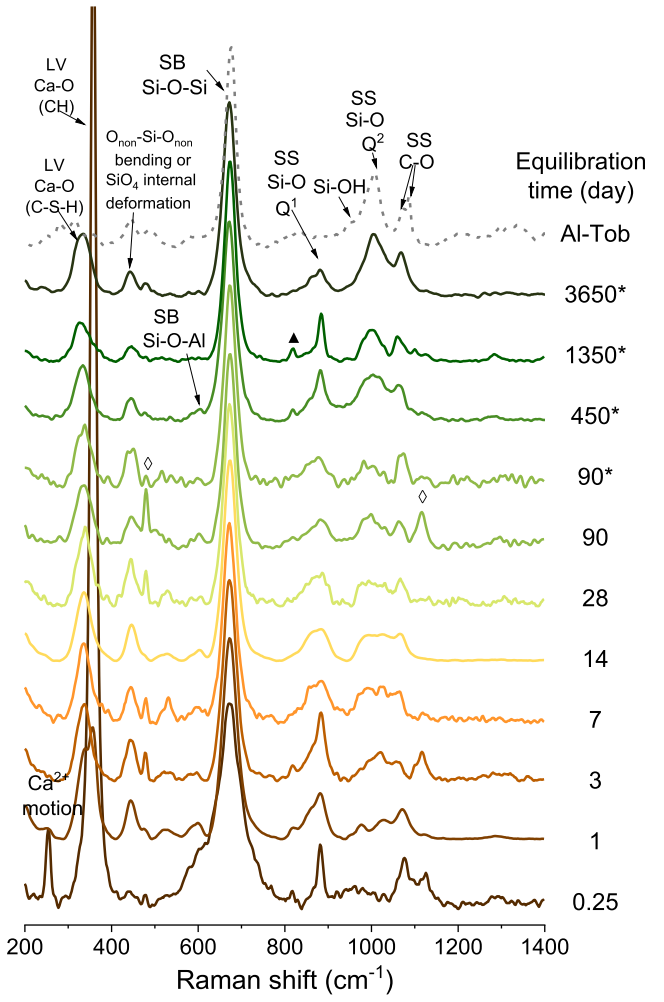

Fig. 6. Raman spectra of C-A-S-H with $Ca/Si_{target} = 1.0$ after different equilibration time synthesized in 0.5 M NaOH and Al-tobermorite [12] for comparison. Normalized to the band related to Si-O-Si symmetrical bending (SB) at ≈672 cm^{-1}. *: samples synthesized with water/solid = 45. ▲, ◊: unidentified peaks from secondary phases.

using Spectragryph [36].

The ^{29}Si MAS NMR single pulse experiments were conducted on Bruker Advance III 400 NMR spectrometer (Bruker BioSpin AG, Fällanden, Switzerland) using a 7 mm CP/MAS probe at 79.50 MHz applying the following parameters: 4500 Hz sample rotation rate, minimum of 10,240 scans, 30° ^{29}Si pulse of 2.5 μs, 20 s recycle time, RF field strength of 33.3 kHz during SPINAL64 proton decoupling. The ^{29}Si NMR chemical shifts were referenced to the most intense resonance at −2.3 ppm of an external sample of an octamethylsilsesquioxane (Aldrich No. 52,683-5) which was referenced to tetramethylsilane (TMS, $\delta^{29}Si = 0.0$ ppm), details are given in [37]. The observed ^{29}Si NMR resonances were assigned using the Q^n classification, where one Si tetrahedron is connected to n Si tetrahedra, where n varies from 0 to 4. The lineshapes of the experimental data were analyzed by non-linear least-square fits using the "Dmfit" software developed by Massiot et al. [38].

Resonances with chemical shifts (δ_{iso}) at approx. −76 ppm (Q^0), −79 ppm (Q^1), −81 ppm ($Q_p^2(1Al)$), −84 ppm (Q_b^2), −85 ppm and −88ppm (Q_{pa}^2, and Q_{pb}^2), −91 ppm ($Q_p^3(1Al)$), and −97 ppm (Q^3) were identified and the line shape analysis was carried out, respecting the following restrictions imposed by the dreierketten model, as discussed in detail in [6,39,40]:

i) $\frac{Q_p^2 - 2\left(Q^3 + Q_p^3(1Al)\right)}{Q_b^2} = 2$

ii) $Q_p^2(1Al) \geq 2Q_p^3(1Al)$

iii) $Q^2 + Q_p^2(1Al) \geq 2\left(Q^3 + Q_p^3(1Al)\right)$

iv) $Q_p^2 - 2\left(Q^3 + Q_p^3(1Al)\right) \geq 0$

v) $Q_p^2(1Al) - 2Q_p^3(1Al) \geq 0$;

where $Q_p^2 = Q_{pa}^2 + Q_{pb}^2$

The single-pulse ^{27}Al MAS NMR experiments were recorded at 104.26 MHz on the same NMR spectrometer using a 2.5 mm CP/MAS probe. The parameters used in the present study are 25′000 Hz spinning speed, at least 3072 scans, π/12 pulses of 1 μs without ^{1}H decoupling, and 0.5 s recycle time. The ^{27}Al NMR chemical shifts were referenced to an external sample of 1.1 m $Al(NO_3)_3$ in D_2O at 0.0 ppm. The ^{27}Al NMR deconvolutions were also conducted with the Dmfit software [38]. The peak shape of Al(*VI*) signal at ~−11 ppm was constraint with a Gaussian shape. The Czjzek model was used for the deconvolution of Al(IV), Al(V) and Al(VI) in C-A-S-H, as outlined in detail in [41]. The assignment to Al $(IV)_a$, Al $(IV)_c$ and Al $(IV)_d$ signals followed the procedure in the recent paper of Yang et al. [40]; the Al $(IV)_b$ signal from the Yang's study could not be distinguished from the Al $(IV)_a$ in this study due to the lower magnetic field used. However, it might still be present and included in the Al $(IV)_a$ signal.

2.2.3. C-S-H composition

The effective Ca/Si ratios in C-S-H ($Ca/Si_{C\text{-}S\text{-}H}$) were obtained indirectly by mass-balance calculations, considering the initial amount of CaO, $CaO{\cdot}Al_2O_3$ and SiO_2 in the system, the fraction of SiO_2, Al_2O_3 and CaO in solution, as well as the amount of secondary phases present, following the procedure outlined in [18,42].

The amount of alkalis bound in the solid was determined following the direct method (i.e. acid digestion of 20 mg of washed and dried C-S-H phase in 10 mL 100 mM HCl). The total amount in the solid was obtained from the measured Ca, Na and Al concentrations in the acid solution as detailed in [20,42].

The effective Al/Si ($Al/Si_{C\text{-}S\text{-}H}$) were obtained indirectly by mass-balance calculations, using the total amount of Al and Si present minus the fraction which remained in the equilibrated solution and the fraction in secondary phases, as quantified from XRD and TGA or ^{27}Al NMR. The effective Al/Si were also obtained directly by HCl dissolution as described above as well as based on the fraction of Si next to an Al-tetrahedron based on the deconvolution of the ^{29}Si NMR signals. The Al/Si fractions from ^{29}Si NMR, are calculated according to the procedure detailed in Myers et al. [6]:

$$(Al/Si)_{C-A-S-H} = \frac{\left[\frac{(Al/Si)_{[NC]}}{\left(1+(Al/Si)_{[NC]}\right)}\right](Al+Si)_{[NC]} + \left[\frac{(Al/Si)_{[C]}}{\left(1+(Al/Si)_{[C]}\right)}\right](Al+Si)_{[C]}}{\left[\frac{1}{\left(1+(Al/Si)_{[NC]}\right)}\right](Al+Si)_{[NC]} + \left[\frac{1}{\left(1+(Al/Si)_{[C]}\right)}\right](Al+Si)_{[C]}} \quad (1)$$

Where $Al/Si_{[C]}$ and $Al/Si_{[NC]}$ are the molar fraction of Al in cross-linked and non-cross-linked bridging sites, obtained by Eqs. (2) and (3):

$$(Al/Si)_{[C]} = \frac{Q^3(1Al)}{Q^1 + Q^2 + Q^2(1Al) + Q^3 + Q^3(1Al)} \quad (2)$$

$$(Al/Si)_{[NC]} = \frac{\left(\frac{1}{2}\right)Q^2(1Al)}{Q^1 + Q^2 + Q^2(1Al)} \quad (3)$$

The incorporation of Al into C-S-H phases can also be expressed in terms of the distribution coefficient (K_d), to quantify the relative affinity for Al to sorb to C-S-H [43]. The K_d values were calculated according to:

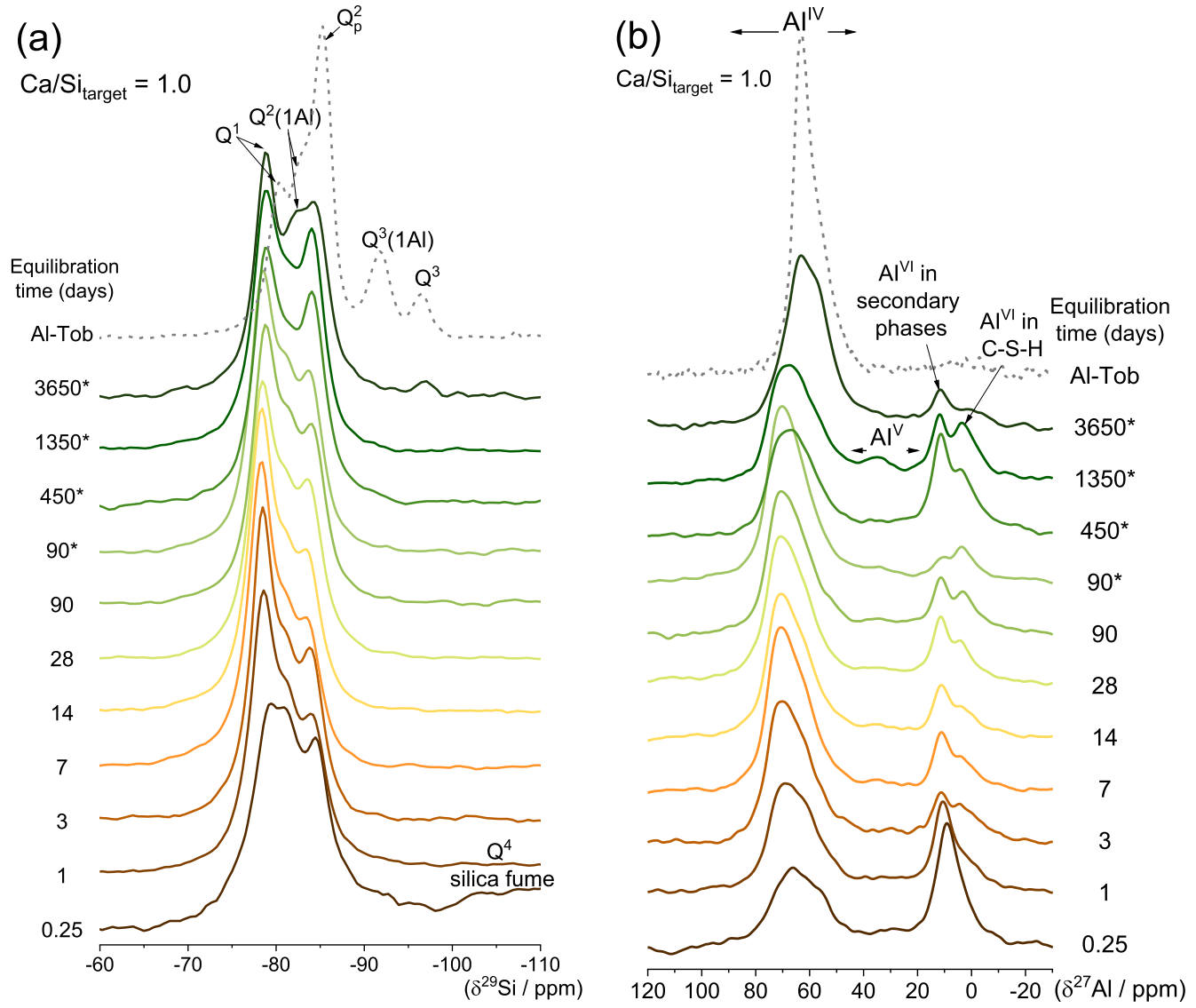

Fig. 7. ^{29}Si and ^{27}Al MAS NMR of aged C-A-S-H with (a) (b): Ca/Si$_{target}$ = 1.0 and (c) (d): Ca/Si$_{target}$ = 0.8 synthesized in 0.5 M NaOH and of Al-tobermorite [12] for comparison. *: samples synthesized with water/solid = 45.

$$K_d = \frac{C_{s,eq}}{C_{l,eq}} \left(\frac{m^3}{kg}\right) \quad (4)$$

where $C_{s,eq}$ is the Al concentration in C-S-H phases [mol/kg], and $C_{l,eq}$ is the aqueous concentration [mol/m^3].

2.3. Thermodynamic modelling

Thermodynamic modelling was carried out with the Gibbs free energy minimization program GEM-Selektor v3.7 [44,45]. GEMS is a geochemical modelling code that computes the equilibrium speciation in aqueous, gas and stable solid phases using the Gibbs free energy minimization algorithm. The thermodynamic data for aqueous species were taken from the PSI-Nagra thermodynamic database [46], while the standard molar properties for cement minerals were taken from the Cemdata18 database [47]. The C-S-H phase with alkali metal- and Al uptake was modelled using the CASH+ solid solution thermodynamic model [29–32], which has been parameterized against experimental data independent of this study. The formation of $CaSiO_2(OH)_2^0$ aqueous complex was described using log K = 4.0 for the reaction $Ca^{2+} + SiO_2(OH)_2^{2-} \Leftrightarrow CaSiO_2(OH)_2^0$ [29], instead of the log K = 4.6 reported in [46]. The log K of gismondine-P1-Na ($Na_6Al_6Si_{10}O_{32}\bullet 12H_2O \Leftrightarrow 6Na^+ + 6Al(OH)_4^- + 10SiO_2^0$) and chabazite ($CaAl_2Si_4O_{12}\bullet 6H_2O \Leftrightarrow Ca^{2+} + 2Al(OH)_4^- + 4SiO_2^0 + 2H_2O^0$) at 20 °C was determined to be −82.2 and −31.4 in parallel studies of zeolite dissolution experiments [48,49].

Ion activity products (IAP) for C-(A-)S-H and saturation indices (SI) for relevant solid phases were calculated from experimentally measured total concentrations. Activity coefficients were calculated using the extended Debye-Hückel equation in Truesdell-Jones form with common ion-size parameter a_i=3.31 Å for NaOH solutions and third parameter b_γ = 0.098 kg/mol [50].

3. Results and discussion

A comprehensive investigation was conducted on various C-(A-)S-H phases, covering a range of target Ca/Si ratios from 0.6 to 1.6. The main focus of this discussion revolves around the impact of aging on C-S-H phases, with specific attention given to Ca/Si$_{target}$ ratios of 0.6, 0.8, 1.0, and 1.4, which represent low, intermediate, and high Ca/Si ratios, respectively. Additional data regarding C-(A-)S-H samples with Ca/Si$_{target}$ ratios of 0.8, 1.2, and 1.6 can be found in Appendix A.

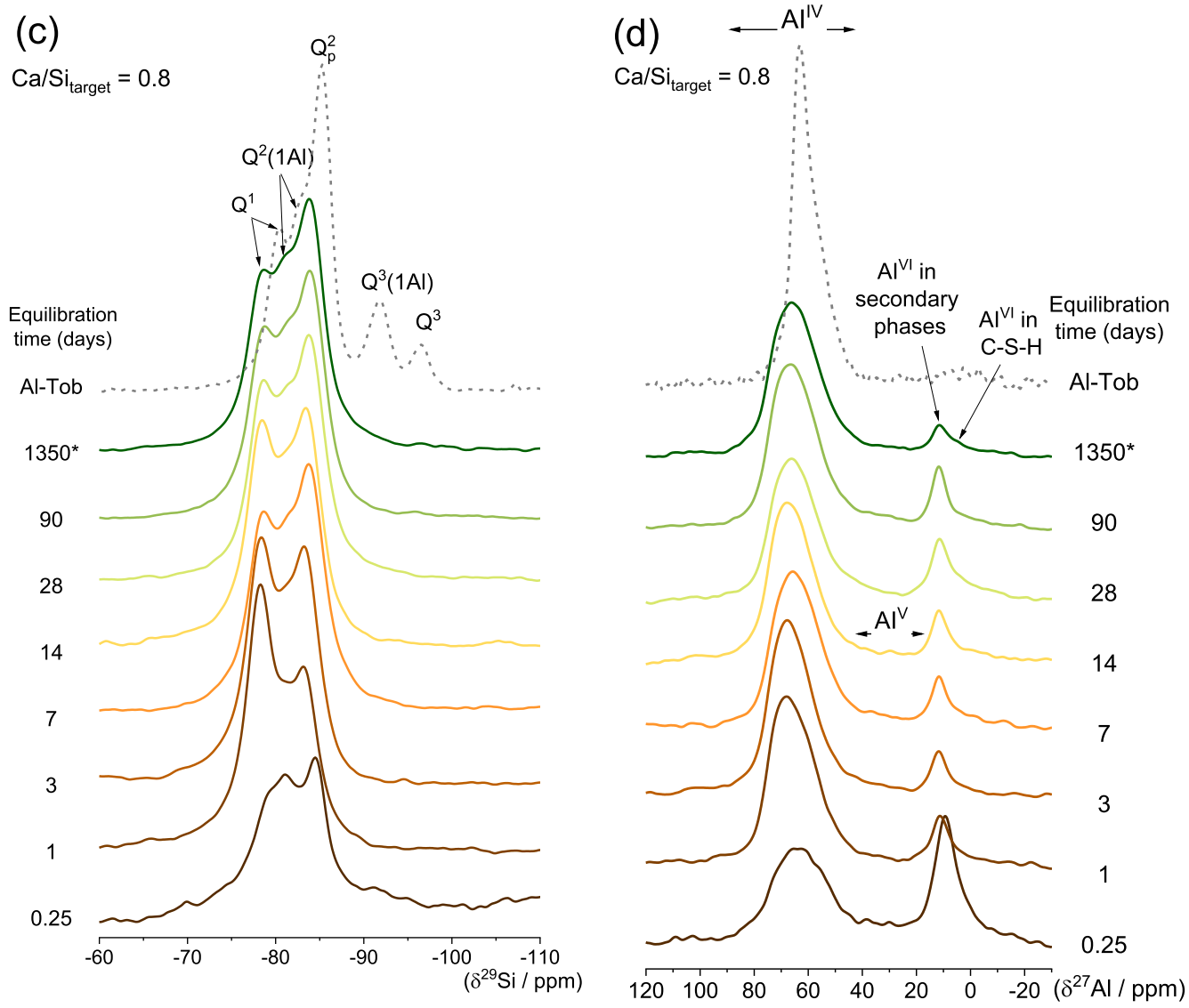

Fig. 7. (*continued*).

3.1. Effect of time on solid phases

3.1.1. Solids present

Fig. 2 shows the solid phase evolution based on XRD and TGA results. C-A-S-H is the main phase in all cases, independent of the Ca/Si$_{target}$ and equilibration time with 2θ Cu $K\alpha$ diffraction maxima at ≈7.4° (12.0 Å), ≈16.7° (5.3 Å), ≈29.1° (3.1 Å), ≈32.0° (2.8 Å), ≈49.8° (1.8 Å), ≈55.0° (1.7 Å), and ≈66.8° (1.4 Å) as detailed in [51,52]. At Ca/Si$_{target}$ = 0.6, 1.0 and 1.4, portlandite precipitates at early age as visible by the characteristic reflection peaks at ≈18.09° (4.9 Å), ≈28.7° (3.11 Å), ≈34.1° (2.63 Å), ≈47.1° (1.93 Å), ≈50.8° (1.80 Å), ≈54.4° (1.69 Å), ≈62.6° (1.48 Å), and ≈64.2° (1.45 Å) [53] observed in the XRD pattern after 6 h. This is related to the initial slow saturation of water with respect with SiO_2, hence a low dissolved Si at early age (slow silica fume dissolution), while the hydration of CaO occurs faster. After 1 day, less portlandite is observed due to its reaction with silica fume (see the FTIR data in Section 3.1.2 C-A-S-H structure). Portlandite is completely consumed after 7 days at Ca/Si$_{target}$ = 0.6 and 1.0, while at Ca/Si$_{target}$ = 1.4 , the quantity of portlandite remains constant after 7 days and longer. The formation of small amount of katoite is observed by XRD (main reflections at ≈17.27° (5.1 Å), ≈31.8° (2.81 Å), ≈39.2° (2.30 Å) and ≈44.4° (2.04 Å) [54]) in most C-A-S-H samples at after 1 or 3 days and longer, which indicates the formation of katoite occurs rapidly. XRD data also show that hemicarbonate and monocarbonate are present in some samples, which is attributed to minor carbonation during sample preparation, drying and measurement. At Ca/Si$_{target}$ = 0.6 after 3 years equilibration time, the formation of a zeolite, gismondine-P1-Na ($Na_6Al_6Si_{10}O_{32}$•$12H_2O$), is observed by XRD with the characteristic reflections at ≈12.5° (7.1 Å), ≈17.65° (5.02 Å), ≈21.7° (4.10 Å) and ≈28.1° (3.18 Å) and ≈33.4° (2.68 Å) [55]. This first observation of zeolite in a suspension of C-N-A-S-H points out that in the long-term at low Ca/Si ratios and high alkali concentrations, zeolitic phases can form, in agreement with other long-term experiments [56] and observations in Roman concrete [1]. After 3 years, also a small amount of portlandite as well as another unidentified phase are observed (see ◆ in Fig. 2).

For C-A-S-H with Ca/Si$_{target}$ = 1.0, after 10 years of hydration, the long-range order of the C-A-S-H products increased (Fig. 2(c)), as visible particularly by the higher intensity and sharpness of the reflections at ≈8° (12.0 Å), ≈16.7° (5.3 Å), as well as by the presence of the reflection at ≈29.9° (3.0 Å) from $d_{2\text{–}22}$ and d_{022} ≈ 42.2° (2.1 Å) from $d_{\text{–}129}$ ≈ 45.0° (2.0 Å) from $d_{3\text{–}25}$ *and* d_{125} [51]. The observations of these reflections are in good agreement with previous research on high temperature C-A-S-H (80 °C) by Myers et al. [11] and indicate a crystallite size of the C-A-S-H in *ab* directions larger than 20 nm according to Grangeon et al. [51].

Table 1
Quantification of the different silicate sites obtained by deconvolution of the ^{29}Si NMR spectra of C-A-S-H with Ca/Si$_{target}$ = 1.0, 0.8 and Al-tobermorite [12] for comparison. *: samples synthesized with water/solid = 45. † signals assigned to unreacted silica. MCL: mean chain length for tetrahedral Al + Si (IV) and for Si only.

Ca/Si$_{target}$	Equilibration time (days)	Q^0		Q^1		Q^2_p(1Al)		Q^2_b		Q^2_{pa}		Q^2_{pb}		Q^3(1Al)		Q^3		MCL (IV)	MCL (Si)	Al/Si in C-A-S-H
		δ_{iso} (ppm)	Rel. amount (%)	δ_{iso} (ppm)	Rel. amount (%)	δ_{iso} (ppm)	Rel. amount (%)	δ_{iso} (ppm)	Rel. amount (%)	δ_{iso} (ppm)	Rel. amount (%)	δ_{iso} (ppm)	Rel. amount (%)	δ_{iso} (ppm)	Rel. amount (%)	δ_{iso} (ppm)	Rel. amount (%)			
1.0	0.25	−75.9	8.6	−78.9	18.9	−81.5	22.1	−84.5	13.7	−86.3	6.0	−88.4	2.2	−91.4	5.0	−96.4	2.3	7.8	3.1	0.155
	1	−75.9	8.1	−78.5	42.3	−81.3	21.7	−83.9	16.5	−85.2	9.6	−88.7	1.8					4.9	2.9	0.108
	3	−75.3	5.9	−78.5	47.5	−81.2	19.0	−83.7	15.7	−84.9	10.9	−87.6	1.0					4.4	2.8	0.095
	7	−74.7	7.8	−78.3	50.7	−81.2	20.3	−83.7	13.9	−84.6	6.9	−88.6	0.4					4.0	2.6	0.102
	14	−74.8	3.8	−78.3	53.3	−81.2	17.2	−83.3	14.4	−84.6	10.0	−87.8	1.5					3.9	2.7	0.086
	28	−75.5	3.0	−78.4	47.3	−81.2	19.8	−83.6	16.4	−84.7	10.9	−88.0	2.6					4.5	2.9	0.099
	90	−74.2	3.9	−78.3	52.4	−81.2	18.3	−83.4	14.7	−84.6	9.9	−87.3	0.9					4.0	2.7	0.092
	90*	−75.5	3.5	−78.4	47.3	−81.2	20.2	−83.6	16.4	−84.7	11.3	−88.1	1.3					4.5	2.9	0.101
	450*	−75.5	3.2	−78.5	41.9	−81.1	18.6	−83.5	18.4	−84.5	15.3	−88.2	2.7					5.1	3.2	0.093
	1350*	−75.5	4.3	−78.5	42.2	−81.2	20.0	−83.7	17.7	−84.3	14.8	−87.4	1.1					5.0	3.1	0.100
	3650*	−74.4	3.6	−78.4	35.5	−80.9	11.3	−82.3	15.7	−84.2	23.7	−86.7	5.5	−90.5	1.8	−96.5	2.8	5.9	4.1	0.086
0.8	0.25	−74.9	9.3	−78.7	13.8	−81.3	22.2	−84.5	22.6	−86.7	2.5	−88.4	2.0	−91.4	7.8	−96.4	3.0	10.7	3.5	0.153
	1	−74.9	9.8	−78.2	42.2	−81.3	25.7	−83.6	16.1	−86.7	5.2	−88.4	1.0					4.9	2.7	0.129
	3	−74.9	7.1	−78.2	35.8	−80.8	12.5	−82.2	19.1	−83.7	22.1	−86.5	3.4					5.5	3.8	0.063
	7	−74.9	4.1	−78.2	24.5	−80.6	14.0	−82.1	23.4	−84.1	26.5	−86.8	7.6					8.4	5.0	0.070
	14	−74.8	4.9	−78.2	31.8	−80.8	15.0	−82.2	21.1	−83.9	22.7	−86.5	4.5					6.4	4.1	0.075
	28	−74.8	2.1	−78.3	27.8	−80.7	12.9	−82.2	23.5	−84.2	26.8	−87.2	6.8					7.5	4.8	0.065
	90	−74.8	2.9	−78.3	26.4	−80.7	12.6	−82.2	23.6	−84.2	28.7	−87.2	5.7					7.8	5.0	0.063
	1350*	−74.8	2.3	−78.2	24.9	−80.7	13.9	−82.2	24.3	−84.2	28.8	−87.2	5.7					8.4	5.0	0.070
	Al-Tob [60]			−80.2	19.6	−82.7	23.7	−84.2	4.6	−85.8	34.2	−88.5	2.6	−91.9	10.6	−96.6	4.6	22.6		0.106

The TGA data show a main water loss between 30 and 300 °C from interlayer and structurally bound water in C-A-S-H. The water loss of C-A-S-H increases from 6 h to 1 day for all Ca/Si$_{target}$, while few changes are observed afterwards up to 3 years (An exception is the decrease in water content at Ca/Si$_{target}$ = 0.6, where gismondine-P1-Na is formed). A water loss at 400–500 °C, marked with ♥, is observed at Ca/Si$_{target}$ = 1.0 at longer equilibration times and tentatively assigned to the thermal decomposition of more ordered water in C-N-A-S-H because none of the other phases identified by TGA, XRD presented here or by ^{27}Al and ^{29}Si MAS NMR (details are given below) can explain the weight loss associated at this temperature. Similar weight losses have also been observed for C-N-A-S-H in the presence of high concentrations of NaOH [17,28] or for samples equilibrated at 50 and 80 °C [11]. TGA indicates also minor carbonation (weight loss <0.6 %) in some samples during sample preparation, storage and/or analysis as visible in the region from 600 to 800 °C. The peak marked with † above 800 °C is assigned to the water loss due to the decomposition of C-A-S-H to wollastonite ($CaSiO_3$) [11,57].

Fig. 3 summarizes the effect of time on the portlandite content in the experiments. As expected, more portlandite is formed at higher Ca/Si ratios. After 6 h of hydration, portlandite is observed at all target Ca/Si ratios, indicating the initial precipitation of portlandite at all target Ca/Si ratios. Independent of Ca/Si ratios, most of the portlandite is consumed during the first day due to the reaction with SiO_2 from the silica fume dissolution. There is a limited further portlandite reduction from 1 day to 14 days, and after 14 days the portlandite content shows little variation. The presence of portlandite in the long-term C-S-H with a target Ca/Si ratio of 0.6 equilibrated for 3 years, suggests a decrease in the calcium content within the silicate structure. This observation potentially indicates heterogeneities within the C-A-S-H suspension or, more likely, the consumption of silicon by a zeolitic phase such as gismondine-P1-Na formation in the C-S-H.

3.1.2. C-A-S-H structure

The C-A-S-H structure evolves with time, as indicated by XRD (Fig. 2), FTIR, Raman and NMR data as shown further below. The positions of basal spacings, d_{001}, of C-A-S-H in the XRD spectra, as shown in Fig. 2(a) (c) and (e), vary only slightly with equilibration time. As an example, the evolution of the basal reflection of the C-A-S-H phase for Ca/Si$_{target}$ = 1.0 is shown in Fig. 4. The basal spacing increases and the full width at half maximum (FWHM) decreases with equilibration time up to 90 days indicating an increase of the crystallite size of the C-A-S-H in c direction [51,58]; little difference is observed after 90 days, except for sample equilibrated for 10 years, where a strong decrease in basal spacing was observed due to a partial transformation of C-A-S-H to 11-Å tobermorite (as discussed further down based on ^{29}Si and ^{27}Al MAS NMR data). The basal spacing of the 1–7 days equilibrated samples showed a larger interlayer distance over short-term hydration, which could be related to the presence of more Al in the dreierketten chain [11,18,42] and/or an increase in crystallite size along c-axis, which shifts the measured reflections to higher 2θ values [51,59].

Moreover, a broad reflection, d_{101}, at ≈17° 2θ (d-spacing ≈5 Å) is observed at Ca/Si$_{target}$ = 0.6 to 1.0, pointing to the occupation of the bridging sites in the silica chain [52]. The d_{101} signal is better visible after 3 days and longer, indicating rearrangement from the initial high Ca/Si C-S-H with mainly silica dimers to longer dreierketten chains over time.

The FTIR spectra of all C-A-S-H samples with Ca/Si$_{target}$ = 0.6, 1.0 and 1.4 (Fig. 5) show the presence of some unreacted silica fume after 6 h. The disappearance of the very broad bands between 1050 and 1300 cm^{-1} indicating the presence of Q^3 and Q^4 tetrahedral silicate sites, shows that silica fume has largely reacted off after 1 day. The band located at 670 cm^{-1}, associated with O–Si–O and/or O–Al–O bending and water librations increases from 6 h to 3 days for all C-A-S-H phases, with no major changes thereafter, indicating that the C-A-S-H phase formed mainly during the first 3 days of hydration.

Table 2
Quantification of Al(IV), Al(V), and Al(VI) fractions in C-A-S-H obtained by deconvolution of the ^{27}Al NMR spectra in C-A-S-H with Ca/Si$_{target}$ = 0.8 and 1.0 and Al-tobermorite [12] for comparison. *: samples synthesized with water/solid = 45.

Ca/Si$_{target}$	Equilibration time (day)	Al (IV)$_a$	Rel. amount	Al (IV)$_c$	Rel. amount	Al (IV)$_d$	Rel. amount	Al(V)	Rel. amount	Al(VI)-CSH	Rel. amount	Al(VI)-secondary phases	Rel. amount	Al/Si in C-A-S-H
		(ppm)	(%)	(ppm)	(%)	(ppm)	(%)	(ppm)	(%)	(ppm)	(%)	(ppm)	(%)	
1.0	0.25	74.0	40.7	65.0	0.7	58.9	5.9	35.4	5.8	8.6	11.3	10.0	35.7	0.064
	1	76.1	58.4	65.0	3.2	59.0	1.0	36.1	3.0	6.5	9.5	11.0	24.9	0.075
	3	75.5	65.1	64.6	6.1	58.1	0.2	35.0	4.1	6.5	10.0	11.4	14.5	0.085
	7	75.9	71.1	64.1	1.8	58.1	0.1	38.2	3.8	6.6	8.1	11.3	15.2	0.085
	14	75.8	63.6	65.3	8.8	56.8	0.1	38.1	4.1	5.6	5.8	11.5	17.6	0.082
	28	75.8	67.3	63.9	3.2	58.4	0.5	38.7	4.0	6.7	7.0	11.5	18.0	0.082
	90	75.6	62.8	64.9	4.2	58.1	2.4	38.0	4.4	6.0	9.0	11.3	17.2	0.083
	90*	75.5	68.5	65.5	11.3	58.3	0.0	38.0	3.6	6.7	7.4	11.0	9.2	0.091
	450*	74.8	45.0	66.4	8.6	58.6	1.1	37.5	2.8	6.7	13.6	11.2	28.9	0.071
	1350*	73.0	58.6	65.7	4.8	59.0	0.7	35.0	4.6	6.5	13.8	12.0	17.6	0.082
	3650*	73.0	23.9	66.3	28.4	60.1	28.7	35.0	3.4	6.5	6.3	12.0	9.3	0.091
0.8	0.25	77.9	17.0	68.5	26.1	57.8	10.0	39.1	4.6	6.5	5.5	9.8	36.9	0.058
	1	77.1	34.6	70.7	37.6	61.4	12.2	39.1	1.4	6.5	1.4	11.5	12.8	0.082
	3	77.7	31.9	70.7	46.2	60.6	7.6	39.1	2.7	6.5	0.6	11.5	10.9	0.083
	7	76.1	33.0	68.7	38.0	59.4	10.5	39.1	3.4	6.5	1.9	11.5	13.1	0.081
	14	78.5	24.8	71.3	45.9	61.6	10.3	39.1	2.9	6.5	2.5	11.5	13.6	0.081
	28	76.8	30.1	69.2	36.0	59.7	9.0	39.1	2.5	6.5	3.4	11.4	19.0	0.076
	90	76.8	33.1	69.7	38.3	60.5	10.3	39.1	3.3	6.5	1.6	11.5	13.4	0.081
	1350*	76.7	34.5	68.9	40.7	59.3	9.8	39.1	3.0	6.5	2.1	11.5	9.9	0.092
	Al-Tob [60]	*73.0*	*9.6*	*65.8*	*66.6*	*57.6*	*16.2*			*6.5*	*7.6*			*0.111*

The formation of C-A-S-H is evident from the main bands with a maxima between 950 and 960 cm^{-1} corresponding to different Si—O vibrations [26,58]. The contributions at ≈ 945 and 963 cm^{-1} are associated with dimeric silicate (Q^1) and oligomeric (Q^2) Si—O stretching vibrations respectively; the bands overlap strongly, such that in most cases only a combined signal is visible. In addition the shoulder related to bridging Q^2_b at ≈900 to 930 cm^{-1} may also contribute to the observed main peak. Thus, for C-A-S-H with Ca/Si$_{target}$ = 0.6 the most intensive band shifts from 957 cm^{-1} at 6 h (where a large fraction of dimeric silica is present) to ≈ 963 cm^{-1} at 1 day and longer as shown in Fig. 5(a). For C-A-S-H with Ca/Si$_{target}$ = 1.0, the signal moves from 957 cm^{-1} at 6 h to 946 cm^{-1} after 3 years of hydration (Fig. 5(b)). For C-A-S-H with Ca/Si$_{target}$ 1.4 the signal moves from 952 cm^{-1} at 6 h to 937 cm^{-1} at 1 day and then back to 952 cm^{-1} after 3 years of hydration (Fig. 5(c)). The dissolution of the silica fume after 1 day and longer leads to a higher polymerization degree as visible by the shift to higher wavenumbers [58,60]. In contrast, the replacement of silica by alumina in C-S-H also lowers the wavenumber of Si—O stretching [61]. For C-A-S-H with Ca/Si$_{target}$ = 0.6 in Fig. 5(a), the shoulders located at ≈ 915 cm^{-1} and 1050 cm^{-1}, assigned to the Si—O stretching of Q^2 silicate (and or aluminate) tetrahedra, start to be observed after an equilibration time of 1 day and increase until 90 days, confirming a higher polymerization degree with longer equilibration time and shows good agreements with the position shift of the peak at ≈ 960 cm^{-1}. For C-A-S-H with Ca/Si$_{target}$ = 1.0 and 1.4 in Fig. 5(b) and (c), the observable shoulders are less visible because of the low amount of Q^2. In Fig. 5(b), a small signal at ≈ 1160 cm^{-1} corresponding to Si—O and/or Al—O stretching of Q^3 silicate (and/or aluminate) tetrahedra is observed in C-A-S-H equilibrated for 10 years, in agreement with previous studies about tobermorite [12,60,62,63].

The intensity of the Q^1 signals located at 815 cm^{-1} and at 490 cm^{-1} increases rapidly between 6 h to 1 day for C-A-S-H with Ca/Si$_{target}$ = 1.0 and 1.4, and more slowly up to 3 days due to the formation of more C-A-S-H. At longer reaction times, however, this Q^1 signal decreases in intensity while the Q^2 signal increases, indicating a slow polymerization of the silicate chains (i.e. chain-growth) over time.

In the Raman spectra (Fig. 6) of the C-A-S-H with Ca/Si$_{target}$ = 1, the narrow peak at 250 cm^{-1} from Ca^{2+} motion [63] can be only observed after 6 h, while the lattice vibration (LV) of Ca—O in portlandite at ≈357 cm^{-1} [64–66] deceases strongly and disappears after 3 days, which is related to the fast consumption of $Ca(OH)_2$ and the formation of C-S-H. The lattice vibration of Ca—O in C-A-S-H at ≈ 335 cm^{-1} [66] is observed at all equilibration times.

The equilibration time does not affect the positions of peaks due to internal deformation of the Si–tetrahedra [63] or to the O–Si–O bending [66] at 445 cm^{-1}, nor to the most pronounced peak at 672 cm^{-1} related to Si–O–Si symmetrical bending (SB). The main SB bending signal, however, narrows significantly between 6 h and 1 day, indicating a much ordered silicate chain [8,67].

The Si—O symmetrical stretching (SS) band at ≈ 840–940 cm^{-1}, assigned to SS Q^1 [63,66,68], decreases in intensity with equilibration time indicating the continuous growth of the silicate chains. In contrast, the peak area of the signal at ≈ 950–1040 cm^{-1}, assigned to SS Q^2 [63,66,68], increases with hydration time, confirming the results from the FTIR data presented above. A small peak at 602 cm^{-1} tentatively assigned to Al–O–Si symmetrical bending [41], decreases with time.

Peaks at 1074 and 1086 cm^{-1} are attributed to the C—O SS vibrations [8,67,69–71]. A sharp peak at 480 cm^{-1} is present at equilibration times of 3, 7, 28, 90 and 3650 days and further signals 1114 cm^{-1}, and 818 cm^{-1} are tentatively assigned to carbonated secondary phases formed during sample handling.

The long-term C-A-S-H phases and the Al-tobermorite showed very similar spectra which confirms that C-A-S-H phases are in the long term analogues to Al-tobermorite. The presence of more Si—O SS Q^1 and more pronounced lattice vibration CaO in C-A-S-H compared with Al-tobermorite are due to the different Ca/Si.

The ^{29}Si MAS NMR spectra of C-A-S-H with Ca/Si = 1.0 and 0.8 after different equilibration time are shown in Fig. 7(a) and (c). Resonances with chemical shifts (δ_{iso}) at approx. −76 ppm (Q^0), −79 ppm (Q^1), −81 ppm ($Q^2_p(1Al)$), −84 ppm (Q^2_b), −85 ppm and −88 ppm (Q^2_{pa}, and Q^2_{pb}), −91 ppm ($Q^3_p(1Al)$), and −97 ppm (Q^3) are identified [40].

In very young C-A-S-H (we subsequently discuss equilibration times of 6 h to 7 days), Q^3 signals related to the presence of unreacted silica are observed after 6 h, which were already absent after the 1st day (see Fig. 7(a) and Table 1). Initially, some Q^0 peaks were observed, decreasing from around 10 % to <5 % on day 7, while the fraction of Q^1 signal increases, due to the processing reaction of silica fume to C-A-S-H. For longer equilibration times, the Q^1 peaks decrease between 7 days and 10 years for C-A-S-H with Ca/Si = 1.0 and between 1 day and 3

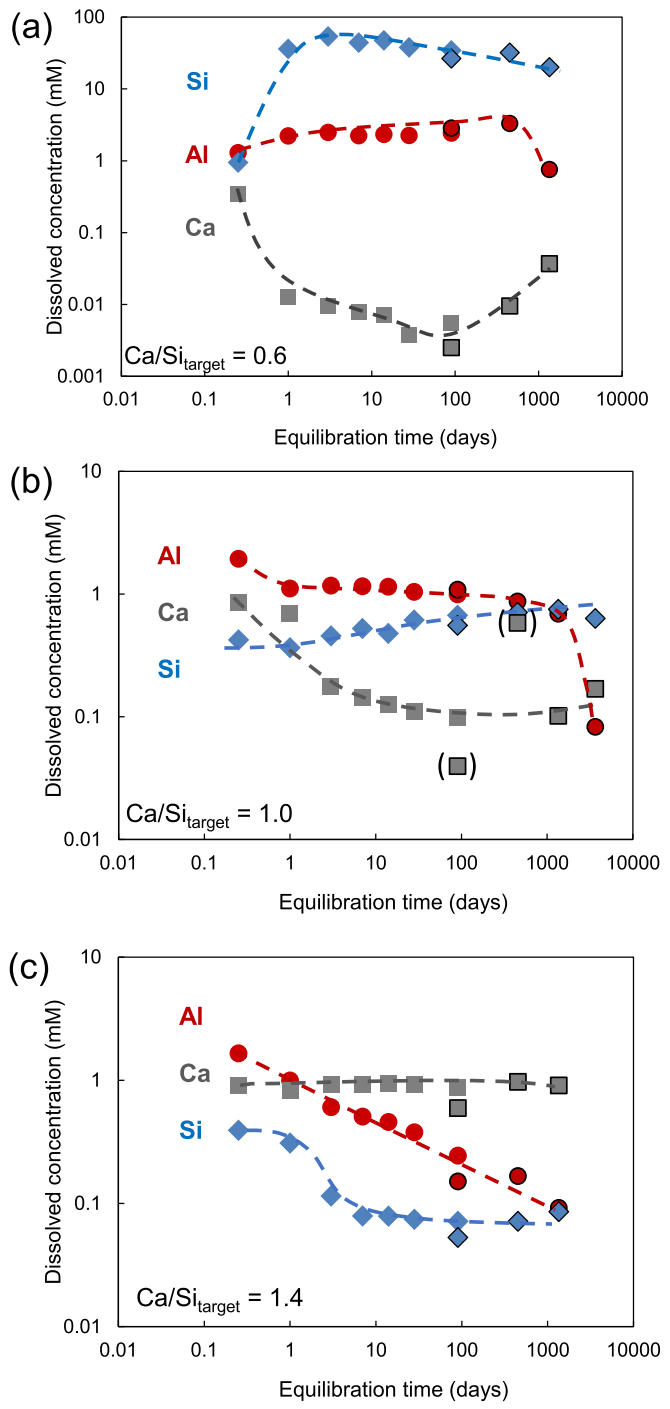

Fig. 8. Evolution of dissolved Al, Si and Ca concentrations in solution for Ca/Si$_{target}$ ratios of (a) 0.6, (b) 1.0 and (c) 1.4 synthesized in 0.5 M NaOH with initial Al/Si 0.1 equilibrated for different time. Two series were studied: Series A: filled symbols: in w/s = 40; Series B: symbols with black border: w/s = 45. The error of the dissolved concentrations are 10 % and the error bars are smaller than the symbols. Symbols in brackets: outlier Ca concentration after 3 months and 1 year (curves added for guidance).

years for C-A-S-H with Ca/Si = 0.8, indicating the growth of longer dreierketten chains. After 10 years of hydration, some Q^3 signals are present indicating cross-linking in the C-A-S-H structure as discussed in C-A-S-H synthesized at 80 °C [11]. The presence of Q^3 resonances characteristic for cross-linked silicate chains in tobermorite is also detectable for the 11-Å tobermorite reference compound (with Al/Si = 0.11 [12]). Compared to C-A-S-H, the ^{29}Si chemical shift of Al-tobermorite is shifted to more negative chemical shift. The proportions of the different silicate sites obtained from the line shape analysis (see Table 1) allowed the calculation of Al/Si and the mean chain length (MCL) (see Fig. A9). Although the error associated with Al/Si appears to be relatively high, the Al/Si of C-A-S-H with both target Ca/Si exhibit a slight increase over time, indicating a slow rearrangement in C-A-S-H structure.

Fig. 7(b) and (d) shows the ^{27}Al MAS NMR spectra of the C-A-S-H with Ca/Si$_{target}$ = 1.0 and 0.8 from 6 h up to 10 years. The ^{27}Al MAS NMR spectra show resonances from Al in tetrahedral (50–80 ppm) and octahedral (0–20 ppm) coordination with a low quantity of aluminium in pentahedral coordination in between. The signal between 50 and 80 ppm is assigned to the Al(IV) in the bridging sites of silicate chains in C-A-S-H structure following the assignments given in Yang et al. [39]. In the octahedral region, resonances at ≈11.5, 10, and 6.5 ppm are observed, which correspond to secondary phases (katoite, AFm phases) as well as to Al(VI) sites associated with the C-A-S-H phase [39], respectively. The deconvolution of the signals allows a rough quantification of the chemical species bound at different sites as summarized in Table 2 (^{27}Al MAS NMR spectra and associated simulated shapes of individual Al sites are detailed in Fig. A3). Initially, approximately 1/3 of the Al was present in secondary phases, with this fraction decreasing over equilibration time. The amount of Al(IV) incorporated in the bridging sites of C-A-S-H increased clearly up to 3 days as more C-A-S-H precipitated, in agreement with the XRD (Fig. 2), FTIR (Fig. 5) and Raman (Fig. 6) results. The deconvolutions allow to distinguish 3 types of Al(IV) at the bridging sites following the procedure outlined in [39]. The resonance Al(IV)$_a$ with its ^{27}Al NMR chemical shift δ_{iso} at ≈75 ppm (peak maximum observed at ≈70 ppm, see Fig. A3), Al(IV)$_c$ at ≈65 ppm (maximum observed at ≈61 ppm) and the Al(IV)$_d$ at ≈58 ppm (maximum observed at ≈55 ppm) show good agreements with Yang et al. [39]. Note that the Al(IV)$_b$ signal as observed at Al MQMAS NMR recorded at 22.3 T from Yang et al. [39] is not visible here. The relative fractions of the Al(IV)$_a$, Al(IV)$_c$, and Al(IV)$_d$ signals obtained by line shape simulations are shown as a function of equilibration time in Table 2 and Fig. A10. In C-A-S-H with Ca/Si$_{target}$ = 1.0, Al(IV)$_a$ was observed predominate from 6 h until 3 years, while after 10 years of equilibration, Al(IV)$_a$ content decreases to 30 %. For comparison, in Al-tobermorite prepared with a similar total Al/(Si + Al) of 0.1, much less Al(IV)$_a$, approximately 10 %, has been observed [12]. In contrast, the Al(IV)$_c$ content increases over time from 1 % in 6 h, to 5 % in 28 days, 16 % in 1 year and 35 % in 10 years. In the Al-tobermorite, more Al(IV)$_c$, 72 %, has been observed. Less than 4 % of Al(IV)$_d$ was observed from 1 day to 3 years, while in the C-A-S-H equilibrated for 10 years, Al(IV)$_d$ occupies 35 % of the Al(IV) positions. In C-A-S-H with Ca/Si$_{target}$ = 0.8, the relative amounts of Al(IV)$_a$, Al(IV)$_c$ and Al(IV)$_d$ remain stable from 1 day to 3 years, at around 40 %, 47 % and 13 %. Al(IV)$_c$ was suggested to correspond to Al(IV) incorporated in the bridging sites charge-balanced by Ca^{2+} or by a combination of Ca^{2+} and Na^+ [39]. In fact, also the "normal" tobermorite with a Ca/(Si + Al) of 0.83 and Al/(Si + Al) of 0.1, used as a reference, shows a more narrow signal of Al(IV) δ_{iso} chemical shift at 66 ppm, which has been assigned to cross-linked Al with Ca^{2+} in its vicinity [12]. Moreover, a maximum Al(IV)$_c$ fraction was also observed at Ca/Si = 0.8 in C-A-S-H with Al/Si = 0.15 and Ca/Si from 0.6 to 1.6 [39], in agreement with the present study. Similar to the FTIR (Fig. 5), Raman (Fig. 6) and ^{29}Si NMR (Fig. 7(a,c)), the ^{27}Al NMR data confirm a slow restructuring in C-A-S-H over years.

3.2. *Effect of time on aqueous phase*

Fig. 8 shows the effect of equilibration time on the dissolved Al, Si and Ca concentrations in solution. The detailed aqueous phase results are shown in Table A2. At Ca/Si$_{target}$ = 0.6, the Al concentration shows a rapid increase from 1.3 mM after 6 h to 2.2 mM after 1 day. It continues to rise slightly, reaching 3.3 mM after 1 year, but eventually drops to 0.76 mM after 3 years. The Si concentration increases from 1 mM after 6

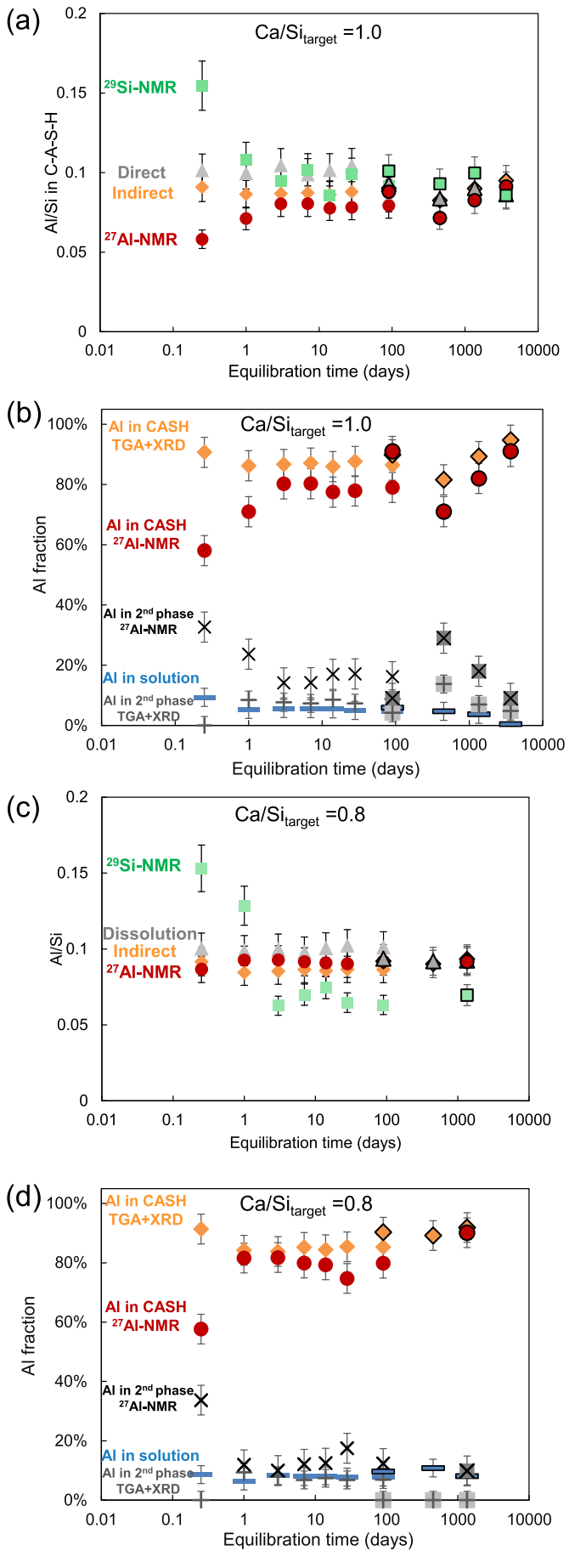

(caption on next column)

Fig. 9. Al/Si ratio in C-A-S-H and distribution of Al in different phases for target Al/Si = 0.1 after different equilibration times in the presence of 0.5 M NaOH determined by different methods: (a) (b) Ca/Si$_{target}$ = 1.0 and (c) (d) Ca/Si$_{target}$ = 0.8. Diamonds: indirect method = mass balance using the filtered solution and XRD and TGA, triangles: dissolution method = complete dissolution of the solid in acid after washing and drying, squares: ^{29}Si NMR quantification results, circles: indirect method combining ^{27}Al NMR quantification results. Two series were studied: Series A: filled symbols: in w/s = 40; Series B: symbols with black border: w/s = 45.

h to 36 mM after 1 day and further to 54 mM after 3 days. It gradually decreases afterwards and over a period of 3 years to 20 mM. As expected, the initial Ca concentration is relatively high at 0.4 mM after 6 h in the presence of portlandite and quickly diminishes to 0.01 mM after 1 day. The Ca concentration continues to decrease slightly over a span of 3 months, but shows a gradual increase to 0.04 mM after 3 years. The early decrease in Ca concentration underlines the fast CaO reaction, while the increase of Si concentration up to 3 days mirrors the slower dissolution progress of silica fume. The minor changes observed up to 1 year are likely related to the slow restructuring of C-A-S-H, as already suspected from the ^{27}Al NMR, ^{29}Si MAS NMR (Fig. 7), FTIR (Fig. 5), Raman (Fig. 6), and XRD (Fig. 2) results. The long-term decrease in Al and Si concentrations and the simultaneous increase in Ca concentrations, may be attributed to the slow restructuring of C-A-S-H and the formation of an additional solid phase, for example the formation of gismondine-P1-Na ($Na_6Al_6Si_{10}O_{32}{\cdot}12H_2O$) observed in the 3 year sample (Fig. 2(a)).

In contrast at Ca/Si$_{target}$ = 1.0, where less silica fume has been added, the Si concentration tends to be lower while the Ca concentration is higher. A relatively high Ca concentration, approximately 1 mM, is determined after 6 h and 1 day, which can be attributed to the rapid hydration of CaO and the initial formation of portlandite, which predominantly influences the Ca concentration during the first day of hydration. As equilibration time extends, dissolved Ca is consumed through C-A-S-H formation, and the gradual changes in Ca and Si concentrations point again towards to slow restructuring of C-S-H over months to years. Interestingly, the Al concentration decreases over time, indicating a gradual and continuous uptake of Al in the solid phase over a span of 10 years.

At Ca/Si$_{target}$ = 1.4, the Ca concentrations remain constant from 6 h to 3 years, primarily influenced by the solubility of portlandite. The Si concentration decreases from approximately 0.4 mM at 6 h to 0.08 mM at 7 days, demonstrating the formation of C-A-S-H, with little changes at later ages (≈0.07 mM). The Al concentration exhibits a continuous decrease, indicating a gradual uptake process up to 3 years. The different concentrations in the aqueous phase as a function of time at different Ca/Si$_{target}$ ratio shows that Ca/Si ratio plays an important role in the kinetics of C-A-S-H formation.

3.3. Al uptake in C-S-H

Fig. 9 compares the effect of different methods on the measured Al/Si in C-A-S-H with Ca/Si$_{target}$ = 1.0 and 0.8 using the indirect method: mass balance and different direct methods: dissolution of solid in acid, measurement from ^{29}Si NMR and ^{27}Al NMR. In terms of alkali uptake in C-S-H, the direct method of dissolution of solid in acid [13] shows clear advantages over the indirect method based on mass balance, offering smaller relative error [13]. When determining Al/Si in C-A-S-H, both direct method with dissolution of solid in acid and indirect methods give comparable results, although the dissolution of solid in acid method is associated with a larger error. The quantification using ^{29}Si NMR and ^{27}Al NMR also provides similar results in most cases. The data obtained from ^{29}Si NMR measurements are subject to significant uncertainties due to the deconvolution of broad and strongly overlapping signals, and only the fraction of Al(IV) can be quantified based on ^{29}Si NMR [39]. On the other hand, the quantification of Al-containing secondary phases by

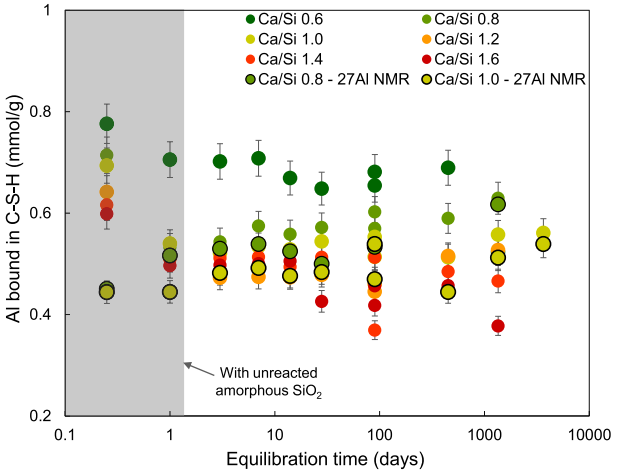

Fig. 10. Effect of equilibration time and Ca/Si on the Al uptake in C-A-S-H expressed Al bound per gram of C-S-A-H based on mass balance combined with XRD/TGA or ^{27}Al NMR. The shaded area indicates the presence of less C-A-S-H as well as the potential underestimation of Al in secondary phases at early stages.

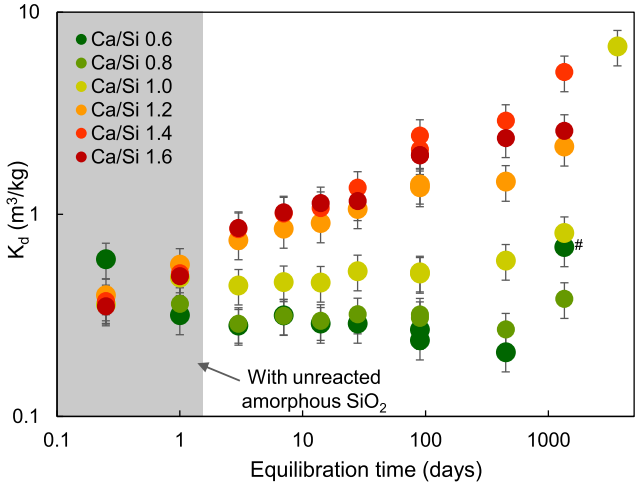

Fig. 11. Effect of equilibration time on the K_d values of Al on C-S-H synthesized in NaOH 0.5 M. #: gismondine-P1Na formation observed after 3 years at Ca/Si_{target} = 0.6.

^{27}Al NMR provides the most accurate results. Notably, for C-A-S-H equilibrated for >3 days, the results obtained from the ^{27}Al NMR and from complete dissolution in acid show remarkable similarity (Fig. 9(a) and (c)).

The Al/Si in C-A-S-H increases from 6 h to 3 days and 1 day for C-A-S-H with Ca/Si_{target} = 1.0 and 0.8 respectively (Fig. 9 (a) and (c)). It is observed that potential secondary phases containing Al precipitate rapidly in the early stages and with the formation of C-A-S-H, they were dissolved. The Al fraction in C-A-S-H shows slight fluctuations from 3 days to 1 year and gradually tends to increase over a span of 10 years, which could account for the very low concentration of Al in the aqueous phase.

Fig. 9 (b) and (d) show the distribution of Al in different phases of C-A-S-H with target Ca/Si at 1.0 and 0.8. The determination of the Al fractions in different phases is based on the aqueous concentrations, and the amount of secondary phases quantified by TGA and XRD, and by ^{27}Al NMR. The major part of Al is bound in C-A-S-H and <20 % of Al is presents in solution and in secondary phases. The results for C-A-S-H with Ca/Si_{target} = 0.6 and 1.2 to 1.6 are shown in the Fig. A7. In C-A-S-H

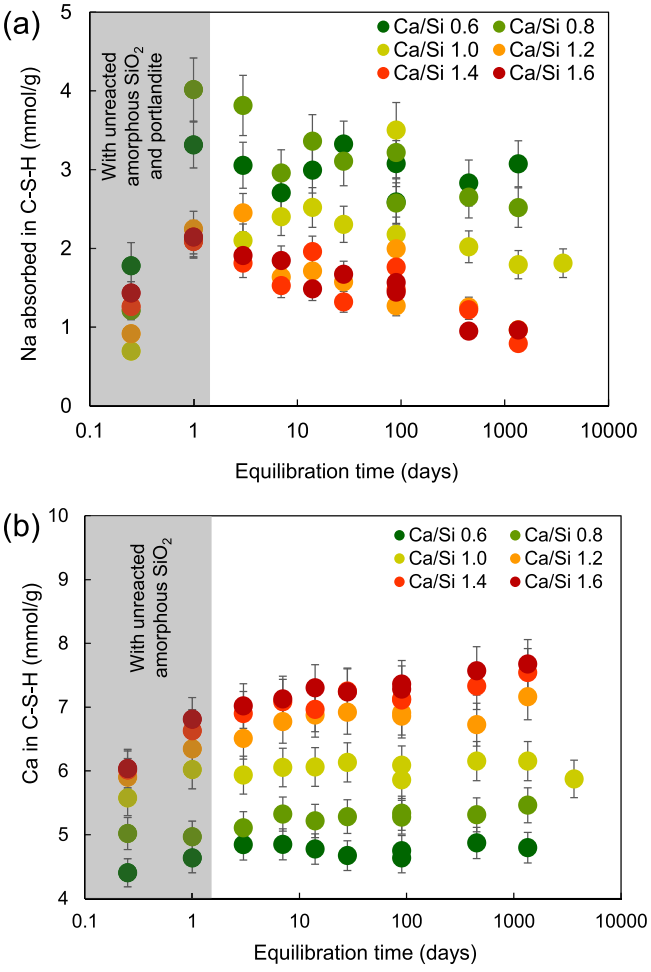

Fig. 12. Effect of equilibration time on the (a) Na absorption and (b) Ca in C-A-S-H. The shaded area indicates the presence of less C-A-S-H at early times. The unreacted amorphous silica was not quantified at early age so the first points at 6 h and 1 day refer to Na/Si in (C-A-S-H incl. silica fume), while the later points refer to C-A-S-H only.

with Ca/Si_{target} = 0.6, the Al fraction in solution increases from 6 h to 1 year, but subsequently drops to 64 % after 3 years of hydration. This is accompanied by a decrease of the Al content in C-A-S-H due to the formation of gismondine-P1-Na. For C-A-S-H with Ca/Si_{target} = 0.8 and 1.0, the amount of Al in solution decreases during the initial days and the quantity of Al in secondary phases observed by ^{27}Al NMR also decreases. It should be noted that that XRD and TGA analysis tend to underestimate the amount of secondary phases, as previously reported in [72], particularly at early reaction times due to the low crystallinity of the secondary phases, as evident from the comparison with the results from ^{27}Al NMR data in Fig. 9(b) and (d). At later ages the difference between NMR and XRD/TGA becomes smaller as the reaction progresses.

The effect of time on Al uptake in C-A-S-H at Ca/Si ratios from 0.6 to 1.6 is summarized in Fig. 10. In general, the fraction of Al bound in C-A-S-H decreases with increasing equilibration time from 6 h to 7 days, although the results at initial equilibration stage might be influenced by the underestimation of secondary phases by XRD and TGA (indicated by the shaded area in Fig. 10). At longer equilibration times, the trends are less clear as the data show a considerable scatter. C-A-S-H with low Ca/Si_{target} takes up more Al per gram of C-S-H than C-A-S-H with higher Ca/Si_{target}. Specifically, C-A-S-H with Ca/Si_{target} = 0.6 is able to incorporate up to 0.7 mmol Al per gram of C-A-S-H, while the Al uptake is about 0.5 mmol Al per gram of C-A-S-H for C-A-S-H with Ca/Si_{target} = 1.0 to 1.6.

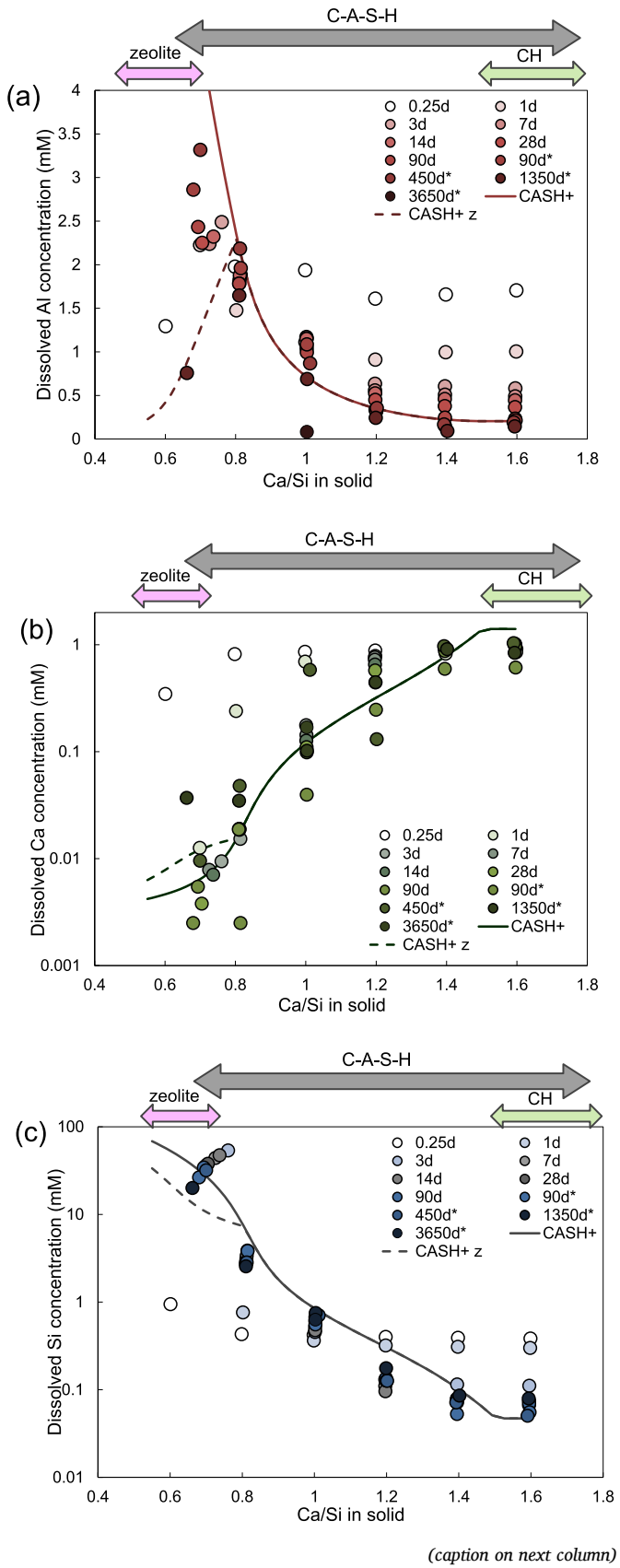

(caption on next column)

Fig. 13. (a) Al, (b) Ca and (c) Si concentrations in the solutions of the C-A-S-H samples prepared in 0.5 M NaOH at different equilibration time as a function of Ca/Si ratios in solids. The estimated absolute errors are ≤ ±0.05 units in the Ca/Si ratios. The estimated relative uncertainty of the IC measurements is ±10 %. Symbols with colour filled from light to dark: synthetic C-A-S-H data with equilibration times from 0.25 to 1350 days. Solid lines: calculated concentrations using the thermodynamic CASH+ model, suppressing the formation of zeolitic phases, which form only slowly. Dashed lines: under consideration of the possible formation of gismondine-P1-Na ($Na_6Al_6Si_{10}O_{32}{\cdot}12H_2O$). *: samples synthesized with water/solid = 45. (For interpretation of the references to colour in this figure legend, the reader is referred to the web version of this article.)

When plotted as the molar ratio of Al/Si in C-A-S-H (Fig. A5), the molar Al/Si distribute between 0.08 and 0.1, with no observable systematic trend is observed between Ca/Si = 0.6 to 1.6, which is due to the lower C-A-S-H weight per mole of Si at C-A-S-H with low Ca/Si.

The Al uptake in C-S-H can also be described by distribution coefficients, K_d values (Fig. 11), which represent the relative affinity of Al to be incorporated by C-S-H compared to the Al concentration I aqueous phase. The K_d values show different trends compared to the Al uptake per unit mass of C-S-H (Fig. 10), mainly due to the definition of K_d as the ratio of the quantity of adsorbed aluminium per unit mass of C-S-H (mol/kg) to the quantity of aluminium remaining in solution (mol/m^3). The contrasting behavior of Al concentration in aqueous phase completely reverses the trends observed.

The long-term K_d values (3 months and 1 year) of C-A-S-H with Ca/Si_{target} = 0.8 are approximately 0.3 m^3/kg, and for C-A-S-H with Ca/Si_{target} = 1.0, they are around 0.6 m^3/kg, consistent with findings from previous studies [41,72]. After longer equilibration times, the K_d values of C-A-S-H with $Ca/Si_{target} \geq 1.0$ increase, while the K_d values of C-A-S-H with $Ca/Si_{target} \leq 0.8$ remain rather constant. An increase of K_d values of C-A-S-H with Ca/Si_{target} = 0.6 and 0.8 from 1 year to 3 years was observed, which can be attributed to precipitation of gismondine-Na-P1 and precursor of zeolitic phases, respectively. The K_d values of C-A-S-H with Ca/Si_{target} at 1.4 and 1.6 are comparable and increase from ≈ 0.25 after 6 h to ≈ 2.6 m^3/kg after 1 year. The increase of K_d values for the C-A-S-H with $Ca/Si_{target} \geq 1.0$ indicates a stabilization of the C-A-S-H structure by the incorporation of Al at a high availability of Ca^{2+} in the interlayer in agreement with molecular modelling results [73]. The K_d value of the 10-year-old C-A-S-H sample with Ca/Si_{target} at 1.0 is relatively high at 6.8 m^3/kg because of the extremely low Al concentration (0.08 mM) in solution.

3.4. Na uptake in C-S-H

In addition to Al, the Na and Ca contents in C-A-S-H also evolve over the years, as illustrated in Fig. 12. Across all Ca/Si_{target} ratios, relatively low Na and Ca uptake was observed after 6 h, which may be related to the presence of less C-A-S-H at this early stage and the initial precipitation of C-A-S-H with high Ca/Si, which can bind fewer alkali ions [41]. The increased uptake of Na and Ca in C-A-S-H at 1 day is attributed to the formation of more C-A-S-H, resulting in a lower Ca/Si in C-A-S-H and thus to a higher alkali uptake. For C-A-S-H at all Ca/Si_{target}, the highest Na binding is observed after 1 day, followed by a gradual decrease. Although Na concentrations in the aqueous phase do not change significantly after 7 days hydration (measured data see Table A2), the continuous decline of Na sorption and increase of Ca sorption indicate the rearrangement of C-A-S-H phases over time. Furthermore, it highlights the preference of Ca over Na in C-A-S-H.

The initial high Na binding observed in the first few days could be related to the rapid initial formation of C-A-S-H with a relatively low $Ca/Si_{C\text{-}S\text{-}H}$, and the high Na concentrations in solution. This co-precipitated Na is partially released again as the C-A-S-H structure rearranges towards its thermodynamic equilibrium composition and with increasing $Ca/Si_{C\text{-}S\text{-}H}$.

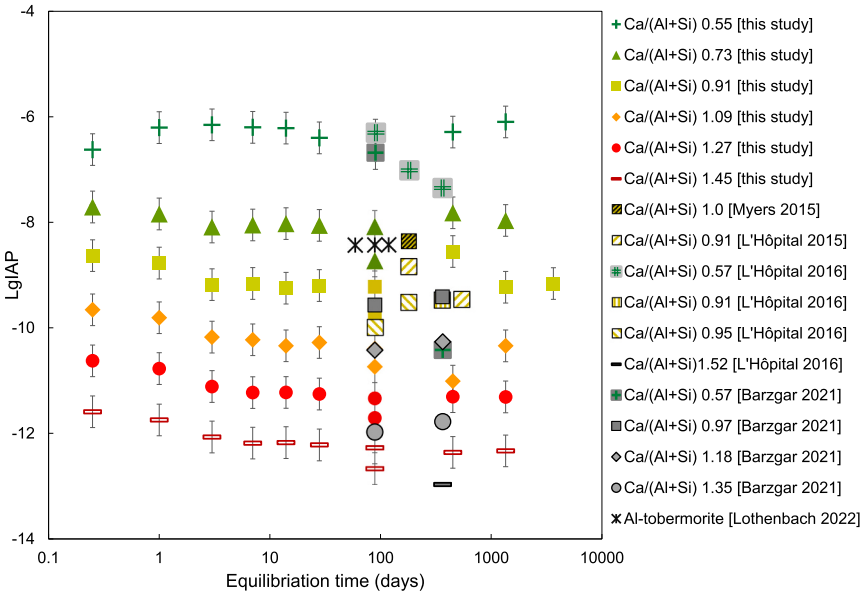

Fig. 14. Calculated $\log_{10}$IAP values for hypothetical C-(A-)S-H and Al-tobermorite at different equilibration times, normalized to $SiO_2 + 0.5Al_2O_3 = 1$. The approximate uncertainty in the $\log_{10}$ (IAP) values are ± 0.3. Colored symbols: C-A-S-H from this study; dark green crosses: Ca/Si_{target} 0.6, olive green triangles: Ca/Si_{target} 0.8, mimosa squaresL: Ca/Si_{target} 1.0, orange diamonds: Ca/Si_{target} 1.2, red circles: Ca/Si_{target} 1.4, dark red rectangles: Ca/Si_{target} 1.6. Grey or patterned symbols: C-A-S-H from Myers et al. [11], L'Hôpital et al. [24,25], Barzgar et al [28] and black stars: Al-tobermorite with Ca/(Al + Si) = 0.83 from Lothenbach et al. [12]. Data from this study and from [11,24,25,28] are obtained from oversaturation experiments, while [12] is obtained from undersaturation experiments. (For interpretation of the references to colour in this figure legend, the reader is referred to the web version of this article.)

The data after 3 days and longer clearly show that more Na is bound in C-A-S-H at low Ca/Si_{target}, as reported in several studies [13,19,58,74]. The sorption of Na in C-A-S-H with $Ca/Si_{target} = 0.6$ and 0.8 is highest with a maximum of ≈ 3 mmol Na per gram of C-S-H. At these low Ca/Si_{target}, Ca concentration in solution is very low (< 0.05 mM Ca), leaving minimal Ca^{2+} to compensate the negative charge of C-S-H [75–77], leading to a strong uptake of Na^+. In contrast, at higher Ca/Si_{target}, competition with Ca^{2+} reduces the Na^+ uptake [5,13]. C-A-S-H phases with $Ca/Si_{target} \geq 1.2$ show a similar capacity to absorb Na^+, which is in agreement with previous observations reported in [13,58]. After 10 years, the amount of Na^+ in C-A-S-H seems to be equal as after 3 years indicating that the exchange of Na by Ca in the C-A-S-H structure.

3.5. Comparison with thermodynamic modelling

Fig. 13 displays the measured dissolved Al, Ca and Si from 6 h to 10 years as a function of the Ca/Si in the solid together with modelled solutions at equilibrium without (solid lines) and with considering the precipitation of zeolites (gismondine-P1-Na, dotted lines). It can been seen that the Ca/Si ratio strongly affects the composition of the solutions. C-A-S-H with higher Ca/Si_{solids} leads to lower Al concentrations and thus a higher Al uptake in C-A-S-H, in agreement with the experimental observations. The simulated concentrations at equilibrium state are in good agreement with the experimental results of samples equilibrated for 90, 450 and 1350 days. The modelled Al concentrations at very low Ca/Si_{solids} (<0.7) are reduced due to the precipitation of gismondine-P1-Na, which also explains the considerable scatter observed in Al concentration. The gismondine-P1-Na formation also leads to shifts in the Ca and Si concentrations at low Ca/Si_{solids}. The measured Si and Ca concentrations for the samples with $Ca/Si_{solids} \leq 0.8$ show some scatter (secondary phases, might be zeolite precursors), while for samples with $Ca/Si_{solids} \geq 1.2$ little variation is observed. At $Ca/Si_{solids} \geq 1.0$ the Al concentration decreases up to 10 years of hydration, indicating the long-term uptake of Al in C-A-S-H.

The experimentally determined ion concentrations in aqueous solution were also used to calculate the ion activity products (IAP) for hypothetical C-A-S-H end-members with chemical compositions corresponding to the bulk chemistry of the systems studied (Ca/Si = 0.6–1.6) and normalized to (Al + Si) = 1, according to the reaction represented by:

$$(CaO)_a(SiO_2)_b(Al_2O_3)_c(H_2O)_f \rightleftharpoons^{IAP} aCa^{2+}_{(aq)} + bHSiO_3^-{}_{(aq)} + 2cAlO_2^-{}_{(aq)} + (2a-b-2c)OH^-_{(aq)} + (c+f-a)H_2O_{(l)} \quad (5)$$

where a, b, c and f are the respective stoichiometric coefficients for CaO, SiO_2, Al_2O_3 and H_2O in the C-A-S-H end members [11]. Thus the IAP of C-A-S-H normalized to one Si + Al (b + 2c =1) is defined as:

$$IAP = \left\{Ca^{2+}_{(aq)}\right\}^a \cdot \left\{HSiO_3^-{}_{(aq)}\right\}^b \cdot \left\{AlO_2^-{}_{(aq)}\right\}^{2c} \cdot \left\{OH^-_{(aq)}\right\}^{(2a-b-2c)} \cdot \left\{H_2O_{(l)}\right\}^{(c+f-a)} \quad (6)$$

In Fig. 14, the IAP calculated for C-A-S-H after different equilibration times are compared to the IAP of C-(A-)S-H and Al-tobermorite reported in literature [11,12,28]. A moderate decrease in the IAP of C-A-S-H was observed between 6 h and 7 days: by ≈ 0.3 log units for $Ca/Si_{target} = 0.8$ and by ≈ 0.6 log units for $Ca/Si_{target} = 1.0$–1.6, while at very low Ca/Si the IAP increased. Some scatter, but no significant differences were observed between 7 days to 3 years, underlining that the aqueous phase reached quasi-equilibrium already after the first 7 days. The IAP of C-A-S-H after 3 months and longer are comparable to the solubility products reported by L'Hôpital et al. [13,24], Barzgar et al. [28] and Myers et al. [11] as shown in Fig. 14. Those IAP with $Ca/Si_{target} = 0.8$ are only slightly higher than the solubility product reported for laboratory-synthesized Al-tobermorite [12] with Ca/(Al + Si) = 0.83, as expected for these structurally and compositionally similar phases.

4. Conclusion

This paper studies the effect of equilibration time on the composition, structure and solubility of synthesized C-A-S-H with a total Al/Si = 0.1. C-A-S-H was the main solid product in all experiments, with a small quantity of secondary phases (mostly katoite and occasionally monocarboaluminate or hemicarboaluminate) observed. At $Ca/Si_{target} = 0.6$,

C-A-S-H was initially formed but partly destabilized to a zeolitic phase (gismondine-P1-Na) between 1 and 3 years. This zeolitic phase in synthetic C-A-S-H was experimentally observed for the first time and could be modelled with recent, accurate thermodynamic data for gismondine-P1-Na.

C-A-S-H was precipitated from CaO, $CaO{\cdot}Al_2O_3$ and silica fume (SiO_2) in 0.5 M NaOH solution. Thus at very early stage, mainly Ca and Al were available, while Si was released slower due to the slow reactivity of silica fume compared to CaO (or $Ca(OH)_2$) and $CaO{\cdot}Al_2O_3$. In all cases, initially portlandite and C-A-S-H with high $Ca/Si_{C\text{-}S\text{-}H}$ formed, which converted within a day to low Ca/Si C-A-S-H depending on the target Ca/Si in the individual experiment. The portlandite initially formed was completely or partially consumed (depending on the target Ca/Si) within the first days and the detected amounts remained stable from day 7 onward, as shown by XRD and TGA results. The dissolved concentrations of Al, Ca and Si changed rapidly between 6 h and 1 day due to the formation of more C-A-S-H and structural rearrangements, while the variations became small after 14 days. The Ca/Si ratio of C-A-S-H played an important role for the changes in aqueous concentrations: an increase in Al concentrations with time was observed for C-A-S-H with $Ca/Si_{target} = 0.6$, whereas a decrease was observed for C-A-S-H with $Ca/Si_{target} \geq 1.0$.

XRD showed that the basal spacings, d_{001}, of C-A-S-H did not change significantly with equilibration time, indicating a small influence of the equilibration time on the interlayer spacing of C-A-S-H. However, results from XRD, ^{29}Si NMR, ^{27}Al NMR, Raman and FTIR spectroscopy indicate that more bridging sites are occupied over time, resulting in longer triple chains. ^{27}Al NMR showed the decrease in the amount of secondary phases and an increasing fraction of Al(IV) in C-A-S-H charge-balanced by Ca^{2+} for C-A-S-H with $Ca/Si_{target} = 1.0$. This is in agreement with the observed decrease of Na^+ and increase of Ca^{2+} in C-A-S-H with time. The investigations showed a slow redistribution of Si and Al in C-A-S-H as well as the partial replacement of Na^+ by Ca^{2+} in the interlayer space with a time span of up to (at least) 10 years. The measured aqueous phase and C-A-S-H compositions at later equilibration time (close to equilibrium) were well reproduced by the thermodynamic CASH+ solid solution model.

In the long-term samples, higher Al uptake was observed in C-A-S-H with high Ca/Si_{target} (if expressed as K_d values), due to the stabilization of Al in the silica chains by Ca^{2+} in the interlayer, while the molar Al/Si (or Al per gram of C-S-H) were rather similar at all Ca/Si_{target} as they depend mainly on the amount of secondary phases present. At high Ca/Si_{target}, competition with Ca^{2+} decreases the uptake of Na^+ by C-A-S-H phases.

The findings of this study can also help for the development of further thermodynamic models to model the effect of equilibration time during hydration and the durability of the PC cements containing large amount of SCMs. The development of a comprehensive thermodynamic model specifically addressing young C-A-S-H would be highly beneficial for researchers and various applications. In addition, enhancing our understanding of the structure and solubility of C-A-S-H over longer term would provide valuable insights for future studies.

Author statement

All persons who meet authorship criteria are listed as authors, and all authors certify that they have participated sufficiently in the work to take public responsibility for the content, including participation in the concept, design, analysis, writing, or revision of the manuscript. Furthermore, each author certifies that this material or similar material has not been and will not be submitted to or published in any other publication before its appearance in the Cement and Concrete Research.

CRediT authorship contribution statement

Y. Yan. and B. Lothenbach. conceived and designed the experiments. Y. Yan conducted the experiments. E. Bernard and D. Rentsch conducted the NMR experiments and supported data interpretation, G. D. Miron and B. Ma supported the thermodynamic modelling, K. Scrivener and B. Lothenbach supervised this work. All authors reviewed the manuscript.

Declaration of competing interest

The authors declare that they have no known competing financial interests or personal relationships that could have appeared to influence the work reported in this paper.

Data availability

Data will be made available on request.

Acknowledgements

The financial support of the Swiss National Science Foundation for the realisation of the project and the NMR hardware (SNF) (projects no. 200021_169014 and 206021_150638/1) is gratefully acknowledged. The authors would like to thank Luigi Brunetti for support during the measurement of elemental concentrations, Rico Muff and Beatrice Fischer for the help with Raman and FTIR measurements, Boris Ingold for the lab support; Emilie L'Hôpital for the synthesis of the 10-year-old samples; Sheng-yu Yang, Andreas Leemann, Jorgen Skibsted, Dmitrii Kulik and Frank Winnefeld are acknowledged for helpful discussions.

Appendix A

Table A1
Mixing proportions used to prepare C-A-S-H (in g per 260 mL of solution for samples with equilibration time from 0.25 day to 90 days, per 180 mL for samples with 90*, 450* and 1350* days and per 90 mL for samples with 3650* days).

Equilibration time (days)	Target Ca/Si ratio	CaO (g)	SiO_2 (g)	$CaO{\cdot}Al_2O_3$ (g)
0.25–90	0.6	2.029	3.952	0.521
	0.8	2.485	3.549	0.467
	1.0	2.856	3.222	0.424
	1.2	3.165	2.950	0.388
	1.4	3.424	2.718	0.357
	1.6	3.648	2.521	0.332
90*	0.6	1.248	2.433	0.323
	0.8	1.528	2.185	0.287
	1.0	1.757	1.982	0.261
	1.2	1.948	1.814	0.239
	1.4	2.107	1.674	0.220

(*continued on next page*)

Table A1 (*continued*)

Equilibration time (days)	Target Ca/Si ratio	CaO (g)	SiO_2 (g)	$CaO{\cdot}Al_2O_3$ (g)
	1.6	2.245	1.552	0.205
450*	0.6	1.249	2.433	0.322
	0.8	1.532	2.184	0.286
	1.0	1.777	1.982	0.263
	1.2	1.949	1.814	0.239
	1.4	2.107	1.674	0.220
	1.6	2.242	1.553	0.208
1350*	0.6	1.255	2.433	0.321
	0.8	1.529	2.184	0.288
	1.0	1.757	1.982	0.262
	1.2	1.947	1.814	0.239
	1.4	2.120	1.674	0.222
	1.6	2.243	1.552	0.205
3650*	1.0	0.879	0.991	0.130

Table A2
Aqueous dissolved concentrations and pH values for the C-(N-)A-S-H samples with different equilibration time (target Al/Si = 0.1). C-A-S-H equilibrated for 0.25–90 days: synthesized with water/solid = 40, C-A-S-H equilibrated for 90*, 450*, 1350* and 3650* days: synthesized with water/solid = 45.

Equilibration time (days)	Target Ca/Si ratio	Si[a] (mM)	Ca[a] (mM)	Al[a] (mM)	Na[a] (mM)	OH^{-}[a] (mM)	pH[b]
0.25	0.6	0.95	0.35	1.3	520	319	13.5
	0.8	0.43	0.82	2.0	528	286	13.5
	1.0	0.42	0.86	1.9	528	302	13.5
	1.2	0.40	0.88	1.6	528	319	13.5
	1.4	0.39	0.91	1.7	536	319	13.5
	1.6	0.38	0.92	1.7	536	337	13.5
1	0.6	36.1	0.013	2.2	499	256	13.4
	0.8	0.76	0.24	1.5	504	302	13.5
	1.0	0.36	0.69	1.1	518	319	13.5
	1.2	0.32	0.79	0.91	521	319	13.5
	1.4	0.31	0.83	1.0	524	337	13.5
	1.6	0.30	0.85	1.0	531	337	13.5
3	0.6	53.9	0.009	2.5	472	217	13.3
	0.8	3.87	0.015	1.9	469	286	13.5
	1.0	0.46	0.18	1.2	491	256	13.4
	1.2	0.13	0.76	0.63	513	302	13.5
	1.4	0.11	0.92	0.61	518	302	13.5
	1.6	0.11	0.96	0.58	522	302	13.5
7	0.6	44.1	0.008	2.2	426	174	13.2
	0.8	3.12	0.019	1.8	427	206	13.3
	1.0	0.52	0.14	1.2	446	230	13.4
	1.2	0.11	0.72	0.56	467	230	13.4
	1.4	0.079	0.92	0.51	470	230	13.4
	1.6	0.074	0.99	0.49	474	230	13.4
14	0.6	47.4	0.007	2.3	433	219	13.3
	0.8	3.39	0.019	1.9	432	247	13.4
	1.0	0.48	0.13	1.1	454	267	13.4
	1.2	0.10	0.65	0.52	479	277	13.4
	1.4	0.079	0.95	0.46	481	277	13.4
	1.6	0.074	1.02	0.44	480	277	13.4
28	0.6	37.8	0.0038	2.3	418	228	13.4
	0.8	2.87	0.019	1.8	416	247	13.4
	1.0	0.61	0.11	1.0	441	256	13.4
	1.2	0.13	0.57	0.45	465	267	13.4
	1.4	0.074	0.93	0.38	471	267	13.4
	1.6	0.067	1.01	0.37	473	277	13.4
90	0.6	34.39	0.0055	2.4	432	195	13.3
	0.8	2.72	0.019	1.8	423	237	13.4
	1.0	0.67	0.10	1.0	453	256	13.4
	1.2	0.14	0.44	0.34	476	256	13.4
	1.4	0.072	0.87	0.25	482	256	13.4
	1.6	0.069	0.97	0.23	489	350	13.5
90*	0.6	26.6	–	2.9	545	147	13.2
	0.8	3.83	–	2.0	542	147	13.2
	1.0	0.56	0.040	1.1	580	154	13.2
	1.2	0.13	0.25	0.32	517	147	13.2
	1.4	0.053	0.59	0.15	522	168	13.2
	1.6	0.055	0.61	0.21	530	176	13.2
450*	0.6	32.00	0.010	3.3	503	425	13.6

(*continued on next page*)

Table A2 (*continued*)

Equilibration time (days)	Target Ca/Si ratio	Si[a] (mM)	Ca[a] (mM)	Al[a] (mM)	Na[a] (mM)	OH^{-}[a] (mM)	pH[b]
	0.8	2.84	0.048	2.2	465	367	13.6
	1.0	0.71	0.58	0.87	479	289	13.5
	1.2	0.13	0.13	0.36	500	336	13.5
	1.4	0.072	0.97	0.17	504	371	13.6
	1.6	0.051	1.04	0.19	505	353	13.5
1350*	0.6	20.1	0.037	0.76	459	321	13.5
	0.8	2.56	0.035	1.6	467	334	13.5
	1.0	0.75	0.10	0.69	496	362	13.6
	1.2	0.18	0.44	0.24	515	348	13.5
	1.4	0.086	0.91	0.09	526	362	13.6
	1.6	0.080	0.84	0.15	524	392	13.6
3650*	1.0	0.63	0.17	0.08	480	348	13.5

[a] Measurement error ± 5 %.
[b] pH measured at ≈24 °C; ±0.1.

Table A3
Saturation indices of the relevant reaction products in C-(A-)S-H system with $Al/Si_{target} = 0.1$ and different Ca/Si as a function of equilibration times. C-A-S-H equilibrated for 0.25–90 days: Synthesized with water/solid = 40, C-A-S-H equilibrated for 90*, 450*, 1350* and 3650* days: Synthesized with water/solid = 45.

Target Ca/Si	Equilibration time (days)	C-A-S-H	AH_3	C_3AH_6	Charbazite	Gismondine-P1-Na	Stratlingite	Protlandite	Amor-SiO_2
0.6	0.25	0.7	−1.9	−1.9	−1.6	−16.5	−0.4	−0.6	−5.1
	1	−0.1	−1.8	−8.1	0.1	0.8	−2.7	−2.7	−3.3
	3	−0.1	−1.8	−9.1	0.3	3.3	−3.1	−3.1	−3.1
	7	−0.4	−1.7	−9.2	0.3	3.0	−3.2	−3.2	−3.1
	14	−0.4	−1.7	−9.4	0.3	3.2	−3.3	−3.2	−3.1
	28	−1.1	−1.7	−10.0	0.2	2.4	−3.7	−3.4	−3.2
	90	−0.8	−1.7	−9.3	0.2	2.0	−3.3	−3.2	−3.2
	90	−1.5	−1.7	−9.5	−0.1	−0.5	−3.8	−3.3	−3.6
	450	−0.3	−1.6	−7.9	0.1	1.3	−2.6	−2.8	−3.4
	1350	0.5	−2.2	−7.0	−0.4	−3.8	−2.4	−2.1	−3.6
0.8	0.25	1.0	−1.7	−0.4	−1.9	−19.1	0.4	−0.2	−5.5
	1	0.2	−1.8	−2.3	−1.7	−16.9	−0.6	−0.8	−5.1
	3	−1.0	−1.7	−6.0	−0.9	−8.7	−2.3	−2.1	−4.4
	7	−1.0	−1.7	−5.8	−0.9	−9.1	−2.1	−2.0	−4.4
	14	−0.9	−1.7	−5.8	−0.9	−8.7	−2.1	−2.0	−4.3
	28	−1.0	−1.7	−5.8	−0.9	−9.3	−2.1	−2.0	−4.4
	90	−1.1	−1.7	−5.8	−1.0	−9.7	−2.1	−2.0	−4.4
	90	−2.7	−1.8	−8.3	−1.0	−9.6	−4.0	−2.8	−4.5
	450	−0.2	−1.6	−4.3	−1.0	−9.6	−1.2	−1.6	−4.5
	1350	−0.6	−1.8	−4.9	−1.1	−10.8	−1.8	−1.7	−4.5
1.0	0.25	1.0	−1.7	−0.3	−16.9	−19.3	0.4	−0.2	−5.5
	1	0.6	−2.0	−1.1	−17.6	−21.1	−0.3	−0.3	−5.5
	3	−0.6	−1.9	−2.8	−17.5	−19.5	−1.3	−0.9	−5.3
	7	−0.6	−1.9	−3.2	−17.0	−18.3	−1.3	−1.0	−5.2
	14	−0.8	−1.9	−3.3	−17.2	−18.8	−1.5	−1.1	−5.2
	28	−0.8	−1.9	−3.6	−16.9	−17.8	−1.6	−1.2	−5.1
	90	−0.8	−2.0	−3.8	−16.9	−17.7	−1.7	−1.2	−5.1
	90	−1.9	−2.0	−4.9	−18.5	−19.8	−2.7	−1.5	−5.4
	450	0.9	−2.0	−1.6	−16.4	−18.4	−0.3	−0.4	−5.1
	1350	−0.8	−2.2	−4.1	−17.3	−18.7	−2.0	−1.2	−5.1
	3650	−0.7	−3.1	−5.2	−19.1	−24.8	−3.5	−0.9	−5.2
1.2	0.25	1.0	−1.8	−0.5	−2.0	−20.0	0.2	−0.2	−5.5
	1	0.5	−2.1	−1.1	−2.2	−22.3	−0.4	−0.2	−5.6
	3	−0.3	−2.2	−1.4	−2.7	−27.0	−1.1	−0.2	−5.9
	7	−0.5	−2.2	−1.6	−2.7	−27.5	−1.2	−0.3	−5.9
	14	−0.7	−2.3	−1.8	−2.8	−28.4	−1.5	−0.3	−6.0
	28	−0.6	−2.3	−2.1	−2.7	−27.3	−1.6	−0.4	−5.9
	90	−0.9	−2.4	−2.7	−2.8	−27.9	−2.0	−0.5	−5.8
	90	−1.6	−2.5	−3.5	−2.9	−28.7	−2.7	−0.7	−5.9
	450	−2.2	−2.4	−4.2	−2.8	−28.2	−3.1	−1.0	−5.9
	1350	−0.8	−2.6	−3.0	−2.8	−28.1	−2.3	−0.5	−5.8
1.4	0.25	1.0	−1.8	−0.4	−2.0	−20.1	0.3	−0.2	−5.5
	1	0.6	−2.0	−1.0	−2.2	−22.2	−0.3	−0.2	−5.6
	3	−0.2	−2.2	−1.2	−2.8	−27.8	−1.1	−0.2	−6.0
	7	−0.5	−2.3	−1.4	−2.9	−29.3	−1.3	−0.2	−6.1
	14	−0.5	−2.3	−1.4	−3.0	−29.7	−1.4	−0.2	−6.1
	28	−0.6	−2.4	−1.6	−3.0	−30.3	−1.6	−0.2	−6.1
	90	−0.8	−2.6	−2.1	−3.2	−31.7	−2.0	−0.2	−6.1
	90	−1.5	−2.8	−3.0	−3.5	−34.7	−3.0	−0.3	−6.3
	450	−0.7	−2.8	−2.3	−3.3	−33.0	−2.3	−0.1	−6.2
	1350	−0.7	−3.1	−2.9	−3.4	−34.0	−2.9	−0.2	−6.1
1.6	0.25	1.0	−1.8	−0.4	−2.0	−20.1	0.3	−0.2	−5.5

(*continued on next page*)

Table A3 (*continued*)

Target Ca/Si	Equilibration time (days)	C-A-S-H	AH_3	C_3AH_6	Charbazite	Gismondine-P1-Na	Stratlingite	Protlandite	Amor-SiO_2
	1	0.6	−2.0	−0.9	−2.2	−22.4	−0.3	−0.2	−5.6
	3	−0.2	−2.2	−1.2	−2.8	−28.1	−1.1	−0.1	−6.0
	7	−0.5	−2.3	−1.3	−3.0	−29.7	−1.3	−0.2	−6.1
	14	−0.5	−2.3	−1.4	−3.0	−30.1	−1.4	−0.1	−6.1
	28	−0.6	−2.4	−1.5	−3.1	−30.9	−1.6	−0.1	−6.2
	90	−0.7	−2.6	−2.0	−3.2	−32.1	−2.0	−0.2	−6.2
	90	−1.4	−2.7	−2.7	−3.4	−33.7	−2.7	−0.3	−6.3
	450	−0.9	−2.7	−2.1	−3.4	−34.2	−2.3	−0.1	−6.3
	1350	−0.8	−2.8	−2.6	−3.3	−33.1	−2.5	−0.2	−6.2

Table A4

Chemical compositions of the C-N-A-S-H products, determined by Rietveld analysis, TGA, ^{27}Al NMR, mass balance and dissolution experiments. The estimated absolute errors are less than ±0.05 units in the Ca/Si ratios, ±0.2 units in the H_2O/Si ratios, and ± 0.03 units in the Na/Si ratios of the C-N-A-S-H products. C-A-S-H equilibrated for 0.25–90 days: synthesized with water/solid = 40, C-A-S-H equilibrated for 90*, 450*, *1350* and 3650* days*: synthesized with water/solid = 45.

Target Ca/Si ratio	Equilibration time (days)	Ca/Si	Na/Si	Al/Si	H_2O/Si	Chemical formula
0.6	0.25[b]	0.54	0.23	0.10	1.2	$(CaO)_{0.54}(Na_2O)_{0.11}(Al_2O_3)_{0.048}(SiO_2)_1(H_2O)_{1.2}$
	1[b]	0.68	0.50	0.10	1.4	$(CaO)_{0.68}(Na_2O)_{0.25}(Al_2O_3)_{0.051}(SiO_2)_1(H_2O)_{1.4}$
	3[b]	0.75	0.51	0.11	1.8	$(CaO)_{0.75}(Na_2O)_{0.26}(Al_2O_3)_{0.055}(SiO_2)_1(H_2O)_{1.8}$
	7[b]	0.72	0.43	0.10	1.6	$(CaO)_{0.72}(Na_2O)_{0.22}(Al_2O_3)_{0.052}(SiO_2)_1(H_2O)_{1.6}$
	14[b]	0.72	0.49	0.10	1.7	$(CaO)_{0.72}(Na_2O)_{0.25}(Al_2O_3)_{0.05}(SiO_2)_1(H_2O)_{1.7}$
	28[b]	0.69	0.58	0.10	1.5	$(CaO)_{0.69}(Na_2O)_{0.29}(Al_2O_3)_{0.047}(SiO_2)_1(H_2O)_{1.5}$
	90[b]	0.68	0.51	0.09	1.5	$(CaO)_{0.68}(Na_2O)_{0.26}(Al_2O_3)_{0.046}(SiO_2)_1(H_2O)_{1.5}$
	90*[b]	0.68	0.45	0.10	1.7	$(CaO)_{0.68}(Na_2O)_{0.23}(Al_2O_3)_{0.050}(SiO_2)_1(H_2O)_{1.7}$
	450*[b]	0.70	0.39	0.10	1.5	$(CaO)_{0.70}(Na_2O)_{0.20}(Al_2O_3)_{0.049}(SiO_2)_1(H_2O)_{1.5}$
	1350*[b]	0.65	0.42	0.07	1.3	$(CaO)_{0.65}(Na_2O)_{0.21}(Al_2O_3)_{0.034}(SiO_2)_1(H_2O)_{1.3}$
0.8	0.25[a]	0.64	0.17	0.06	1.2	$(CaO)_{0.64}(Na_2O)_{0.09}(Al_2O_3)_{0.029}(SiO_2)_1(H_2O)_{1.2}$
	1[a]	0.79	0.75	0.08	1.8	$(CaO)_{0.79}(Na_2O)_{0.37}(Al_2O_3)_{0.041}(SiO_2)_1(H_2O)_{1.8}$
	3[a]	0.80	0.70	0.08	1.7	$(CaO)_{0.80}(Na_2O)_{0.35}(Al_2O_3)_{0.042}(SiO_2)_1(H_2O)_{1.7}$
	7[a]	0.80	0.50	0.08	1.5	$(CaO)_{0.80}(Na_2O)_{0.25}(Al_2O_3)_{0.041}(SiO_2)_1(H_2O)_{1.5}$
	14[a]	0.80	0.61	0.08	1.6	$(CaO)_{0.80}(Na_2O)_{0.30}(Al_2O_3)_{0.040}(SiO_2)_1(H_2O)_{1.6}$
	28[a]	0.80	0.56	0.08	1.5	$(CaO)_{0.80}(Na_2O)_{0.28}(Al_2O_3)_{0.038}(SiO_2)_1(H_2O)_{1.5}$
	90[a]	0.80	0.57	0.08	1.5	$(CaO)_{0.80}(Na_2O)_{0.29}(Al_2O_3)_{0.040}(SiO_2)_1(H_2O)_{1.5}$
	90*[b]	0.81	0.40	0.09	1.7	$(CaO)_{0.81}(Na_2O)_{0.20}(Al_2O_3)_{0.046}(SiO_2)_1(H_2O)_{1.7}$
	450*[b]	0.81	0.41	0.09	1.7	$(CaO)_{0.81}(Na_2O)_{0.21}(Al_2O_3)_{0.045}(SiO_2)_1(H_2O)_{1.7}$
	1350*[a]	0.81	0.37	0.09	1.5	$(CaO)_{0.81}(Na_2O)_{0.18}(Al_2O_3)_{0.046}(SiO_2)_1(H_2O)_{1.5}$
1.0	0.25[a]	0.73	0.10	0.06	1.1	$(CaO)_{0.73}(Na_2O)_{0.05}\ (Al_2O_3)_{0.032}(SiO_2)_1(H_2O)_{1.1}$
	1[a]	0.96	0.39	0.08	1.7	$(CaO)_{0.96}(Na_2O)_{0.19}(Al_2O_3)_{0.038}(SiO_2)_1(H_2O)_{1.7}$
	3[a]	0.99	0.42	0.09	2.0	$(CaO)_{0.99}(Na_2O)_{0.21}(Al_2O_3)_{0.043}(SiO_2)_1(H_2O)_{2.0}$
	7[a]	0.99	0.44	0.09	1.8	$(CaO)_{0.99}(Na_2O)_{0.22}(Al_2O_3)_{0.043}(SiO_2)_1(H_2O)_{1.8}$
	14[a]	0.99	0.49	0.08	1.7	$(CaO)_{0.99}(Na_2O)_{0.24}(Al_2O_3)_{0.041}(SiO_2)_1(H_2O)_{1.7}$
	28[a]	0.99	0.44	0.08	1.7	$(CaO)_{0.99}(Na_2O)_{0.22}(Al_2O_3)_{0.041}(SiO_2)_1(H_2O)_{1.7}$
	90[a]	0.99	0.57	0.08	1.7	$(CaO)_{0.99}(Na_2O)_{0.29}(Al_2O_3)_{0.042}(SiO_2)_1(H_2O)_{1.7}$
	90*[a]	0.99	0.37	0.09	1.8	$(CaO)_{0.99}(Na_2O)_{0.18}(Al_2O_3)_{0.046}(SiO_2)_1(H_2O)_{1.8}$
	450*[a]	0.99	0.33	0.07	1.8	$(CaO)_{0.99}(Na_2O)_{0.16}(Al_2O_3)_{0.036}(SiO_2)_1(H_2O)_{1.8}$
	1350*[a]	0.99	0.29	0.08	1.8	$(CaO)_{0.99}(Na_2O)_{0.15}(Al_2O_3)_{0.041}(SiO_2)_1(H_2O)_{1.8}$
	3650*[a]	1.00	0.28	0.09	1.8	$(CaO)_{1.00}(Na_2O)_{0.14}(Al_2O_3)_{0.046}(SiO_2)_1(H_2O)_{1.8}$
1.2	0.25[b]	0.81	0.15	0.09	1.1	$(CaO)_{0.81}(Na_2O)_{0.073}(Al_2O_3)_{0.044}(SiO_2)_1(H_2O)_{1.1}$
	1[b]	1.08	0.47	0.09	1.6	$(CaO)_{1.08}(Na_2O)_{0.23}(Al_2O_3)_{0.044}(SiO_2)_1(H_2O)_{1.6}$
	3[b]	1.16	0.55	0.08	1.9	$(CaO)_{1.16}(Na_2O)_{0.27}(Al_2O_3)_{0.042}(SiO_2)_1(H_2O)_{1.9}$
	7[b]	1.17	0.33	0.08	1.9	$(CaO)_{1.17}(Na_2O)_{0.17}(Al_2O_3)_{0.040}(SiO_2)_1(H_2O)_{1.9}$
	14[b]	1.17	0.37	0.08	1.7	$(CaO)_{1.17}(Na_2O)_{0.18}(Al_2O_3)_{0.040}(SiO_2)_1(H_2O)_{1.7}$
	28[b]	1.17	0.34	0.08	1.7	$(CaO)_{1.17}(Na_2O)_{0.17}(Al_2O_3)_{0.040}(SiO_2)_1(H_2O)_{1.7}$
	90[b]	1.17	0.43	0.08	1.7	$(CaO)_{1.17}(Na_2O)_{0.21}(Al_2O_3)_{0.039}(SiO_2)_1(H_2O)_{1.7}$
	90*[b]	1.16	0.21	0.07	1.8	$(CaO)_{1.16}(Na_2O)_{0.11}(Al_2O_3)_{0.036}(SiO_2)_1(H_2O)_{1.8}$
	450*[b]	1.19	0.24	0.09	2.2	$(CaO)_{1.19}(Na_2O)_{0.12}(Al_2O_3)_{0.045}(SiO_2)_1(H_2O)_{2.2}$
	1350*[b]	1.17	0.15	0.09	1.6	$(CaO)_{1.17}(Na_2O)_{0.073}(Al_2O_3)_{0.043}(SiO_2)_1(H_2O)_{1.6}$
1.4	0.25[b]	0.88	0.22	0.09	1.2	$(CaO)_{0.88}(Na_2O)_{0.11}(Al_2O_3)_{0.045}(SiO_2)_1(H_2O)_{1.2}$
	1[b]	1.17	0.45	0.09	1.7	$(CaO)_{1.17}(Na_2O)_{0.23}(Al_2O_3)_{0.045}(SiO_2)_1(H_2O)_{1.7}$
	3[b]	1.23	0.41	0.09	1.7	$(CaO)_{1.23}(Na_2O)_{0.21}(Al_2O_3)_{0.046}(SiO_2)_1(H_2O)_{1.7}$
	7[b]	1.25	0.35	0.09	1.7	$(CaO)_{1.25}(Na_2O)_{0.18}(Al_2O_3)_{0.045}(SiO_2)_1(H_2O)_{1.7}$
	14[b]	1.26	0.47	0.09	1.7	$(CaO)_{1.26}(Na_2O)_{0.23}(Al_2O_3)_{0.044}(SiO_2)_1(H_2O)_{1.7}$
	28[b]	1.27	0.30	0.09	1.7	$(CaO)_{1.27}(Na_2O)_{0.15}(Al_2O_3)_{0.045}(SiO_2)_1(H_2O)_{1.7}$
	90[b]	1.27	0.41	0.09	1.7	$(CaO)_{1.27}(Na_2O)_{0.21}(Al_2O_3)_{0.046}(SiO_2)_1(H_2O)_{1.7}$
	90*[b]	1.20	0.25	0.06	1.7	$(CaO)_{1.20}(Na_2O)_{0.12}(Al_2O_3)_{0.031}(SiO_2)_1(H_2O)_{1.7}$
	450*[b]	1.29	0.21	0.09	1.8	$(CaO)_{1.29}(Na_2O)_{0.11}(Al_2O_3)_{0.043}(SiO_2)_1(H_2O)_{1.8}$
	1350*[b]	1.28	0.13	0.08	1.6	$(CaO)_{1.28}(Na_2O)_{0.065}(Al_2O_3)_{0.039}(SiO_2)_1(H_2O)_{1.6}$
1.6	0.25[b]	0.91	0.27	0.09	1.2	$(CaO)_{0.91}(Na_2O)_{0.14}(Al_2O_3)_{0.045}(SiO_2)_1(H_2O)_{1.2}$
	1[b]	1.25	0.51	0.09	1.5	$(CaO)_{1.25}(Na_2O)_{0.26}(Al_2O_3)_{0.046}(SiO_2)_1(H_2O)_{1.5}$
	3[b]	1.31	0.46	0.09	1.8	$(CaO)_{1.31}(Na_2O)_{0.23}(Al_2O_3)_{0.047}(SiO_2)_1(H_2O)_{1.8}$
	7[b]	1.33	0.47	0.09	1.7	$(CaO)_{1.33}(Na_2O)_{0.23}(Al_2O_3)_{0.047}(SiO_2)_1(H_2O)_{1.7}$
	14[b]	1.36	0.37	0.09	1.8	$(CaO)_{1.36}(Na_2O)_{0.19}(Al_2O_3)_{0.047}(SiO_2)_1(H_2O)_{1.8}$

(*continued on next page*)

Table A4 (*continued*)

Target Ca/Si ratio	Equilibration time (days)	Ca/Si	Na/Si	Al/Si	H_2O/Si	Chemical formula
	28[b]	1.28	0.39	0.08	2.0	$(CaO)_{1.28}(Na_2O)_{0.19}(Al_2O_3)_{0.037}(SiO_2)_1(H_2O)_{2.0}$
	90[b]	1.31	0.35	0.08	1.6	$(CaO)_{1.31}(Na_2O)_{0.17}(Al_2O_3)_{0.040}(SiO_2)_1(H_2O)_{1.6}$
	90*[b]	1.30	0.28	0.07	1.7	$(CaO)_{1.30}(Na_2O)_{0.14}(Al_2O_3)_{0.038}(SiO_2)_1(H_2O)_{1.7}$
	450*[b]	1.39	0.17	0.08	1.9	$(CaO)_{1.39}(Na_2O)_{0.084}(Al_2O_3)_{0.042}(SiO_2)_1(H_2O)_{1.9}$
	1350*[b]	1.34	0.17	0.07	1.8	$(CaO)_{1.34}(Na_2O)_{0.083}(Al_2O_3)_{0.033}(SiO_2)_1(H_2O)_{1.8}$

[a] Al/Si determined by TGA, ^{27}Al NMR, mass balance and dissolution experiments.
[b] Al/Si determined by TGA, Rietveld analysis, mass balance and dissolution experiments.

Table A5
Solid phase assemblages of the C-N-A-S-H samples, as determined by TGA and XRD Rietveld analysis. The estimated absolute error is ±0.2 wt%. C-A-S-H equilibrated for 0.25–90 days: synthesized with water/solid = 40, C-A-S-H equilibrated for 90*, 450*, *1350* and 3650* days*: synthesized with water/solid = 45.

Equilibration time (days)	target Ca/Si ratio	C-(N,*K*)-A-S-H	CH	C3AH6	Hemicarbonate	Monocarbonate	Gismondine-P1-Na
		(wt%)	(wt%)	(wt%)	(wt%)	(wt%)	(wt%)
0.25	0.6	96.5	3.5				
	0.8	91.8	8.2				
	1.0	86.9	13.1				
	1.2	82.6	17.0	0.4			
	1.4	79.4	20.6				
	1.6	74.5	25.5				
1	0.6	98.6	0.9	0.5			
	0.8	98.9		1.1			
	1.0	98.0	1.0	1.0			
	1.2	94.6	4.5	0.9			
	1.4	91.2	8.4	0.4			
	1.6	87.5	12.2	0.3			
3	0.6	99.3		0.7			
	0.8	99.0		1.0			
	1.0	99.1		0.9			
	1.2	97.8	0.9	1.3			
	1.4	93.3	6.2	0.5			
	1.6	89.8	9.9	0.3			
7	0.6	99.3		0.7			
	0.8	99.1		0.9			
	1.0	99.2		0.8			
	1.2	98.0	0.3	1.7			
	1.4	93.9	5.5	0.6			
	1.6	90.5	9.2	0.3			
14	0.6	98.7		1.3			
	0.8	99.1		0.9			
	1.0	99.0		1.0			
	1.2	98.2		1.8			
	1.4	94.3	4.9	0.8			
	1.6	91.2	8.5	0.3			
28	0.6	98.5		1.5			
	0.8	99.1		0.9			
	1.0	99.1		0.9			
	1.2	98.2		1.8			
	1.4	94.8	4.4	0.8			
	1.6	86.0	11.1	0.4	0.3	2.2	
90	0.6	98.5		1.5			
	0.8	99.1		0.9			
	1.0	99.0		1.0			
	1.2	97.8		2.2			
	1.4	94.7	4.6	0.7			
	1.6	87.9	9.9	0.3	0.1	1.8	
90*	0.6	100.0					
	0.8	100.0					
	1.0	99.3			0.7		
	1.2	97.2		2.1	0.7		
	1.4	90.2	5.0	1.2	1.7	1.9	
	1.6	87.4	9.3	0.0		3.3	
450*	0.6	99.8		0.2			
	0.8	100.0					
	1.0	98.3		1.3		0.4	
	1.2	99.0		0.3		0.7	
	1.4	95.0	3.1	0.4		1.5	
	1.6	91.5	6.4	0.5		1.6	
1350*	0.6	92.0	2.0	0.9			5.1
	0.8	100.0					
	1.0	99.2		0.8			
	1.2	98.0				2.0	
	1.4	93.6	3.4	0.4		2.6	

(*continued on next page*)

Table A5 (*continued*)

Equilibration time (days)	target Ca/Si ratio	C-(N,*K*)-A-S-H	CH	C3AH6	Hemicarbonate	Monocarbonate	Gismondine-P1-Na
		(wt%)	(wt%)	(wt%)	(wt%)	(wt%)	(wt%)
	1.6	88.7	7.1	0.9		3.3	
3650*	0.8	100.0					

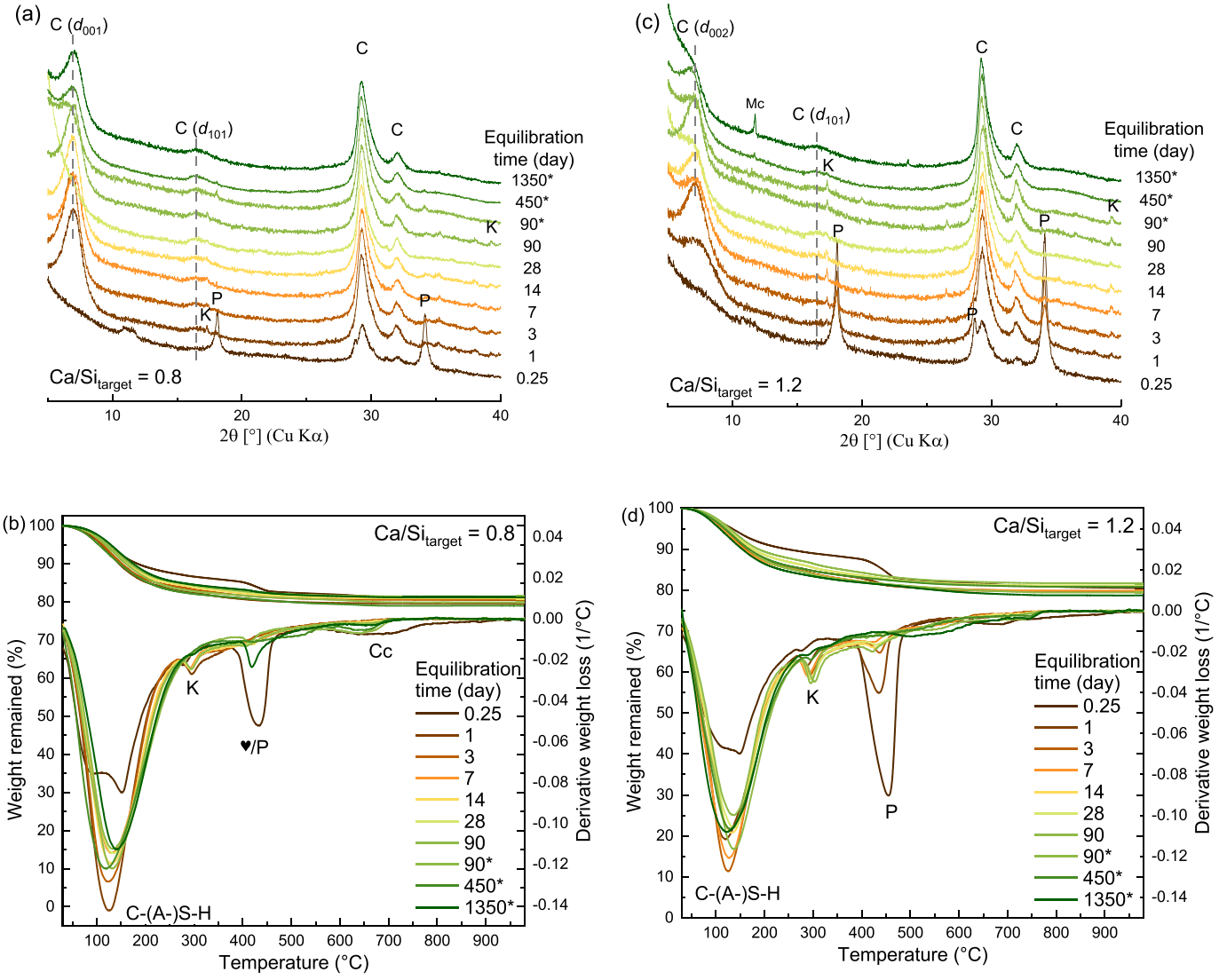

Fig. A1. XRD and TGA of C-A-S-H with (a) and (b) Ca/Si$_{target}$t = 0.8, (c) and (d) Ca/Si$_{target}$t = 1.2, (e) and (f) Ca/Si$_{target}$t = 1.6 equilibrated for different time from 0.25 day to 1350 day. C: C-A-S-H, P: portlandite ($Ca(OH)_2$, PDF# 00-004-733), K: katoite ($Ca_3Al_2(OH)_6$, PDF# 00-024-0217), Hc: hemicarbonate ($Ca_4Al_2(OH)_{12}(OH)(CO_3)_{0.5}(H_2O)_5$, PDF# 00-029-0285), Mc: monocarbonate ($Ca_4Al_2(OH)_{12}(OH)(CO_3)(H_2O)_5$, PDF# 00-029-0285), Cc: carbonates. ▲: unidentified phase.

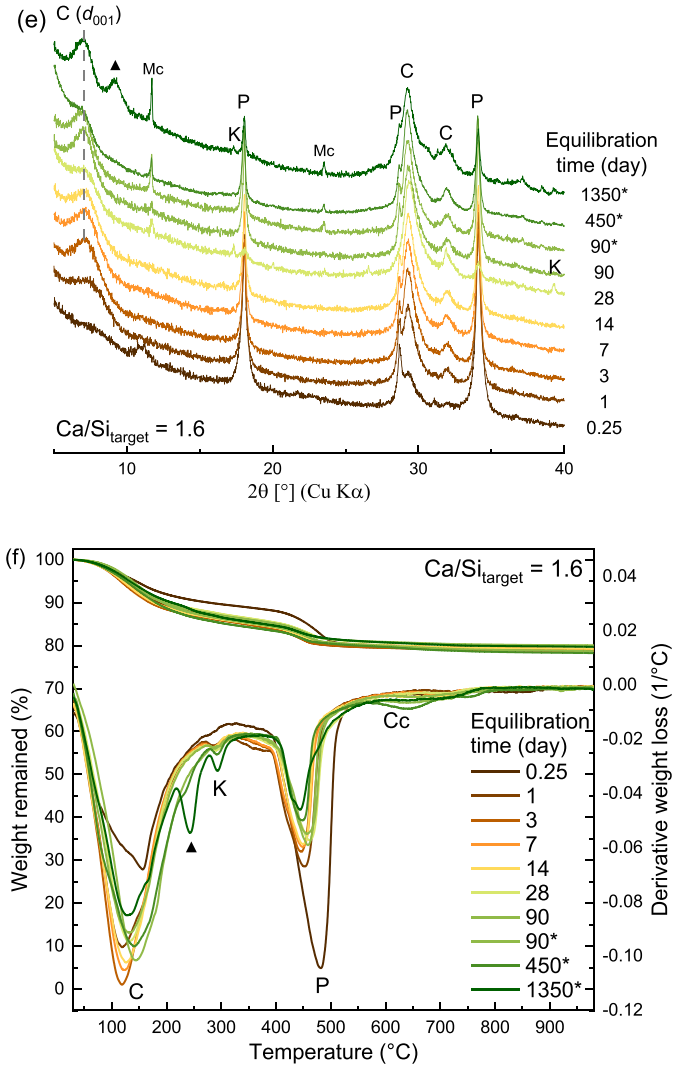

Fig. A1. (*continued*).

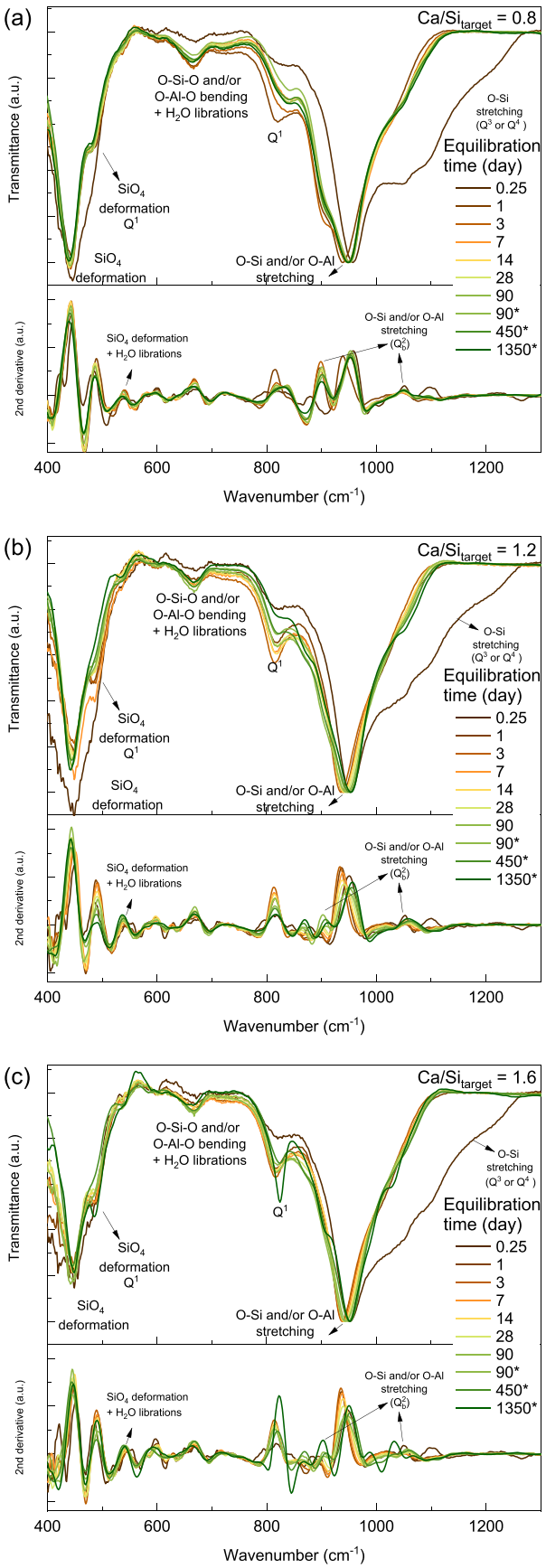

Fig. A2. FTIR and second derivative spectra of C-A-S-H with Ca/Si$_{target}$ = (a) 0.6, (b) 1.0 and (c) 1.4 after different equilibration time synthesized in 0.5 M NaOH. Normalized to the most intensive band at ≈ 950 cm^{-1} of FTIR. C-A-S-H equilibrated for 0.25–90 days: synthesized with water/solid = 40, C-A-S-H equilibrated for 90*, 450* and 1350*: synthesized with water/solid = 45.

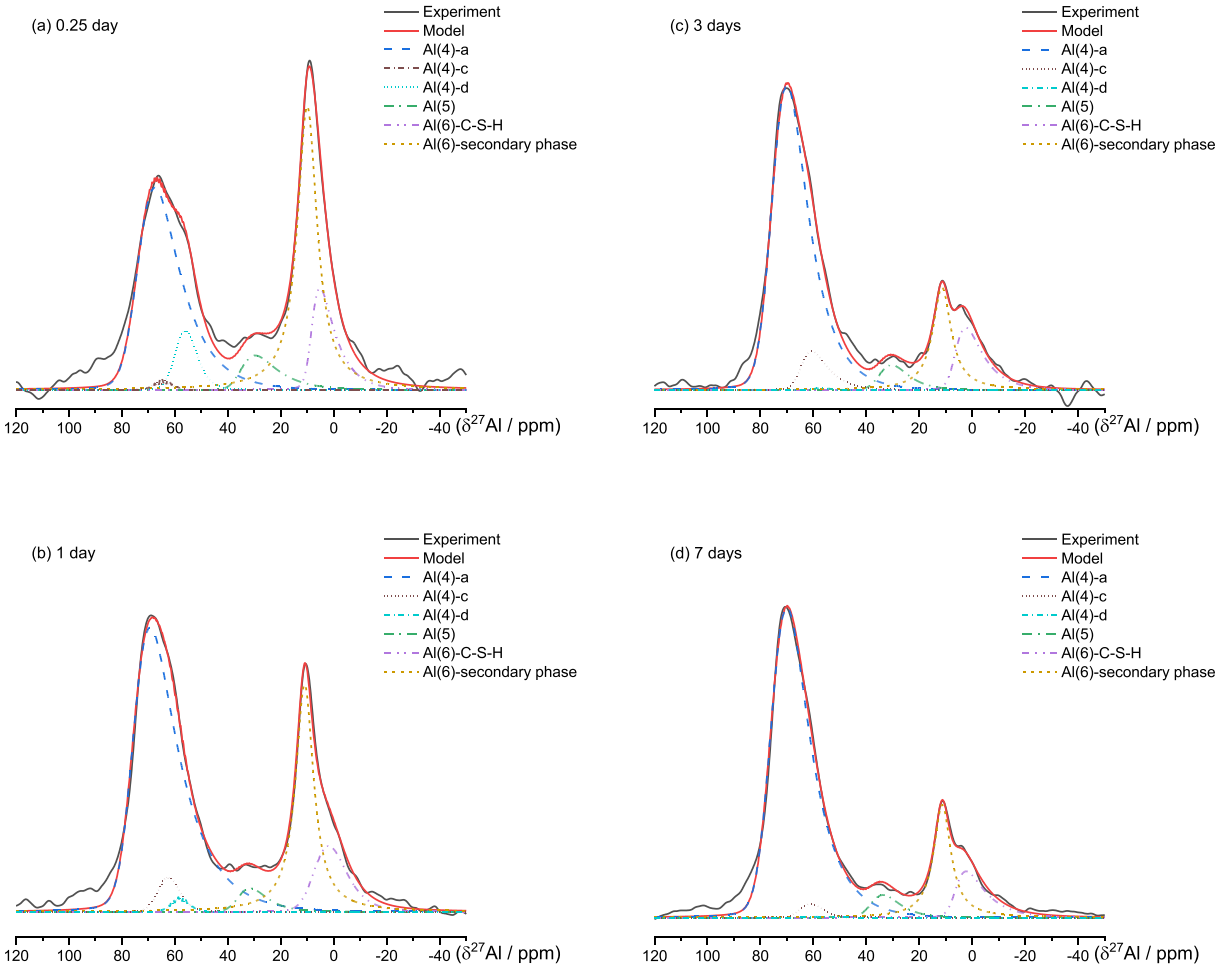

Fig. A3. ^{27}Al NMR: Experimental spectra and results from deconvolution obtained for C-A-S-H with (a)-(k) $Ca/Si_{target} = 1.0$ and (l)-(s) $Ca/Si_{target} = 0.8$ equilibrated from 0.25 day to 3650 days (target Al/Si = 0.1). C-A-S-H equilibrated for 0.25–90 days: synthesized with water/solid = 40, C-A-S-H equilibrated for 90*, 450*, 1350* and 3650* days: synthesized with water/solid = 45.

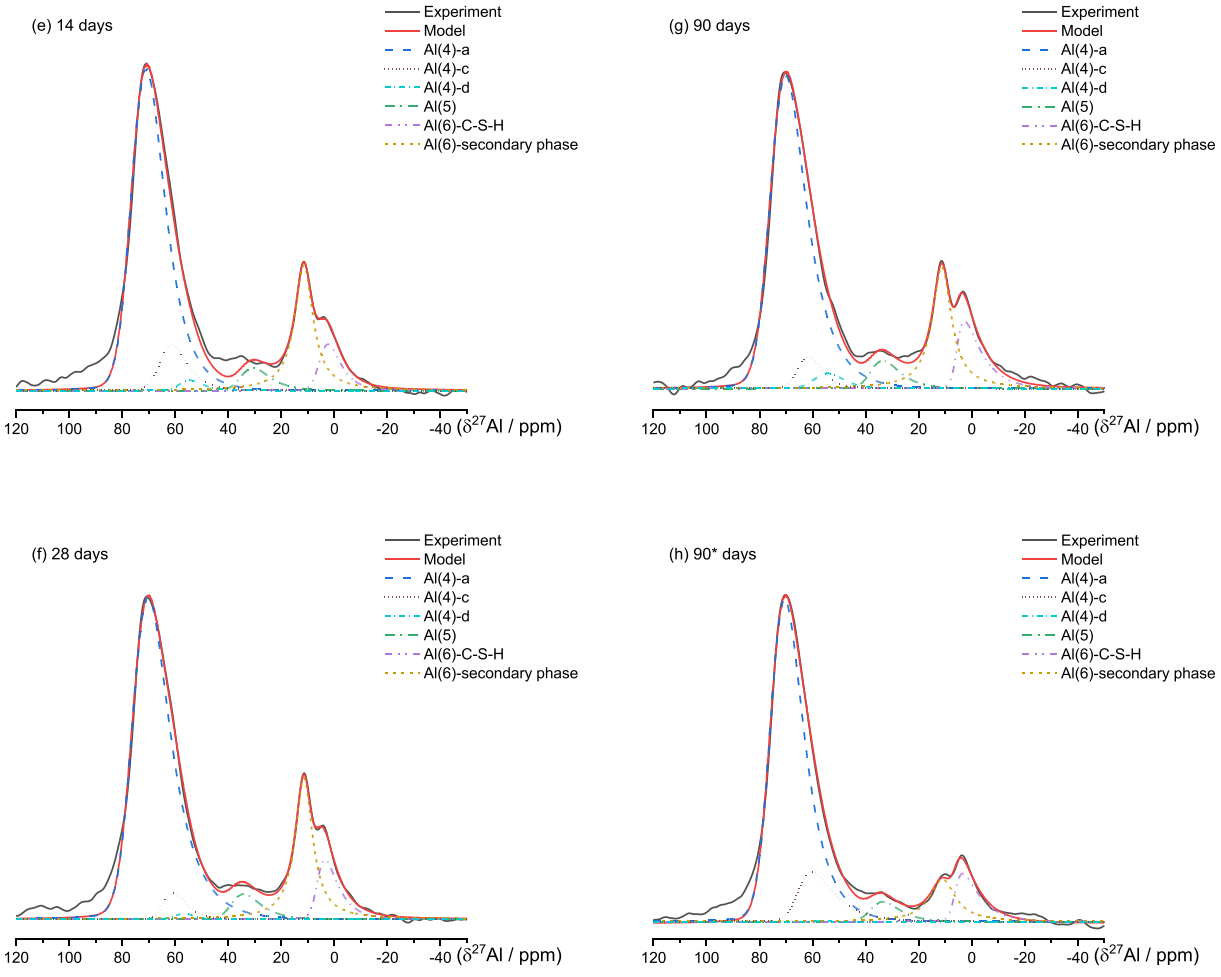

Fig. A3. (*continued*).

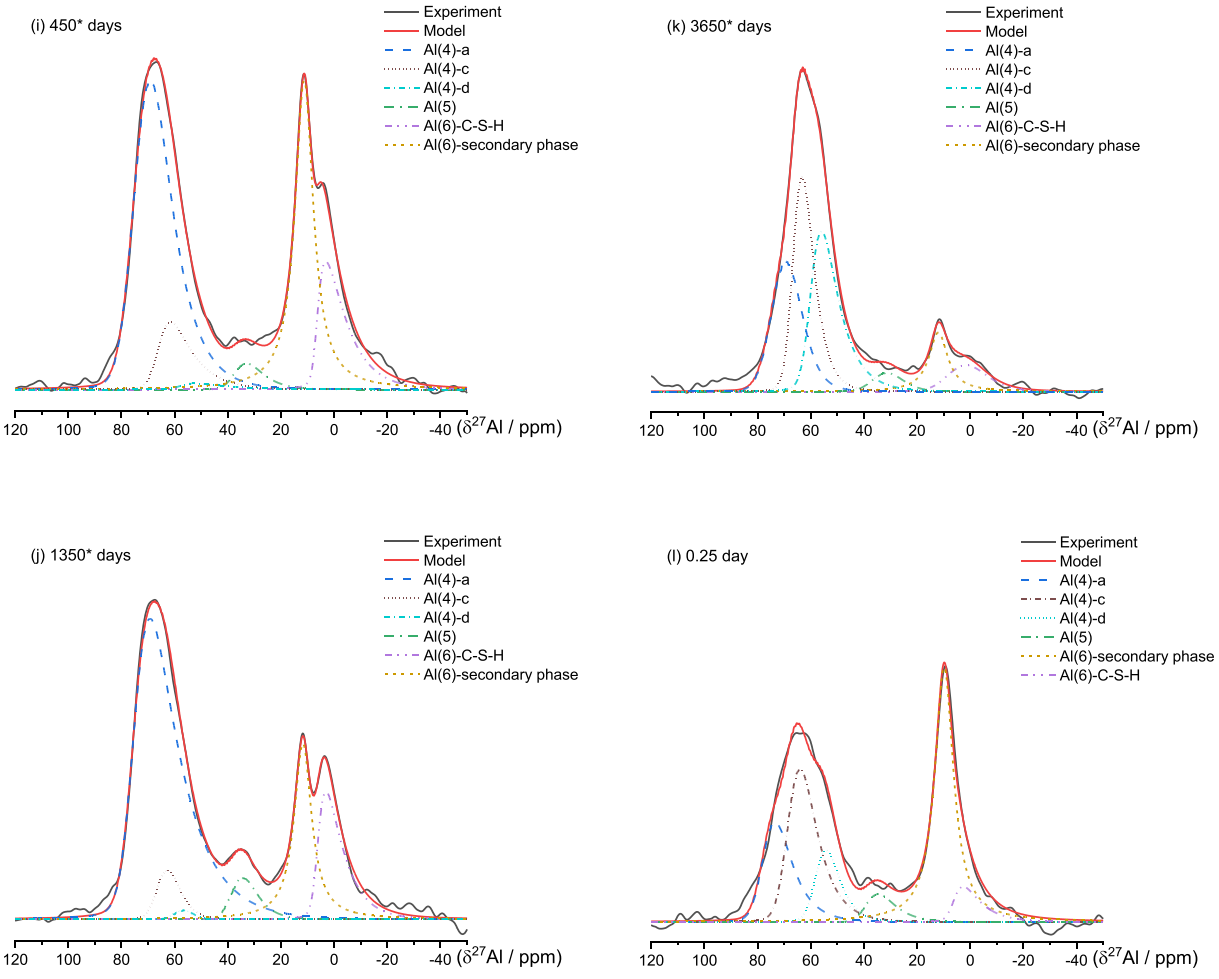

Fig. A3. (*continued*).

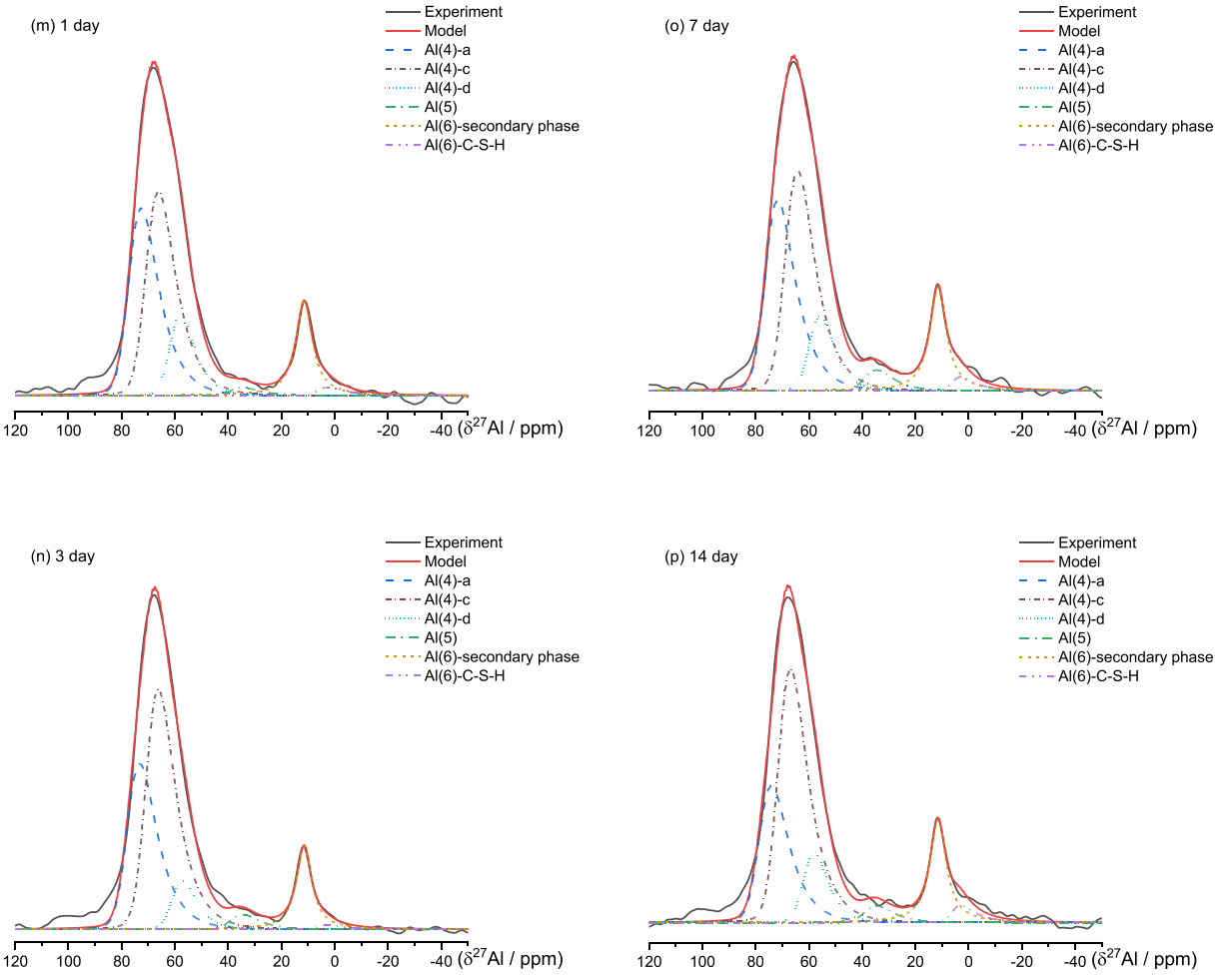

Fig. A3. (*continued*).

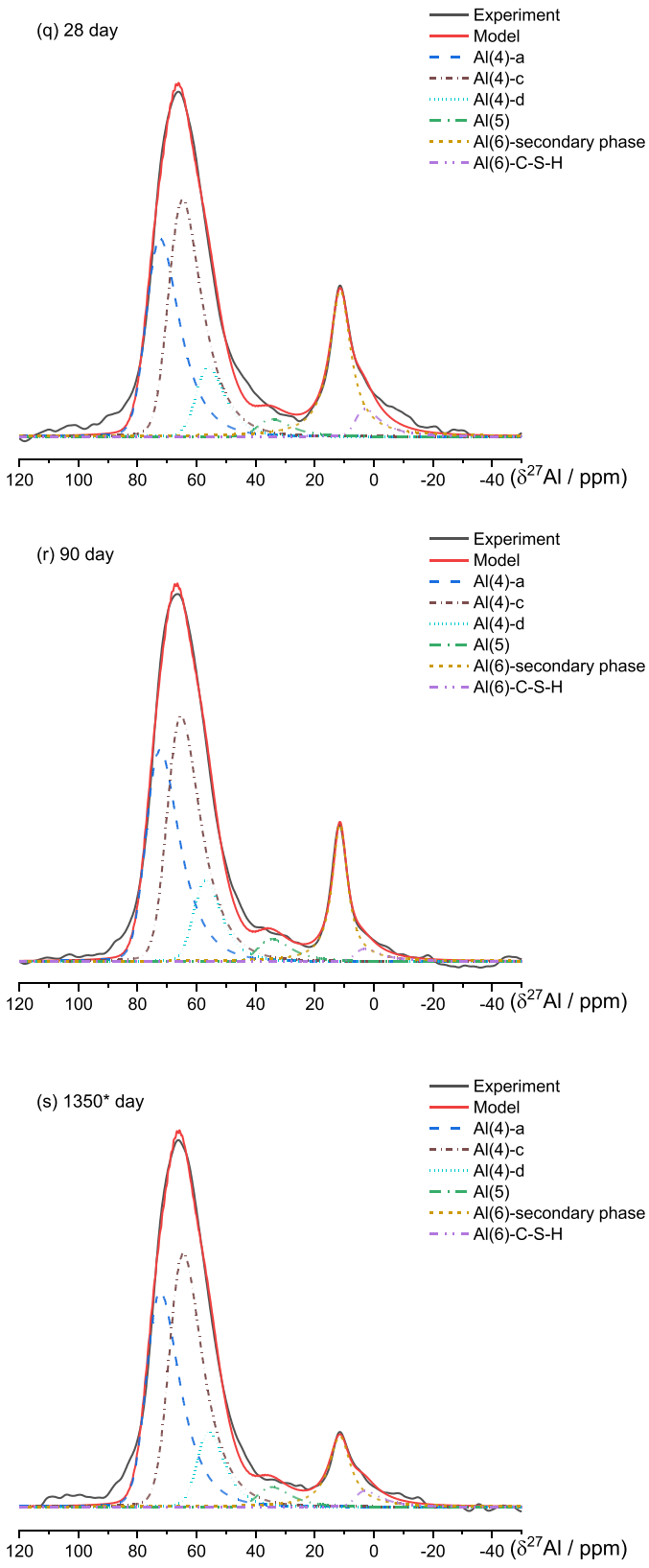

Fig. A3. (*continued*).

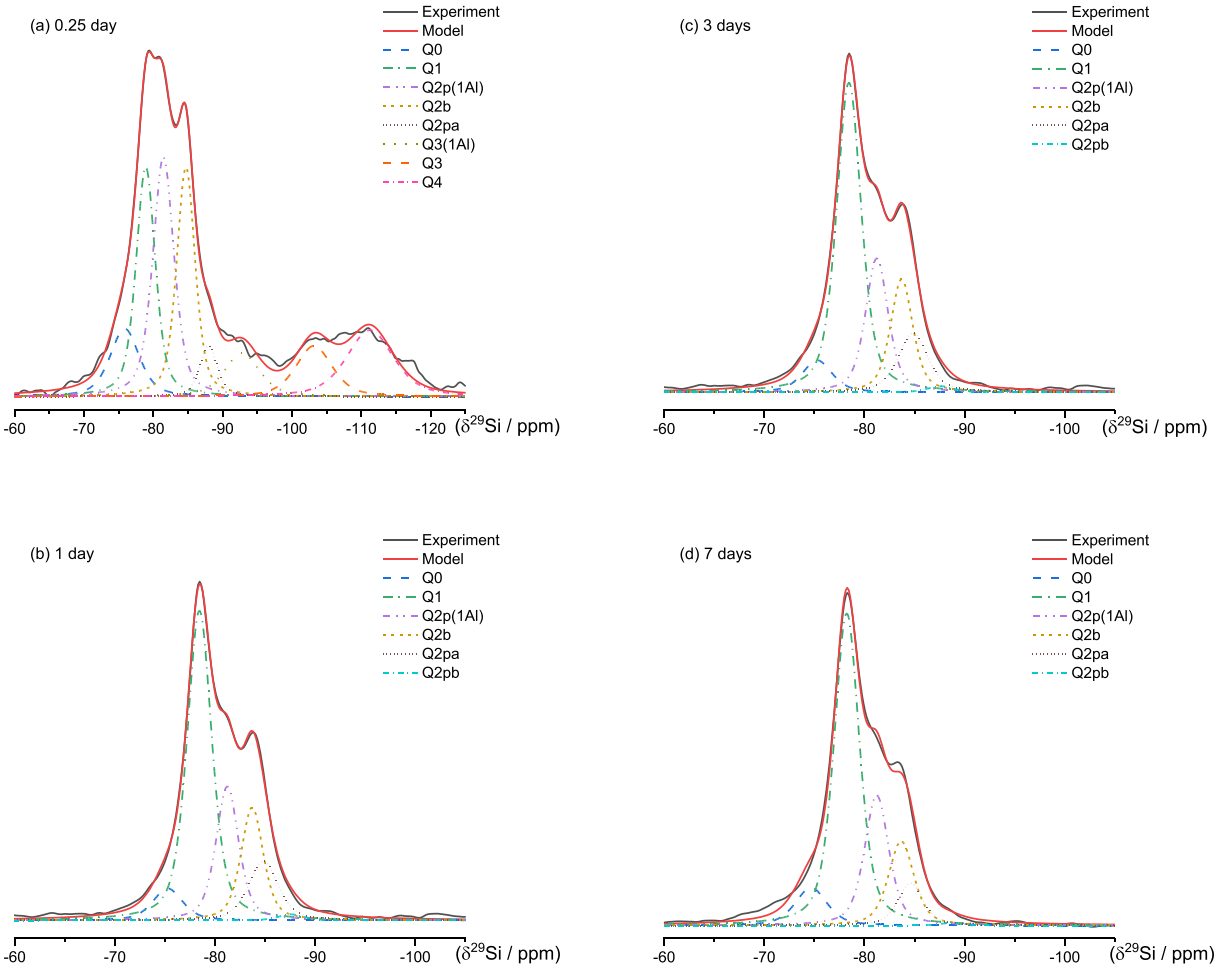

Fig. A4. ^{29}Si NMR Experimental spectra and results from deconvolution obtained for C-A-S-H with (a)-(k) Ca/Si$_{target}$ = 1.0 and (l)-(s) Ca/Si$_{target}$ = 0.8 equilibrated from 0.25 day to 3650 days (target Al/Si = 0.1). C-A-S-H equilibrated for 0.25–90 days: synthesized with water/solid = 40, C-A-S-H equilibrated for 90*, 450*, 1350* and 3650* days: synthesized with water/solid = 45.

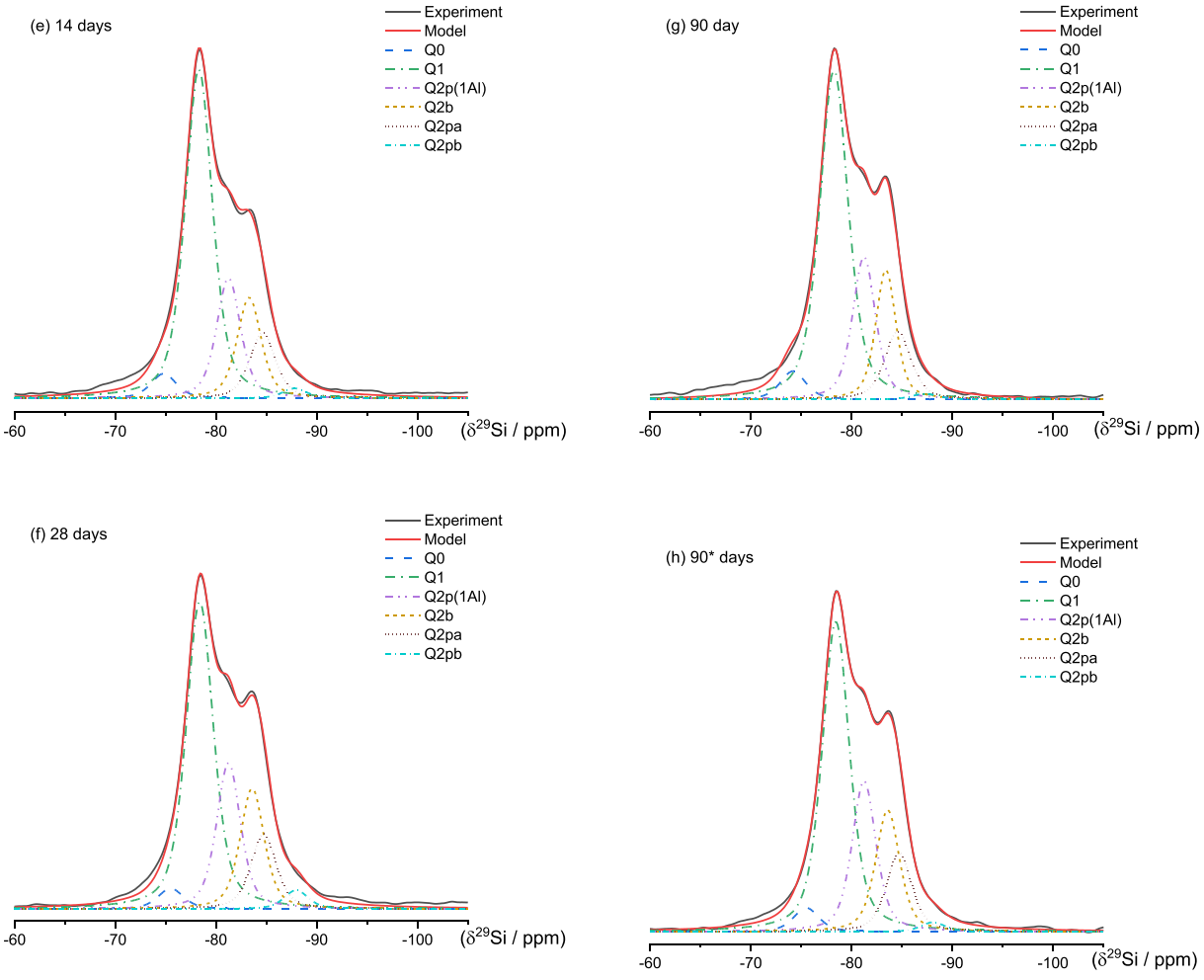

Fig. A4. (*continued*).

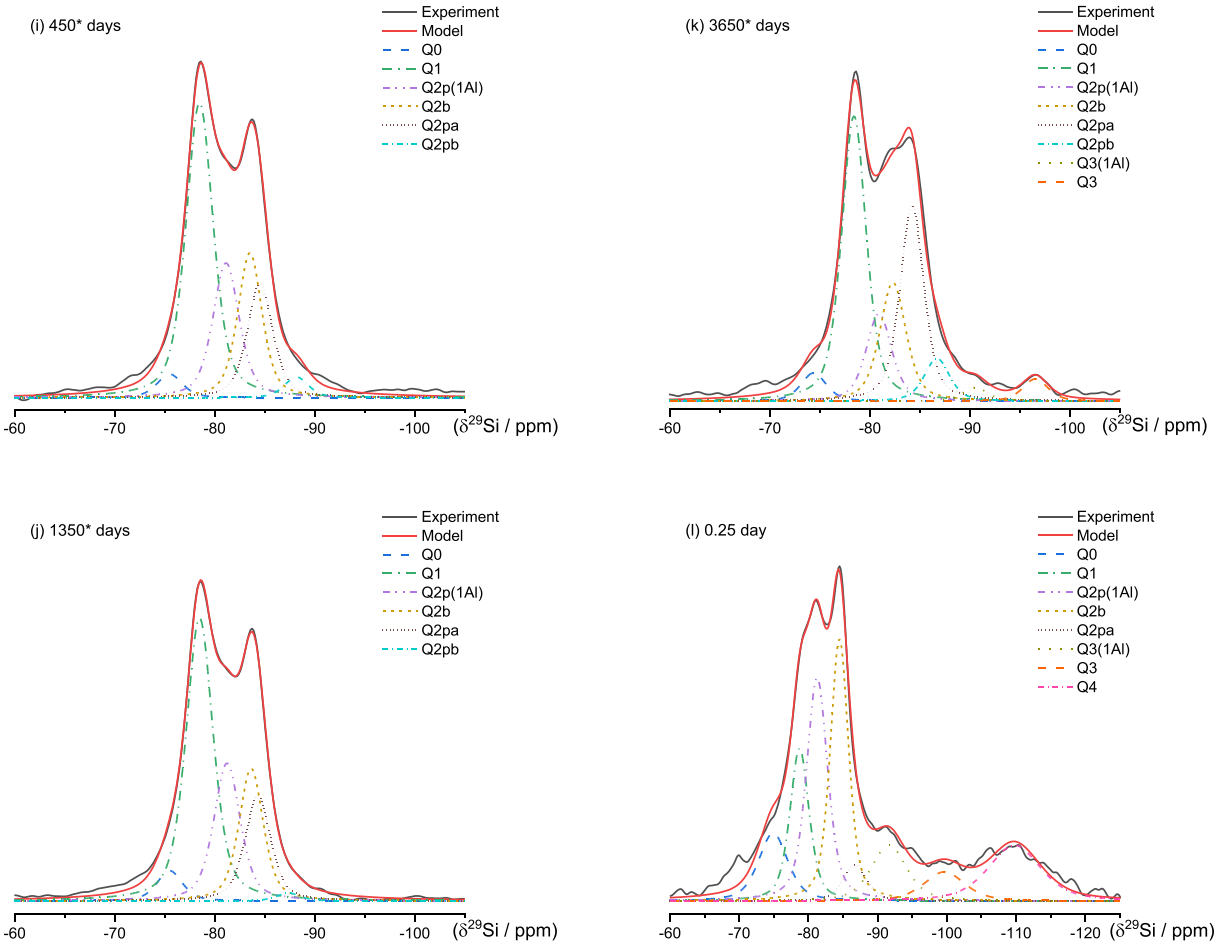

Fig. A4. (*continued*).

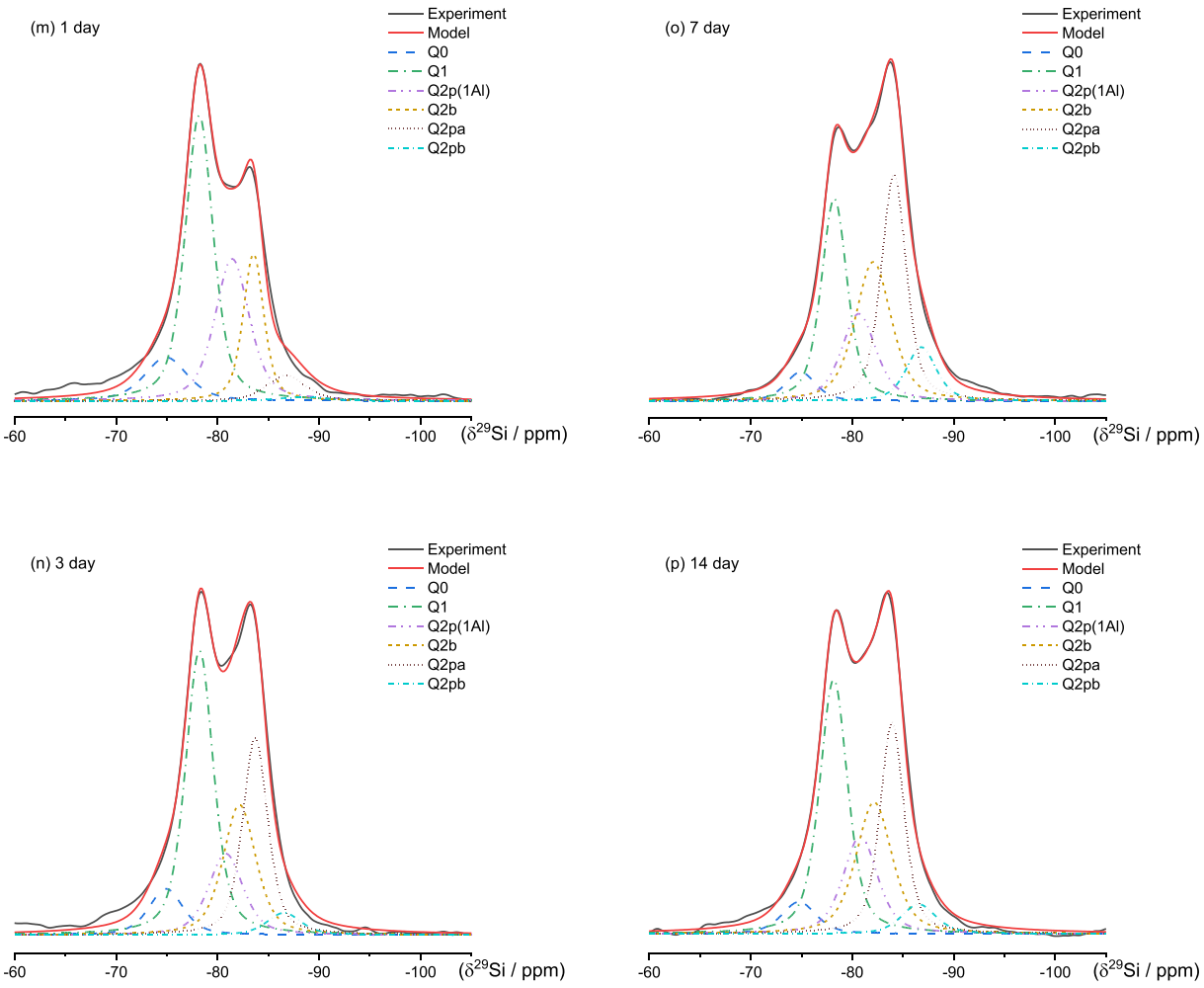

Fig. A4. (*continued*).

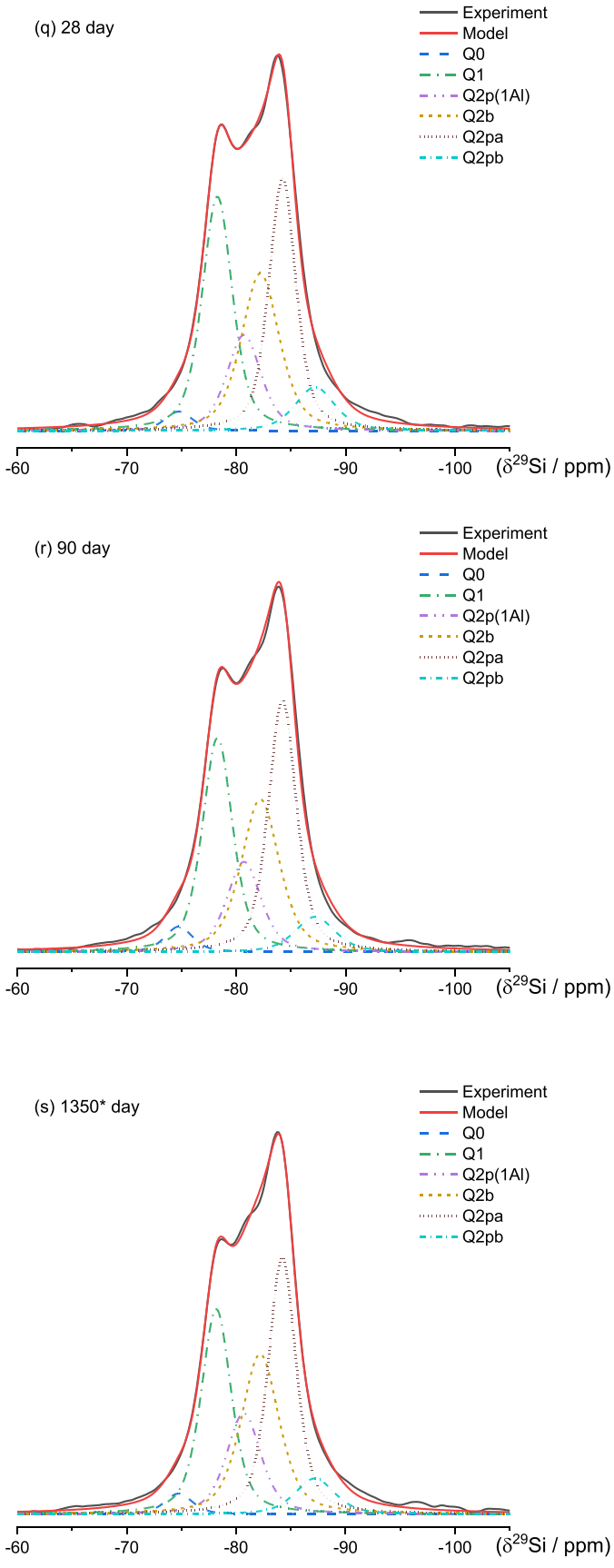

Fig. A4. (*continued*).

Fig. A5 shows the Al/Si in C-S-H for all Ca/Si studied, as a comparison of Fig. 10. The Al uptake between the different Ca/Si C-S-H is comparable if plotted as molar Al/Si in C-S-H (Fig. A5) but much higher at low Ca/Si if plotted as Al per g of C-S-H (Fig. 10), due to lower C-S-H weight per mol Si at low Ca/Si C-S-H.

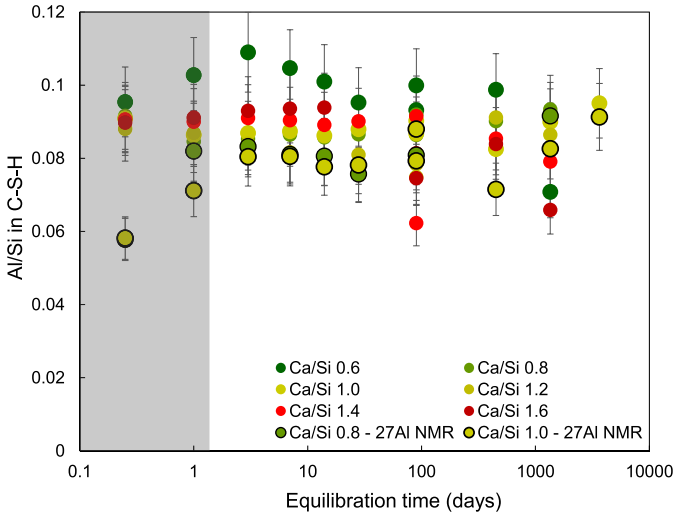

Fig. A5. Effect of time on the Al sorption in C-A-S-H expressed Al/Si in C-S-H. The shade area indicates the presence of less C-A-S-H as well as the potential underestimation of Al in secondary phases at early stages.

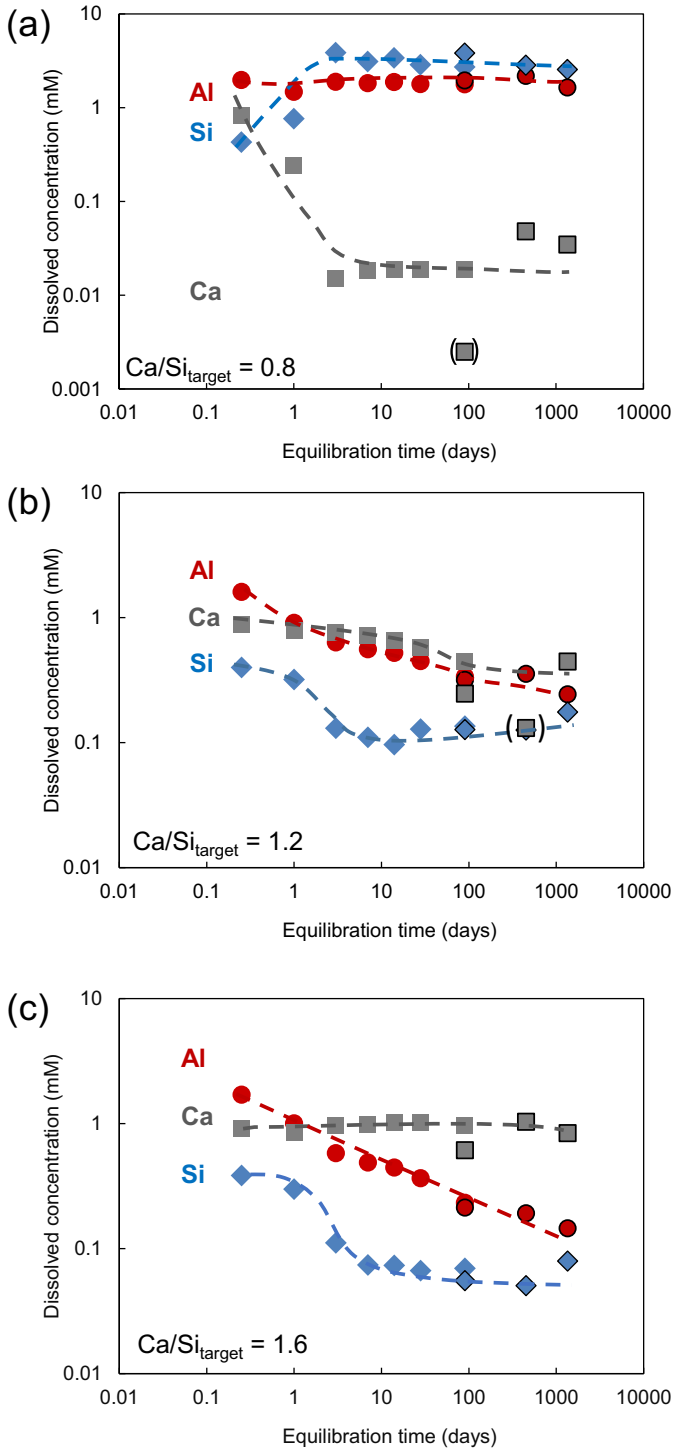

Fig. A6. The evolution of dissolved Al, Si and Ca concentrations in solution for Ca/Si$_{target}$ ratios of (a) 0.8, (b) 1.2 and (c) 1.6 synthesized in NaOH 0.5 M with initial Al/Si 0.1 equilibrated for different time. Two series were studied: Series A: filled symbols: in w/s = 40; Series B: symbols with black border: w/s = 45. The error of the dissolved concentrations are 10 % and the error bars are smaller than the symbols. Symbols in brackets: outlier Ca concentration after 3 months and 1 year (curves added for guidance).

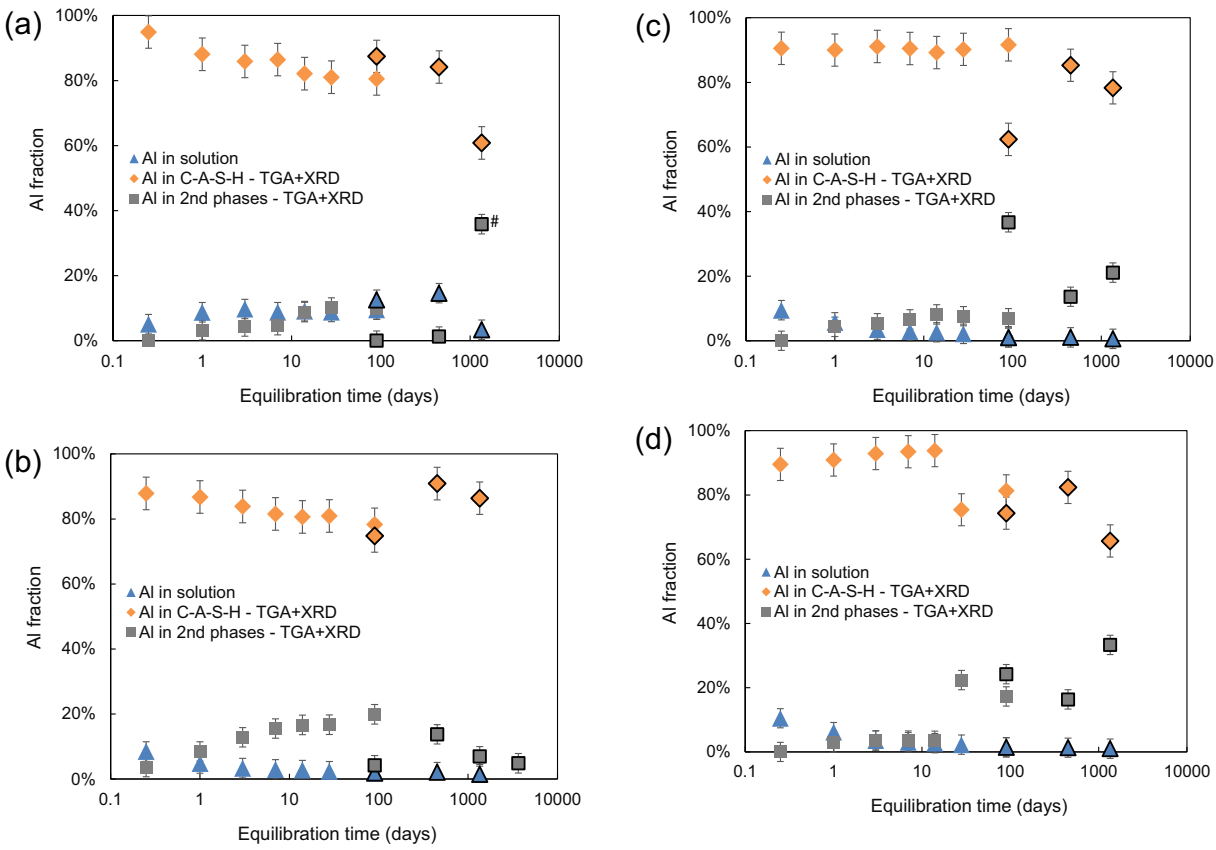

Fig. A7. Distribution of Al between C-A-S-H, aqueous phase and different secondary phases for target Ca/Si = (a) 0.6, (b) 1.2, (c) 1.4 and (d) 1.6 after different equilibration time in the presence of 0.5 M NaOH. Two series were studied: Series A: filled symbols: in w/s = 40; Series B: symbols with black border: w/s = 45. #: gismondine-P1-Na formation observed after 3 years at Ca/Si = 0.6.

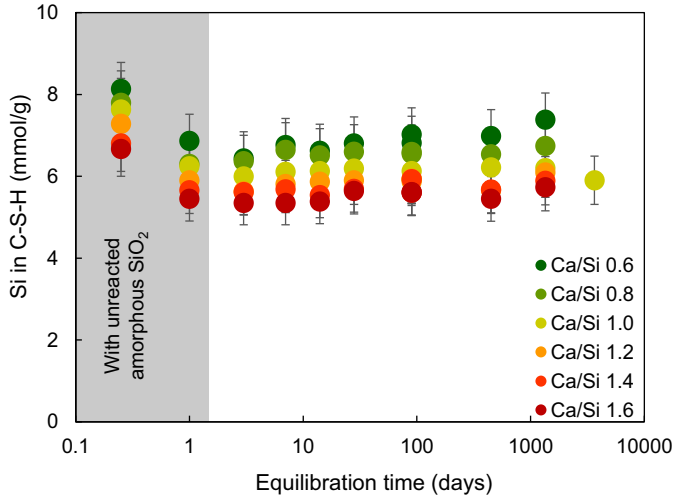

Fig. A8. Effect of equilibration time on the Si evolution in C-A-S-H.

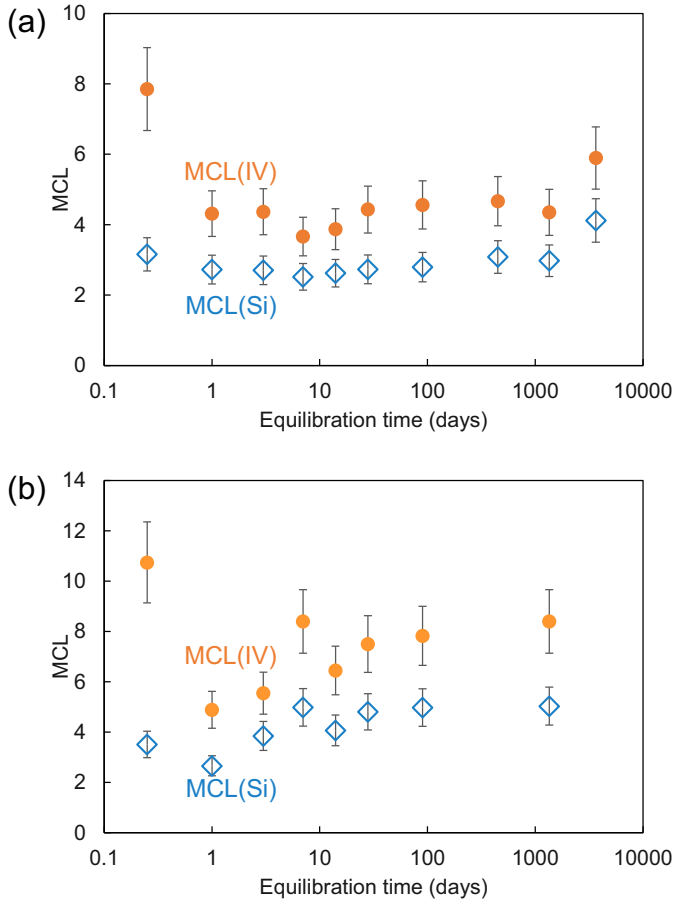

Fig. A9. Effect of equilibration time on MCL: (a) $Ca/Si_{target} = 1.0$ and (b) $Ca/Si_{target} = 0.8$.

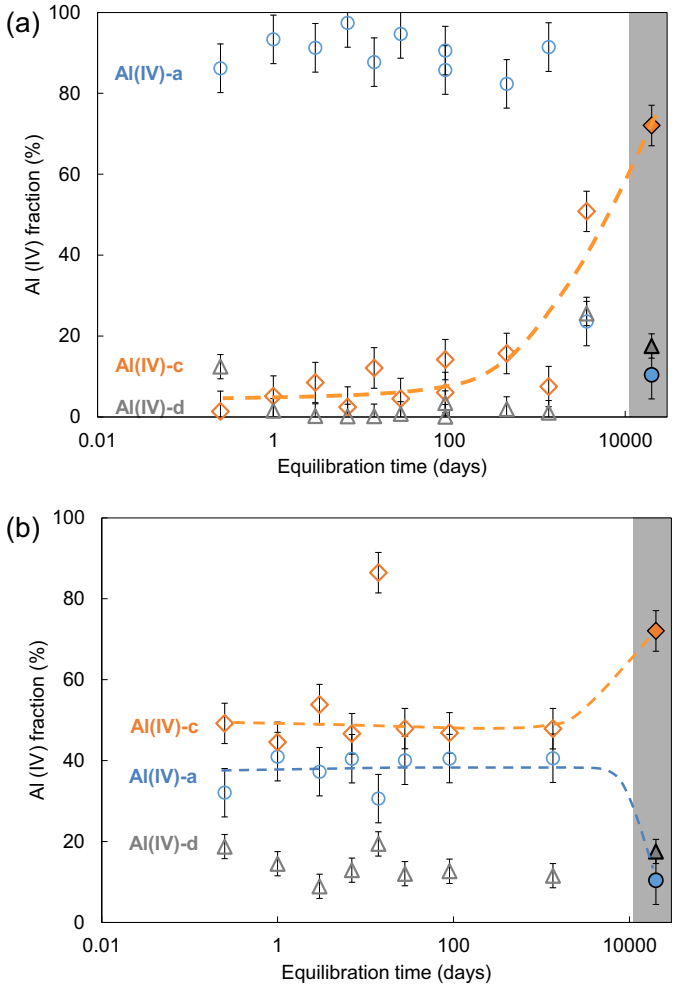

Fig. A10. Relative ^{27}Al NMR fraction of the different Al(IV) sites as a function of equilibration time of the C-A-S-H with (a) Ca/Si$_{target}$ = 1.0 and (b) Ca/Si$_{target}$ = 0.8 synthesized in 0.5 M NaOH and Al-tobermorite [12]. Empty symbols: C-A-S-H, solid symbols: Al-tobermorite. The fractions are derived from fittings of ^{27}Al NMR spectra in Fig. 7 and summarized in Table 2. The shaded area shows the Al-tobermorite in equilibrium (curves added for guidance).

References

[1] M.D. Jackson, S.R. Mulcahy, H. Chen, Y. Li, Q. Li, P. Cappelletti, H.R. Wenk, Phillipsite and Al-tobermorite mineral cements produced through low-temperature water-rock reactions in Roman marine concrete, Am. Mineral. 102 (2017) 1435–1450.

[2] X. Pardal, F. Brunet, T. Charpentier, I. Pochard, A. Nonat, 27Al and 29Si solid-state NMR characterization of calcium-aluminosilicate-hydrate, Inorg. Chem. 51 (2012) 1827–1836.

[3] J. Skibsted, M.D. Andersen, The effect of alkali ions on the incorporation of aluminum in the calcium silicate hydrate (C-S-H) phase resulting from Portland cement hydration studied by 29Si MAS NMR, J. Am. Ceram. Soc. 96 (2013) 651–656.

[4] G.K. Sun, J.F. Young, R.J. Kirkpatrick, The role of Al in C-S-H: NMR, XRD, and compositional results for precipitated samples, Cem. Concr. Res. 36 (2006) 18–29.

[5] B. Lothenbach, A. Nonat, Calcium silicate hydrates: solid and liquid phase composition, Cem. Concr. Res. 78 (2015) 57–70.

[6] R.J. Myers, S.A. Bernal, R.S. Nicolas, J.L. Provis, Generalized structural description of calcium-sodium aluminosilicate hydrate gels: the cross-linked substituted tobermorite model, Langmuir 29 (2013) 5294–5306.

[7] J.L. Provis, The Role of Al in Cross-Linking of Alkali-Activated Slag Cements 1004, 2015, pp. 996–1004.

[8] S. Ortaboy, J. Li, G. Geng, R.J. Myers, P.J.M.M. Monteiro, R. Maboudian, C. Carraro, Effects of CO2 and temperature on the structure and chemistry of C-(A-)S-H investigated by Raman spectroscopy, RSC Adv. 7 (2017) 48925–48933.

[9] J. Li, W. Zhang, K. Garbev, G. Beuchle, P.J.M. Monteiro, Influences of cross-linking and Al incorporation on the intrinsic mechanical properties of tobermorite, Cem. Concr. Res. 136 (2020), 106170.

[10] G. Geng, R.J. Myers, J. Li, R. Maboudian, C. Carraro, D.A. Shapiro, P.J. M. Monteiro, Aluminum-induced dreierketten chain cross-links increase the mechanical properties of nanocrystalline calcium aluminosilicate hydrate, Sci. Rep. 7 (2017) 44032.

[11] R.J. Myers, E. L'Hôpital, J.L. Provis, B. Lothenbach, Effect of temperature and aluminium on calcium (alumino)silicate hydrate chemistry under equilibrium conditions, Cem. Concr. Res. 68 (2015) 83–93.

[12] B. Lothenbach, D. Jansen, Y. Yan, J. Schreiner, Solubility and characterization of synthesized Al-tobermorite, Cem. Concr. Res. 159 (2022), 106871.

[13] S.-Y. Hong, F.P. Glasser, Alkali sorption by C-S-H and C-A-S-H gels: part II. Role of alumina, Cem. Concr. Res. 32 (2002) 1101–1111.

[14] M.D. Andersen, H.J. Jakobsen, J. Skibsted, Incorporation of aluminum in the calcium silicate hydrate (C-S-H) of hydrated Portland cements: a high-field 27Al and 29Si MAS NMR investigation, Inorg. Chem. 42 (2003) 2280–2287.

[15] G. Renaudin, J. Russias, F. Leroux, F. Frizon, C. Cau-dit-Coumes, Structural characterization of C-S-H and C-A-S-H samples-part I: long-range order investigated by Rietveld analyses, J. Solid State Chem. 182 (2009) 3312–3319.

[16] I.G. Richardson, Model structures for C-(A)-S-H(I), Acta Crystallogr. Sect. B Struct. Sci. Cryst. Eng. Mater. 70 (2014) 903–923.

[17] R.J. Myers, E.L. Hôpital, L. Provis, B. Lothenbach, Composition-solubility-structure relationships in calcium (alkali) aluminosilicate hydrate (C-(N,K-)A-S-H), Dalton Trans. 44 (2015) 13530–13544.

[18] E. L'Hôpital, B. Lothenbach, G. Le Saout, D. Kulik, K. Scrivener, Incorporation of aluminium in calcium-silicate-hydrates, Cem. Concr. Res. 75 (2015) 91–103.

[19] E. L'Hôpital, B. Lothenbach, D.A. Kulik, K. Scrivener, Influence of calcium to silica ratio on aluminium uptake in calcium silicate hydrate, Cem. Concr. Res. 85 (2016) 111–121.

[20] E. L'Hôpital, B. Lothenbach, K. Scrivener, D.A.A. Kulik, Alkali uptake in calcium alumina silicate hydrate (C-A-S-H), Cem. Concr. Res. 85 (2016) 122–136.

[21] S.V. Churakov, C. Labbez, Thermodynamics and molecular mechanism of Al incorporation in calcium silicate hydrates, J. Phys. Chem. C 121 (2017) 4412–4419.

[22] G. Geng, R.N. Vasin, J. Li, M.J.A. Qomi, J. Yan, H.R. Wenk, P.J.M. Monteiro, Preferred orientation of calcium aluminosilicate hydrate induced by confined compression, Cem. Concr. Res. 113 (2018) 186–196.
[23] J. Li, G. Geng, R. Myers, Y.S. Yu, D. Shapiro, C. Carraro, R. Maboudian, P.J. M. Monteiro, The chemistry and structure of calcium (alumino) silicate hydrate: a study by XANES, ptychographic imaging, and wide- and small-angle scattering, Cem. Concr. Res. 115 (2019) 367–378.
[24] J. Li, W. Zhang, K. Garbev, P.J.M. Monteiro, Coordination environment of Si in calcium silicate hydrates, silicate minerals, and blast furnace slags: a XANES database, Cem. Concr. Res. 143 (2021), 106376.
[25] S. Barzgar, B. Lothenbach, M. Tarik, A. Di Giacomo, C. Ludwig, The effect of sodium hydroxide on Al uptake by calcium silicate hydrates (C-S-H), J. Colloid Interface Sci. 572 (2020) 246–256.
[26] E. John, D. Stephan, Calcium silicate hydrate—in-situ development of the silicate structure followed by infrared spectroscopy, J. Am. Ceram. Soc. 104 (2021) 6611–6624.
[27] X. Pardal, I. Pochard, A. Nonat, Experimental study of Si-Al substitution in calcium-silicate-hydrate (C-S-H) prepared under equilibrium conditions, Cem. Concr. Res. 39 (2009) 637–643.
[28] S. Barzgar, M. Tarik, C. Ludwig, B. Lothenbach, The effect of equilibration time on Al uptake in C-S-H, Cem. Concr. Res. 144 (2021), 106438.
[29] D.A. Kulik, G.D. Miron, B. Lothenbach, A structurally-consistent CASH+ sublattice solid solution model for fully hydrated C-S-H phases: thermodynamic basis, methods, and ca-Si-H2O core sub-model, Cem. Concr. Res. 151 (2022), 106585.
[30] G.D. Miron, D.A. Kulik, Y. Yan, J. Tits, B. Lothenbach, Extensions of CASH+ thermodynamic solid solution model for the uptake of alkali metals and alkaline earth metals in C-S-H, Cem. Concr. Res. 152 (2022), 106667.
[31] G.D. Miron, Y. Yan, D.A. Kulik, B. Lothenbach, Extensions of CASH+ Thermodynamic Solid Solution Model for the Uptake of Aluminium in C-S-H (in preparation), 2023.
[32] G.D. Miron, D.A. Kulik, B. Lothenbach, Porewater compositions of Portland cement with and without silica fume calculated using the fine-tuned CASH+NK solid solution model, Mater. Struct. 55 (2022) 212.
[33] B. Traynor, H. Uvegi, E. Olivetti, B. Lothenbach, R.J. Myers, Methodology for pH measurement in high alkali cementitious systems, Cem. Concr. Res. 135 (2020), 106122.
[34] B. Lothenbach, P. Durdzinski, K. De Weerdt, Thermogravimetric analysis, in: K. L. Scrivener, R. Snellings, B. Lothenbach (Eds.), A Pract. Guid. to Microstruct. Anal. Cem. Mater, CRC Press, Oxford, UK, 2016, pp. 177–212.
[35] S.T. Merlino, E.L. Bonaccorsi, T.H. Armbruster, The real structure of tobermorite 11Å: normal and anomalous forms, OD character and polytypic modifications, Eur. J. Mineral. 13 (2001) 577–590.
[36] F. Menges, Spectragryph - optical spectroscopy software, Version 1.2.15. http://www.effemm2.de/spectr, 2020.
[37] E. Bernard, B. Lothenbach, D. Rentsch, Influence of sodium nitrate on the phases formed in the MgO-Al2O3-SiO2-H2O system, Mater. Des. 198 (2021), 109391.
[38] D. Massiot, F. Fayon, M. Capron, I. King, L. Calv, B. Alonso, J.O. Durand, B. Bujoli, Z. Gan, G. Hoatson, S. Le Calvé, B. Alonso, J.O. Durand, B. Bujoli, Z. Gan, G. Hoatson, Modelling one- and two-dimensional solid-state NMR spectra, Magn. Reson. Chem. 40 (2002) 70–76.
[39] R.J. Myers, S.A. Bernal, J.L. Provis, A thermodynamic model for C-(N-)A-S-H gel: CNASH_ss. Derivation and validation, Cem. Concr. Res. 66 (2014) 27–47.
[40] S.-Y. Yang, Y. Yan, B. Lothenbach, J. Skibsted, Sodium and tetrahedral aluminium in cementitious calcium-aluminate-silicate hydrate phases (C-A-S-H), J. Phys. Chem. C 125 (2021) 27975–27995.
[41] J.B. d'Espinose de Lacaillerie, C. Fretigny, D. Massiot, MAS NMR spectra of quadrupolar nuclei in disordered solids: the Czjzek model, J. Magn. Reson. 192 (2008) 244–251.
[42] Y. Yan, B. Ma, G.D. Miron, D.A. Kulik, K. Scrivener, B. Lothenbach, Al uptake in calcium silicate hydrate and the effect of alkali hydroxide, Cem. Concr. Res. 162 (2022), 106957.
[43] D.W. Oscarson, H.B. Hume, Effect of the Solid: Liquid Ratio on the Sorption of Sr2+ and Cs+ on Bentonite, Woodhead Publishing Limited, 1998.
[44] T. Wagner, D.A. Kulik, F.F. Hingerl, S.V. Dmytrievava, Gem-selektor geochemical modeling package: TSolMod library and data interface for multicomponent phase models, Can. Mineral. 50 (2012) 1173–1195.
[45] D.A. Kulik, T. Wagner, S.V. Dmytrieva, G. Kosakowski, F.F. Hingerl, K. V. Chudnenko, U.R. Berner, GEM-Selektor geochemical modeling package: revised algorithm and GEMS3K numerical kernel for coupled simulation codes, Comput. Geosci. 17 (2013) 1–24.
[46] T. Thoenen, W. Hummel, U. Berner, E. Curti, The PSI/Nagra Chemical Thermodynamic Database 12/07, 5232 Villigen PSI, 2014.
[47] B. Lothenbach, D.A. Kulik, T. Matschei, M. Balonis, L. Baquerizo, B. Dilnesa, G. D. Miron, R.J. Myers, Cemdata18: a chemical thermodynamic database for hydrated Portland cements and alkali-activated materials, Cem. Concr. Res. 115 (2019) 472–506.
[48] B. Ma, B. Lothenbach, Tetrahedral Atom Ordering and Si/Al Ratio on Thermodynamic Properties of Selected Zeolites, 2023.
[49] B. Ma, B. Lothenbach, Thermodynamic study of cement/rock interactions using experimentally generated solubility data of zeolites, Cem. Concr. Res. 135 (2020), 106149.
[50] H.C. Helgeson, D.H. Kirkham, G.G. Flowers, Theoretical prediction of the thermodynamic behavior of aqueous electrolytes at high pressure and temperature: IV. Calculation of activity coefficients, osmotic coefficients, and apparent molal and standard and relative partial molal properties to 600°C a, Am. J. Sci. 281 (1981) 1249–1516.
[51] S. Grangeon, F. Claret, Y. Linard, C. Chiaberge, X-ray diffraction: a powerful tool to probe and understand the structure of nanocrystalline calcium silicate hydrates, Acta Crystallogr. Sect. B: Struct. Sci. Cryst. Eng. Mater. 69 (2013) 465–473.
[52] S. Grangeon, F. Claret, C. Roosz, T. Sato, S. Gaboreau, Y. Linard, IUCr, structure of nanocrystalline calcium silicate hydrates: insights from X-ray diffraction, synchrotron X-ray absorption and nuclear magnetic resonance, J. Appl. Crystallogr. 49 (2016) 771–783.
[53] O. Chaix-Pluchery, J. Pannetier, J. Bouillot, J.C. Niepce, Structural prereactional transformations in Ca(OH)2, J. Solid State Chem. 67 (1987) 225–234.
[54] G.A. Lager, R.T. Downs, M. Origlieri, R. Garoutte, High-pressure single-crystal X-ray diffraction study of katoite hydrogarnet: evidence for a phase transition from Ia3d → I4¯3d symmetry at 5 GPa, Am. Mineral. 87 (2002) 642–647.
[55] C. Baerlocher, W.M. Meier, The crystal structure of synthetic zeolite na-p 1, an isotype of gismondine, Z. Krist. - New Cryst. Struct. 135 (1972) 339–354.
[56] B. Lothenbach, E. Bernard, U. Mäder, Zeolite formation in the presence of cement hydrates and albite, Phys. Chem. Earth 99 (2017) 77–94.
[57] E. Tajuelo Rodriguez, K. Garbev, D. Merz, L. Black, I.G. Richardson, Thermal stability of C-S-H phases and applicability of Richardson and Groves' and Richardson C-(A)-S-H(I) models to synthetic C-S-H, Cem. Concr. Res. 93 (2017) 45–56.
[58] Y. Yan, S.Y. Yang, G.D. Miron, I.E. Collings, E. L'Hôpital, J. Skibsted, F. Winnefeld, K. Scrivener, B. Lothenbach, Effect of alkali hydroxide on calcium silicate hydrate (C-S-H), Cem. Concr. Res. 151 (2022), 106636.
[59] K. Mesecke, L.N. Warr, W. Malorny, Structure modeling and quantitative X-ray diffraction of C-(A)-S-H, J. Appl. Crystallogr. 55 (2022) 133–143.
[60] P. Yu, R.J. Kirkpatrick, B. Poe, P.F. McMillan, X. Cong, Structure of calcium silicate hydrate (C-S-H): near-, mid-, and far-infrared spectroscopy, J. Am. Ceram. Soc. 48 (1999) 742–748.
[61] N.V. Chukanov, Infrared Spectra of Mineral Species: Extended Library, Springer Science & Business Media, 2014.
[62] N.Y. Mostafa, A.A. Shaltout, H. Omar, S.A. Abo-El-Enein, Hydrothermal synthesis and characterization of aluminium and sulfate substituted 1.1 nm tobermorites, J. Alloys Compd. 467 (2009) 332–337.
[63] X. Qu, Z. Zhao, X. Zhao, Microstructure and characterization of aluminum-incorporated calcium silicate hydrates (C-S-H) under hydrothermal conditions, RSC Adv. 8 (2018) 28198–28208.
[64] R.J. Kirkpartick, J.L. Yarger, P.F. McMillan, P. Yu, X. Cong, Raman spectroscopy of C-S-H, tobermorite, and jennite, Adv. Cem. Based Mater. 5 (1997) 93–99.
[65] M. Tarrida, M. Madon, B. Le Rolland, P. Colombet, An in-situ Raman spectroscopy study of the hydration of tricalcium silicate, Adv. Cem. Based Mater. 2 (1995) 15–20.
[66] C.S. Deng, C. Breen, J. Yarwood, S. Habesch, J. Phipps, B. Craster, G. Maitland, Ageing of oilfield cement at high humidity: a combined FEG-ESEM and Raman microscopic investigation, J. Mater. Chem. 12 (2002) 3105–3112.
[67] K. Garbev, P. Stemmermann, L. Black, C. Breen, J. Yarwood, B. Gasharova, Structural features of C-S-H(I) and its carbonation in air-a Raman spectroscopic study. Part I: fresh phases, J. Am. Ceram. Soc. 90 (2007) 900–907.
[68] L. Black, C. Breen, J. Yarwood, K. Garbev, P. Stemmermann, B. Gasharova, Structural features of C-S-H(I) and its carbonation in air-a Raman spectroscopic study. Part II: carbonated phases, J. Am. Ceram. Soc. 90 (2007) 908–917.
[69] I.G. Richardson, J. Skibsted, L. Black, R.J. Kirkpatrick, Characterisation of cement hydrate phases by TEM, NMR and Raman spectroscopy, Adv. Cem. Res. 22 (2010) 233–248.
[70] S. Martinez-Ramirez, S. Sanchez-Cortes, J.V. Garcia-Ramos, C. Domingo, C. Fortes, M.T. Blanco-Varela, Micro-Raman spectroscopy applied to depth profiles of carbonates formed in lime mortar, Cem. Concr. Res. 33 (2003) 2063–2068.
[71] T. Runčevski, R.E. Dinnebier, O.V. Magdysyuk, H. Pöllmann, Crystal structures of calcium hemicarboaluminate and carbonated calcium hemicarboaluminate from synchrotron powder diffraction data, Acta Crystallogr. Sect. B Struct. Sci. 68 (2012) 493–500.
[72] J.T. Kloprogge, D. Wharton, L. Hickey, R.L. Frost, Infrared and Raman study of interlayer anions CO32−, NO3−, SO42− and ClO4− in Mg/Al-hydrotalcite, Am. Mineral. 87 (2002) 623–629.
[73] S. Barzgar, Y. Yan, M. Tarik, J. Skibsted, C. Ludwig, B. Lothenbach, A long-term study on structural changes in calcium aluminate silicate hydrates, Mater. Struct. 55 (2022) 243.
[74] A. Kunhi Mohamed, P. Moutzouri, P. Berruyer, B.J. Walder, J. Siramanont, J. Siramanont, M. Harris, M. Negroni, S.C. Galmarini, S.C. Parker, S.C. Parker, K. L. Scrivener, L. Emsley, P. Bowen, The atomic-level structure of cementitious calcium aluminate silicate hydrate, J. Am. Chem. Soc. 142 (2020) 11060–11071.
[75] S. Hong, F.P. Glasser, Alkali binding in cement pastes: part I. The C-S-H phase, Cem. Concr. Res. 29 (1999) 1893–1903.
[76] C. Labbez, I. Pochard, B. Jönsson, A. Nonat, C-S-H/solution interface: experimental and Monte Carlo studies, Cem. Concr. Res. 41 (2011) 161–168.
[77] E. Bernard, Y. Yan, B. Lothenbach, Effective cation exchange capacity of calcium silicate hydrates (C-S-H), Cem. Concr. Res. 143 (2021), 106393.